UNIVERSITY OF SOUTHAMPTON
ENERGY AND COASTS GROUP
School of Civil Engineering and the Environment

Hydrostatic Pressure Converters for the Exploitation of Very Low Head Hydropower Potential

by

James Alexander Senior

Thesis for the degree of Doctor of Philosophy

February 2009

UNIVERSITY OF SOUTHAMPTON

ABSTRACT

ENERGY AND COASTS GROUP

SCHOOL OF CIVIL ENGINEERING AND THE ENVIRONMENT

Doctor of Philosophy

HYDROSTATIC PRESSURE CONVERTERS FOR THE EXPLOITATION OF VERY LOW HEAD HYDROPOWER POTENTIAL

by James Alexander Senior

Much of the world's available hydropower potential has been exploited, and within the western world attention is increasingly being focussed on hydropower sites with very low head differences. These are sites where the vertical distance through which water falls is less than five metres, and remain unexploited as there is a recognised lack of hydropower technology avaiable to exploit these low-power sites economically. The aim of this work was therefore to develop a novel hydropower machine which could be used to viably exploit very low head differences in river environments.

A review of the hydropower technologies determined that the established machinery is primarily driven by the operational principles of impulse, reaction, or potential. It was however noticed that some less well established designs appear to be driven directly by the hydrostatic pressure which could be generated by a depth of flowing water. This observation had not been previously acknowledged. It was also recognised that investigation into this operational principle could potentially result in machines that were both relatively simple, and have high flow and power capacities when compared to the established technologies.

It was identified that there could be two approaches to exploiting hydrostatic pressure, and ideal theories were developed to describe both approaches. The resulting physical concepts were called *Hydrostatic Pressure Converters*. Scale models of these concepts were hydraulically tested, verifiying the proposed theories, and providing data from which estimates of full scale performance were made. These predicted that the two proposed designs of Hydrostatic Pressure Converter were suitable for head differences below 2.5m, normally the domain of the traditional waterwheel. They would operate with high hydraulic efficiency, at around 80%, but have a significantly greater flow capacity and power output per unit width of machine, at 500% that possible using a traditional waterwheel.

In conclusion this work has identified, analysed and prototyped a novel approach to exploiting very low head hydropower potential. The resulting Hydrostatic Pressure Converters are a significant and promising development in the field of very low head hydropower.

Contents

List of Figures

List of Tables

Author's Declaration

I, James Alexander Senior, declare that the thesis entitled *Hydrostatic Pressure Converters for the Exploitation of Very Low Head Hydropower Potential* and the work presented in the thesis are both my own, and have been generated by me as the result of my own original research.
I confirm that:

- This work was done wholly while in candidature for a research degree at this University.
- Where any part of this thesis has previously been submitted for a degree or any other qualification at this Unversity or any other institution, this has been clearly stated.
- Where I have consulted the published work of others, this is always clearly attributed.
- Where I have quoted from the work of others, the source is always given. With the exception of such quotations, this thesis is entirely my own work.
- I have acknowledged all main sources of help.
- Where the thesis is based on work done by myself jointly with others, I have made clear exactly what was done by others and what I have contributed myself.
- Parts of this work has been published as Senior et al. 2007 and 2008.

Signed:.....

Date:.....

Acknowledgements

I wish to thank Dr Gerald Müller for his supervision during the last three years, and for sharing his great enthusiasm for all things innovative, scientific and engineering. I have greatly enjoyed the discussions we held and the projects we conducted.

I also want to thank everyone who assisted me at various times, including my brother Nick, who wrote the rotational speed tracking program I used, Derek Clarke for his additional supervision, and all of the technicians in the laboratories for their good humour and interest in my work.

Finally I wish to thank my good friend Patrick Wiemann, with whom I had a highly entertaining time working as consultants, conducting site surveys, and attending conferences.

Glossary:

Efficiency: Describes a hydropower machine's ability to convert the hydraulic power of the flowing water to mechanical power.

Filling ratio: Describes the proportion of a cell of a waterwheel which is occupied by water during operation.

Flow capacity: The volume of water being proceesed by a hydropower machine at the point of maximum power output.

Free surface: Describes the boundary between open water and the atmosphere.

Inertial reaction force: The reaction force exerted by the installation as a whole to the acceleration of water through the installation.

Load: The resistance of a device to which power is delivered.

Operational principle: The fundamental mechanism or process by which a hydropower machine is driven.

Rotational quality: Describes the smoothness which which a hydropower machine rotates, with pulsation being undesirable.

Specific cost: The initial cost of installation per rated kWh.

'Type one' HPC: Hydropower machines where the working surface extends from the channel bed to the *upstream* water surface.

'Type two' HPC: Hydropower machines where the working surface extends from the channel bed to the *downstream* water surface.

Working surface: The moving surface, such as a blade, upon which force is being exerted, thus doing work.

List of Abbreviations:

EL: Energy Line

FP7: Seventh Framework Programme.

HPC: Hydrostatic Pressure Converter.

M-HPC: Middleshot Hydrostatic Pressure Converter.

SDM: *Staudruckmaschine*.

SHP: Small Hydropower (installations under 10MW).

U-HPC: Undershot Hydrostatic Pressure Converter.

SI Units:

Quantity	Unit Name	Unit Symbol	Equivalent Units
Pressure	Pascals	Pa	N/m^2
Force	Newtons	N	kg m/s^2
Work	Joules	J	N m
Power	Watts	W	Nm/s
Frequency	Hertz	Hz	s^{-1}

Table 1: SI Units

List of Symbols:

Symbol	Description	Units
d_b	Water depth at the blade	m
d_c	Water depth in channel, prior to drop within shroud (U-HPC)	m
$\triangle_d$	Drop in head resulting from the acceleration of flow (M-HPC)	m
$\triangle_Z$	Height of sharp crested measurement weir	m
d_1	Depth of water in the in upstream	m
d_2	Depth of water in the downstream	m
ε	Filling ratio of waterwheel cells	-
f	F|requency of rotation	s^{-1}
F_A	Reaction force to the acceleration of flow (M-HPC)	N
F_P	Force exerted by hydrostatic pressure on the working blade (M-HPC)	N
F_T	Force on the working blade which results from thurbulent losses	N
F_1	Force exerted on the upstream side of working blade	N
F_2	Force exerted on the downstream side of the working blade	N
g	Acceleration due to gravity	m/s^2
g_b	Depth of gap beneath working blade	m
g_s	Width of gap beside working blade	m
H	Head difference	m
H_{wave}	Wave height	m
l	Blade length	m
$m_{counterweight}$	Mass of the Prony Brake counterweight	kg
m_{weight}	Mass of the Prony Brake weight	kg
n	Number of blades	-
η	Efficiency	-
$\eta_{leakage\,adjusted}$	Efficiency, adjusted to account for leakage losses	-
$\eta_{leakage\,and\,turbulence\,adjusted}$	Efficiency, adjusted to account for leakage and turbulent losses	-
P	Power	W
P_d	Power developed on the downstream side of the working blade (U-HPC)	W
P_{evac}	Power associated with the 'type one' HPC evacuation process	W
$P_{friction}$	Power lost to friction	W
P_{max}	max power out	W
P_{out}	Power output	

Table 2: List of Symbols

Symbol	Description	Units
$P_{out,\,leakage\,adjusted}$	Power output, adjusted to account for leakage losses	W
$P_{out,\,leakage\,and\,turbulence\,adjusted}$	Power output, adjusted to account for leakage and turbulent losses	W
$P_{out,measured}$	Power output as measured by Prony Brake	W
P_u	Power developed on the upstream side of the working blade (U-HPC)	W
P_{wave}	Wave Power	W/m
Q	Flow rate	m^3/s
$Q_{leakage}$	Leakage flow rate (through gaps)	m^3/s
Q_{max}	Flow rate at point of maximum power output	m^3/s
Q_{total}	Total flow rate, estimated by combining Q_{wheel} and $Q_{leakage}$	m^3/s
Q_{wheel}	Flow rate through the wheel (excluding leakage)	m^3/s
R	Radius	m
r_d	Radius to central point where F_2 acts on downstream side of working blade	m
r_u	Radius to central point where F_1 acts on upstream side of working blade	m
ρ	Density	kg/m^3
T_{wave}	Wave period	s
t_1	Water depth upstream from sharp crested measurement weir	m
V	Volume of cells	m^3
v_b	Velocity of blade	m/s
v_c	Velocity of flow in channel	m/s
v_d	Velocity of blade at radius r_d on downstream side of working blade	m/s
v_u	Velocity of blade at radius r_u on upstream side of working blade	m/s
v_1	Flow velocity in upstream	m/s
v_2	Flow velocity in downstream	m/s
W	Width	mm
W_{blade}	Width of working blade	m
$W_{channel}$	Width of channel upstream from HPC	m
ω	Angular speed of rotation	s^{-1}

Table 3: List of Symbols continued

Chapter 1

Introduction

1.1 Background

In the western world much of the large scale, high output, hydropower sites have now been exploited. Within Europe the focus has now shifted to Small Hydro-Power, which is installations with power outputs beneath 10MW. The European target is to achieve an additional 2.4GW of power generation from Small Hydro-Power plants by 2010, relative to the 2005 generation levels. Within this bracket are sites with 'very low head' which refers to sites where the vertical distance through which flowing water falls over structures or terrain is less than 5m. At this point in time, no technology for this bracket satisfactorily meets the economic and ecological requirements required by investors and the authorities. As a result, the Seventh Framework Programme's 'Research Priorities for the Renewable Energy sector' set by the European Union includes the development of small turbines for very low heads under 5m as one of its long term targets.

1.2 Aims and Objectives

The aim of this work is to develop a novel technology to viably exploit very low head hydropower installations in river environments.

This is to be achieved by meeting the following objectives:

- Identify the core issues which govern the viability of very low head hydropower installations.
- Investigate the existing hydropower technologies and their limitations.
- Identify any opportunities that exist for technical development or novel technologies.
- Support the design of any new concepts developed within this work with scientific theory.
- Verify any new theories through the use of hydraulic scale modelling.
- Indicate the potential full scale performance of any concepts developed.

Chapter 2

Literature Review: Part A Background

This Chapter, Part A of the literature review, provides an introduction as to what hydropower is, and the demand that exists to exploit it. The aim of developing a novel and viable technology that operates at very low head differences is justified, and the principle requirements of this new technology are identified. Additional factors relevant to hydropower such as environmental and operational considerations are raised. These considerations are not fundamental to addressing the aim of this research, but do provide additional perspective required to recommend further work, if the novel technology were ever to be implemented. This is followed by Part B of the literature review, which describes the current hydropower technology that exists for exploiting very low head hydropower.

2.1 Introduction to Hydropower

Hydropower is the exploitation of flowing water to generate electrical or mechanical power. The source of water in the majority of cases is natural, ranging from streams flowing down mountains to rivers and canals flowing along plains. An additional source of hydropower potential of increasing interest is that resulting from tidal flow through estuaries.

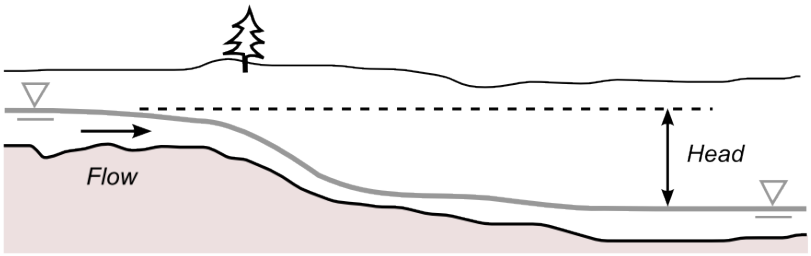

Figure 2.1: Fundamentals of hydropower

The power available for extraction from flowing water is a function of the quantity of flowing water and the vertical distance through which the water falls, as demonstrated by Figure 2.1 representing a cross section of a stream where the water surface is indicated by the inverted triangles. These variables are called the *flow rate*, Q, measured in m^3/s, and the *head* ,H, measured as the distance between two water surface levels in m. The maximum theoretical power available at a given hydropower site can be calculated using Equation 2.1.

$$P = H\,\rho\,g\,Q \tag{2.1}$$

Where:

P	power, W
H	head, m
ϱ	density of working fluid, kg/m^3
g	Acceleration due to gravity, m/s^2
Q	flow rate, m^3/s

For any potential hydropower site to be exploited, the head and flow rate must be determined so that appropriate *hydropower machinery* can be selected. How much of the hydraulic power can be converted to useful power depends on the efficiency of the components that comprise the installation. The components of an installation are commonly broken down into three groups:

- The hydropower machine converts the hydraulic power of the flowing water into mechanical power, normally in the form of a rotating shaft. The effectiveness of this conversion, or the *hydraulic efficiency*, primarily depends on the *operational principle* through which the machine operates. This is discussed further in Chapters 3 and 4.

- The mechanical output of the hydropower machine often requires modification to be utilised effectively. This may be in the form of a transmission or gearbox, delivering the mechanical power to the machine being driven, known as the *load*. These components will incur losses due to friction and have an associated *mechanical efficiency*.

- The majority of hydropower is exploited to generate electricity. In these installations, the load is an electrical generator. The generator, and its control system will have an associated *electrical efficiency*.

With a careful assessment of the hydropower resource and the available hydropower machinery, it can be determined whether a solution is technically feasible. It should be noted however that a technically feasible hydropower installation will often only be constructed if it is also deemed to be economically feasible, and environmentally acceptable.

2.2 Hydropower Potential

Hydropower installations generate about 17% (2,700 TWh/yr) of the world's supply of electricity (WEC 2004). This is 97% of all renewable power generation (Bakis 2007). Globally, hydropower potential is estimated at 40,000 TWh/yr of which 14,400 TWh/yr is technically feasible for development and 8000TWh/yr is economically feasible (WEC 2001). When considering large scale hydropower installations (10MW-100's MW), only 33% of the worlds technically and economically feasible hydropower is exploited, however this statistic does not apply to all regions equally. Whilst huge resources remain untapped in Asia, Africa and South Africa, the majority of the economical hydropower in North America and Europe has been exploited (WEC 2004). Much of the remaining potential is *Small Hydro-Power* (SHP), which is defined as installations beneath 10MW by the European Small Hydropower Association (however this value varies country by country, being up to under 25MW in China). In Europe SHP provides 8GW of electricity and an estimated 18GW remain, and in China SHP potential is estimated to exceed 70GW (Paish 2002).

2.3 Demand for New Very Low Head Technology

In Europe, a White Paper proposing a strategy and action plan for renewables currently targets an additional 2.4GW of power generation from Small Hydro-Power plants by 2010, relative to the 2005 generation levels (European Commission 1997, 2007). This has been followed by a comprehensive document for the European Commission titled 'Proposals for a European Strategy of Research, Development and Demonstration for Renewable Energy from Small Hydropower' (TNSHP 2005). This document thoroughly examined all aspects currently limiting the exploitation of SHP including the economic, public image, technology, and environmental issues. In its *priorities summary*, the development of low-head and very low head turbines was classified as "essential to reach White Paper objectives by year 2010". *Very low head* sites are those with fall heights beneath 5m. The findings of the proposal have been adopted in the Seventh Framework Programme's (FP7) 'Research Priorities for the Renewable Energy sector' (EURECA 2005) where one of the long term targets is to develop small hydro turbines for very low heads under 5m. This finding supports the observation commonly made in SHP studies: that no economically feasible solution exists for sites with very low heads in the range 1-3m (e.g.: ETSU 1982). In these SHP studies, head differences below 1m are ignored completely (e.g.: Bacon 2004).

The established low head technologies can be seen in Figure 2.2, which is updated from Giescke and Monsonyi (1998) to include traditional waterwheels (see section 3.1). Indicated on the graph, is the area of demand which must be targeted if the power output and economics of very low head hydropower are to be improved. This constitutes head differences under 5m with flow rates greater than $5m^3/s$ per unit.

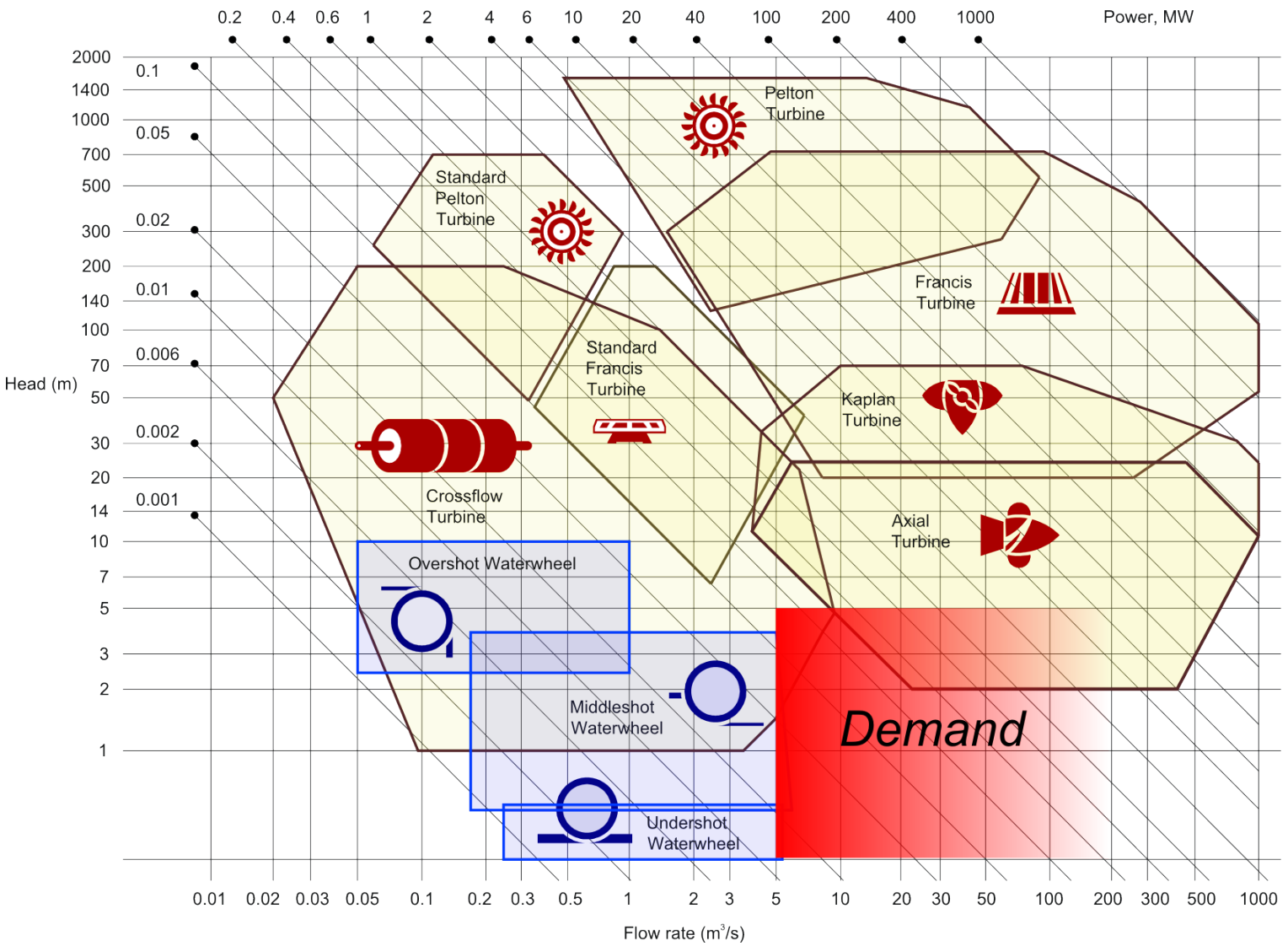

Figure 2.2: Established hydropower machines and demand for new technology, modified from Giescke and Monsonyi (1998)

2.4 Hydropower Considerations

This section introduces the main factors which must be taken into account when planning and building hydropower installations. They are all design and site specific, and as such do not directly impact on the stated aim of developing a new technology for exploiting very low heads. They will however assist in indicating the direction of further work to be conducted on any concepts developed in this document.

2.4.1 Hydropower site location

Very low head hydropower sites below 5m head do not take the form of large dams and reservoirs, which are associated with medium and high head installations with between 20m and 2,000m head. Instead they are mostly installed directly on natural or man-made rivers and canals, or on some rare occasions in estuaries or bays exploiting tidal flows.

2.4.1.1 River locations

The majority of very low head hydropower installations are found on natural or man-made rivers and canals with little or no water storage capacity. This means that the availabile hydropower at any time is predominantly determined by the natural river conditions, and not the electricity generator personnel. Man-made sites include industrial sites such as water treatment plants, navigation and irrigation canals. Installations on rivers come in the two forms shown in Figure 2.3 (Kaltschmitt 2007).

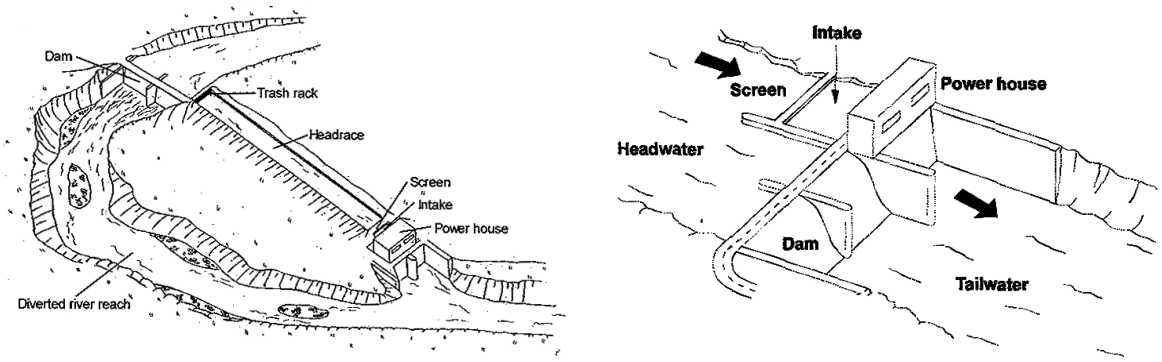

Figure 2.3: Low head river installation types: 'Diversion' and 'Run-of-river' (Kaltschmitt 2007)

The *Diversion* type hydropower station is situated outside of the actual riverbed at the end of a canal connecting the river before and after a dam or weir, which generates the head difference. Depending on the ecological and environmental protection laws, a certain flow rate must remain in the original portion of the river bed which has been bypassed. In the UK, the minimum residual flow is normally set at Q_{95}, the minimum flow present in the river 95% of the year (Bacon 2004). *Run-of-river* type hydropower installations are built into the actual riverbed. Many layouts of Diversion and Run-of-river installations exist depending on the geography and types of hydropower machine used.

An indication of the number of potential sites for very low head hydropower was made by NRW (2005) which counted the number of weir structures in a German federal state with an area of 1,000 km^2. This found 1,304 potential sites with heads between 0.2 m and 1.0 m which would suggest that tens of thousands of sites must exist throughout Europe. Several reports identify that potential developments could be installed at previously utilised sites such as disused Mills, but that these sites are only small and short term solutions. Medium to long term solutions exist at existing weir structures which could be redeveloped to exploit hydropower (Bacon, 2004). According to Ciocci (2003), fewer than 3% of significant dams in the United States have been exploited.

2.4.1.2 Tidal installations

An alternative to very low head sites on rivers and canals can be found in estuaries and other coastal environments and structures such as wetlands or even ports. The heads at these sites are driven by the tides and unlike river scenarios, are variable and alternating resulting in bi-directional currents. Unlike river locations which are dependent on precipitation and ground-water levels, tidal levels are reliable and predictable.

Large scale tidal projects come in two forms. The first is the Barrage type as proposed for the river Severn in the UK. These are large structures spanning estuaries which artificially create head differences by impeding the natural flow of the water. The second and more modern approach is to extract the kinetic energy from the current itself without using a barrage. The problem with both approaches is that the natural heads and flows can be significantly altered by the installation of the machine itself. An approximate guideline is that only 10% of the 'raw energy flux' produced by the tide can be extracted without adversely modifying the natural

flow characteristics (Bryden and Couch 2006). Kinetic energy type converters resemble wind turbine technology and are available for very low tidal variation down to 1m, such as the Davis turbine (Davis 1997).These turbines require deep channels so they can be fully submersed and safe from shipping traffic, and the flow velocities need to be high, normally beyond 3m/s. Also no significant head is measurable directly before and after the turbine. These types of turbine are not suitable for river installations as the depths and velocities required do not exist often if at all.

There are however examples of a tidal installations from the past where the hydro machinery is subjected to channel depths and flow velocities closer in form to river installations. One of these is Eling Tide Mill in the UK which operates by allowing sea water to fill a mill pond (Eling 2005). This is stored and released back to the sea through a hydropower machine when the tide is out as shown in Figure 2.4. The purpose of introducing tidal flows is merely to indicate that sites suitable for river type hydro machinery can present themselves, and that these can have bi-directional flows.

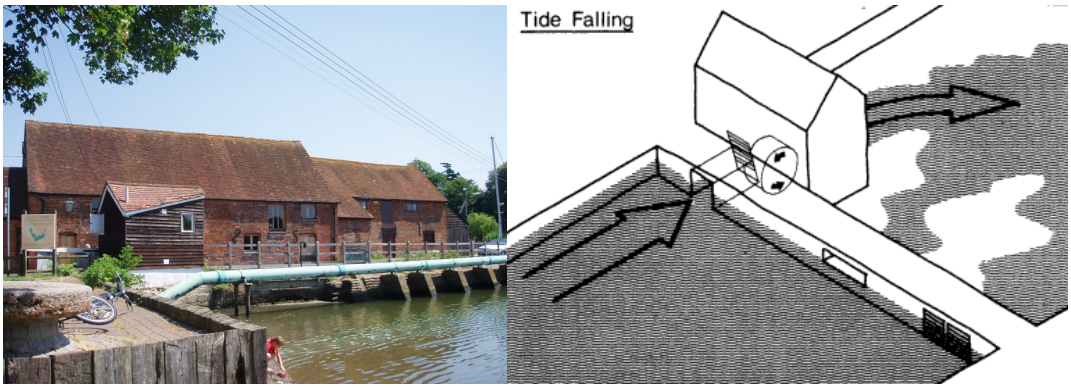

Figure 2.4: Eling Tide Mill, (Eling 2005)

2.4.2 Site hydrology

Two of the most important features of a potential hydropower installation are its flow and head profiles. These indicate how the flow rate and head vary throughout a year, and are especially important for low head installations as there is normally no storage capacity upstream to damp out any variation. As a result the daily power output of the installation is directly related to the flow and resulting head on that day. Figure 2.5 provides an example of a flow and head profile. The flow rate in the rivers is usually greatest during the winter months and smallest in

the summer months, in the Northern Hemisphere. Hydropower installations are conventionally designed with suitable control systems such that the upstream water level remains constant, however the machine has no ability to control the downstream water level, as the water runs away. Thus it can be seen that for most rivers there is an inverse relationship between the flow rate and head, as the downstream level drops with reducing flow (Kaltschmitt 2007). This is not always the case, as in some scenarios an adjustable weir may be positioned downstream of an installation which maintains a constant downstream water level. It must be noted that flow profiles are extremely site specific, depending on the location and the size of the catchment area - the area from which precipitation contributes to the river flow. Mountainous sites tend to have greater heads and smaller flows, whilst low-land sites tends to have much greater flows but much smaller heads. Most medium and large rivers within the UK have gauging stations which accurately record flow data. As there is annual variation, it is always ideal to obtain as much data as possible so that appropriate installation sizing can be conducted. This is the selection of the most economical hydropower machinery for an installation, and usually tends towards giving optimum performance at or above the average flow of the river, as opposed to giving optimum performance during maximum flow present during the year. In very low head cases, it can in some circumstances make more economic sense to install a relatively small and cheap hydropower plant if it can be run at full capacity for a greater proportion of the year (Bacon 2004).

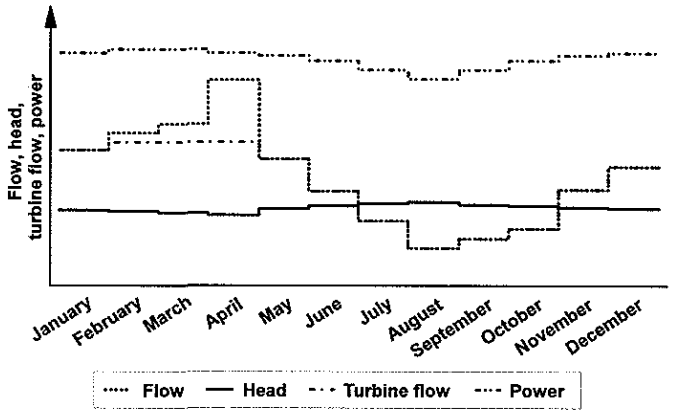

Figure 2.5: River flow and head profiles (Kaltschmitt 2007)

2.4.3 Economic considerations

The economics of hydropower installations are a very complicated discipline into which many decades of research and knowledge are applied. Included in the conventional analysis of costs and revenues are detailed trends and estimates over time in costs, revenues, interest rates, flow duration curves and even government policy. At its most basic level, if electricity is sold to the distribution network, the revenue is a function of the number of Kilowatt hours (kWh) generated. The costs encountered come from many sources and are specific for each project and site. These include the costs of design, land acquisition, planning approval, construction, installation, connection to the national grid, abstraction licenses from the Environment Agency (in the UK), maintenance and more.

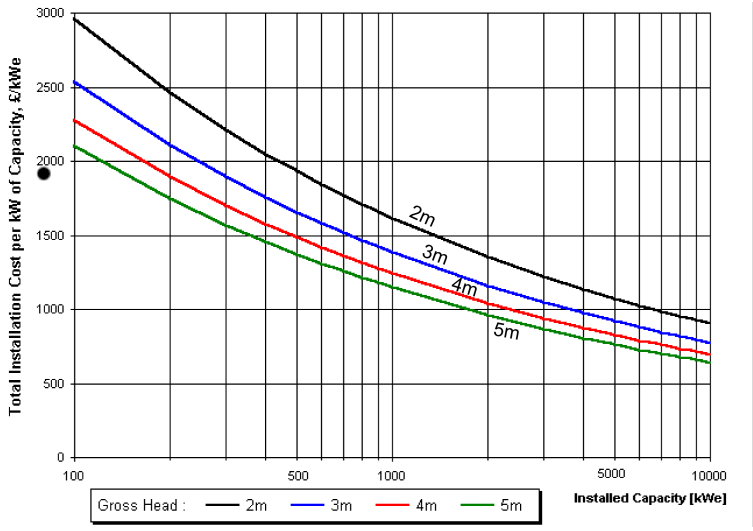

Figure 2.6: Hydropower project installation costs (Bacon 2004)

General observations made are that the *specific cost*, the investment cost per kW of installed capacity, increases with decreasing flow capacity and head as shown in Figure 2.6. The result is that using current technology, low head installations are not as favourable as high head installations; indeed Bacon (2004) concluded that installations below 3m head or 100kW were not attractive. These values are of course dependent on the price that can be earned per kWh and available grants, which are subject to change. It is also observed that the specific cost for low head sites can be reduced by using simpler technology and using as few units per site as possible (Goldsmith 1993).

2.4.4 Environmental considerations

There are several environmental considerations which must be satisfied for a hydropower installation to gain approval and remain operational. These include fish passage, changes in ecology, sediment transport, river bank and bed erosion, river management issues and water quality. In all cases the aim must be to alter these as little as possible from their natural states, although this can be difficult to define. These issues either have to be addressed in the initial design, or in some cases rectified following assessment (Bacon 2004, Kaltschmitt 2007). Other issues which are much harder to assess and require further research include the visual and audible impact of installations.

2.4.4.1 Fish passage

Figure 2.7: Example of a Fish ladder

Fish passage describes the movement of migratory and non-migratory fish, traveling both up- and down-stream. This can be adversely influenced by the introduction of installations which create unnatural head differences and falls at dams or weirs which they can not cross. Trash racks and fine screens normally prevent the passage of fish through the machinery itself, as the fish can be damaged by the localised acceleration of flow or by mechanical strike. Sudden and localised acceleration of flow occurs within most high speed turbines, and results in sudden pressure changes, sometimes even sub-atmospheric, which can harm the fish. Mechanical strike describes physical contact between fish and the rotating blades of the hydropower machine. It occurs not only with fast rotating machines such as turbines, but also potentially with slow rotating

machines such as waterwheels. A study into a traditional waterwheel found that fish were generally not attracted towards the installation. However, when forced to enter, the action of the blades passing the channel bed was compared to a guillotine, as fish would be cut. Although the fish were potentially fast enough to avoid impact, they tended to drift downstream into peril (Ely 2003). Conclusions can not yet be made with regards to fish passage through waterwheels, as Ely contradicts an historical source (Gerhardt 1893), which described how fish often passed though waterwheels without harm. As Ely's finding may have resulted from the manner in which the fish were fed into the installation, and Gerhardt's method to assess the well being of the fish is unknown, it can only be concluded that further study is required in this area.

The direct effect on the fish population depends on the characteristics of the machinery being used and the species of fish present. This is very site specific. In most cases it is required to add a *fish passage* which is a natural gradient stream, or a *fish ladder* which consist of many pools of water in a series of steps, as shown in figure 2.7. These bypass the hydropower installation allowing natural fish passage, but are very complicated to design and build effectively. Physical or behavioral screens are required to divert the fish into these passages. The construction of fish passages and screens reduces the flow available for energy extraction, and can comprise a considerable addition to the initial investment cost to construct. Hydropower installations also influence other areas of river ecology, including organisms, plants and insects. This is because they alter the natural depths and water velocities of the original river. Doing so can change the temperature and oxygenation levels in the water so that existing organisms can no longer survive.

2.4.4.2 Sediment transport

Sediment transport describes the natural movement of sediment such as sand, stones and soil within flowing water moving downstream. Most conventional hydropower installations dramatically reduce the natural sediment transport. This occurs for different reasons, intentional and non-intentional. For example, silt traps are often built upstream from turbines to remove the sediment which would otherwise erode the blades of the turbine and reduce operational efficiency. As the water exiting the turbine usually contains very little suspended sediment, scouring of river beds and loss of riverbanks can occur without replenishment (Bakis 2007). Sediment is also reduced by larger, slow rotating machines such as traditional waterwheels, where surface erosion would not influence the performance. This occurs at curved sections of river bed which partially extend around the wheels, acting like a dam or weir to create a head difference by increasing the depth of the upstream water. The flow velocity in the upstream is thus reduced, allowing some of the sediment to settle and build up behind the installation. The impact of sediment transport reduction is two fold. Firstly the sediment which collects upstream must be periodically flushed or dredged out. Also, the downstream portion of the river is no longer replenished with fresh sediment and erodes accordingly, altering the natural condition of the river.

2.4.5 Operational considerations

There are at least two important criteria which must be satisfied if a hydropower installation that generates electricity is to operate successfully. These are addressing the debris often found in natural river flows, and generating electricity of sufficient quality to export to the national grid.

2.4.5.1 Trash racks

Practically all forms of hydropower machinery can not handle debris in river flow. Debris can be natural, for example in the form of weed or logs, or man made, such as litter or larger items discarded into the river. Depending on the size of the debris, the result can be clogging of the installation intakes, seizure of the machinery, or damage to rotating components such as turbine blades. The standard solution since the introduction of waterwheels has been the use of raked bar screens, an example of which is shown in figure 2.8.

Figure 2.8: Raked bar screen (Bacon 2004)

These consist of many vertical bars, normally equidistantly spaced at around 20mm, placed immediately upstream from the machinery creating a screen to prevent passage of the debris into the machine. This system has drawbacks, as the debris which collects must be removed regularly otherwise a head difference will be generated across the screen, either raising the upstream water level or decreasing the head across the hydraulic machinery. In the worst case scenario a large build up of debris can block the inlet completely. The removal of the debris from the screen is either achieved manually using hand-held rakes or by expensive automated systems using hydraulically operated rakes. The second problem is that any debris removed

from rivers can not legally be returned to the river. This either means that the debris must be disposed of, requiring the continual hire of waste disposal skips, or the installation must be designed so that the debris can be diverted away and bypassed from the hydraulic machinery without it being removed from the river itself. This solution is normally difficult in practice as it is limited by the site layout. An alternative debris removal system is available whereby a mesh, in the form of a predominanly submersed horizontal cyclinder, rotates at a very slow speed to lift the debris above the water level. These types of debris screens are powered by the flowing water itself, but are often only cost effective for very low flow rates under $1m^3/s$ (Bacon 2004). The important consideration is the size of debris which can enter any given hydraulic machinery without damage. The finer the rack needs to be, the greater the quantity of debris that will collect, requiring more frequent maintenance and expense.

2.4.5.2 Power generation and distribution

The majority of hydropower installations are connected to the national grid whilst other small scale installations, normally in remote areas, are 'stand alone' using battery storage or heat dumps to provide the load. Grid connection is considered to be the best route as excess power generated can be dumped onto the grid and sold, and the grid can provide the reactive power to drive commonly used induction generators. In order to gain permission for grid connection, the generated power must be of a certain quality, specifically 50Hz and 230V ($\pm$10%) in the UK. Licenses must also be obtained and commissioning of the equipment must be conducted, all depending on the power output of the installation (DGCG 2004). The details of this are in the realm of the electrical engineer, however the generator type and quality requirement must be acknowledged by the hydropower machinery engineer.

The generator types used in the hydropower industry are similar to those used by the wind power industry. These include constant speed and variable speed generators which require suitable power electronics and converters to process the output power for grid connection (Khater 1996). The least expensive and most commonly used generators are constant speed induction types and need to be run at just over 1,500 rpm. This means that the rotational speed of the hydro machinery must be matched to that of the generator. Variable speed generators also have design ranges of speed that will require some speed matching. This is normally achieved using gearboxes, belt drives, or a combination of the two depending on the rotational speeds

and torques. An additional option is to construct large multi-pole generators which run at lower rotational speeds thus not requiring a gearbox. These are very large and heavy, and being custom built are considerably more expensive than 'off the shelf' induction motors used as generators. Typical generator efficiencies for low head applications are between 90% and 95% (Kaltschmitt 2007).

The type of generator will be selected based upon the size of the installation and the best operating regime for the hydraulic machinery (constant or variable speed). Pulsation in the rotation of the hydraulic machinery can be damaging to gearboxes and generating equipment, and if severe, can make grid connection impossible if the frequency and voltage fluctuate beyond acceptable limits. Ideally, the machinery must be designed to rotate as smoothly as possible. In this document this property is referred to as the *rotational quality*.

2.5 Conclusion

Within the Western world, much of the available hydropower potential has already been exploited. What remains, and what is now targeted is Small Hydropower, defined as installations beneath 10MW power output. Within this target area is locations where the head difference, the vertical fall between two water levels, is very low, under 5m. Although established hydropower machinery does exist for exploiting such low heads, including traditional waterwheels and turbines, it is generally observed that it is not economically viable to do so. This is due to the limited available hydraulic power resulting from the low head, and the relatively high cost of the machinery required to exploit it. As a result there is a stated demand from sources as significant as the European Commission to develop new technologies that are suitable for exploiting very low head hydropower.

The aim in developing any new technology is therefore to provide a solution that is more economically viable than established technologies. This can be achieved by reducing the cost and increasing the power output of the machinery. Although the hydraulic efficiency of any new technology is important to the power output, maximising it is not an objective as it is associated with additional complexity and cost. *Instead the approach to developing a more viable technology is to create a hydropower machine that is fundamentally both relatively simple in design and construction, and also has a relatively high flow capacity, defined as the flow rate that can be processed per unit. The target operational range is for heads below 5m, and flow rates above* $5m^3/s$ *per unit.*

It has also been shown that hydropower installations are influenced by environmental and operational considerations. Following the development of a new hydropower technology in principle, it is these considerations as well as design optimisation which will dictate the direction of further work to be pursued, if the new technology is ever to be implemented.

Chapter 3

Literature Review: Part B

Hydropower Technologies

Part A of the literature review provided a background of hydropower, and concluded that a new viable technology needs to be developed for exploiting hydropower potential with very low head differences. This second part of the literature review, Part B, describes all of the relevant low head technologies already in existence. This is conducted in three sections; the first two covering the long established technologies of waterwheels and turbines, and the third covering contemporary technologies developed within the last few decades. Attention should be payed to the waterwheel terminology, Section 3.1.2, as it is used throughout the document.

The review is only from a technical perspective, indicating the heads, flow rates and efficiencies at which the machines operate. Most importantly, the *operational principles* proposed by the manufacturers of each machine are indicated. These describe the fundamental principles behind how each machine exploits the hydraulic power of the water, converting it to mechanical power. This chapter has no conclusions, but leads directly to a discussion on the operational principles observed.

3.1 Established Technologies: Waterwheels

3.1.1 History

Waterwheels were first employed to extract energy from flowing water over 2,000 years ago and have been analysed by many renowned engineers, scientists and mathematicians including Da Vinci, Bernoulli and Smeaton (Smith 1976). This attention began at a time when an understanding of hydraulics and even energy and its conversion did not exist. To demonstrate this, in 1704 Antoine Parent published his theory on jets which limited the hydraulic efficiency of all waterwheels to just 14.8%. His analysis was mathematically incorrect and not applicable to all types of waterwheel. The result was that a form of waterwheel called the 'undershot' waterwheel was incorrectly favoured over the 'overshot' waterwheel until 1756, when John Smeaton published experimental data which conclusively proved the opposite (Lockett 2001, Smith 1976). By the time the theories and manufacturing methods of the accepted waterwheel forms neared perfection, the most developed waterwheel technology took a significant leap into the realm of turbines and waterwheel development effectively ceased (Denny 2003).

To indicate the number of sites within Europe which previously used waterwheels, by 1820 France had 60,000 installations (Denny 2003), by 1850 England had 25-30,000, and as late as 1925 Germany had 33,500 (Müller and Kauppert 2004, quoting McGuigan 1978, and Müller 1939). The use of waterwheels began to decline with the introduction of the steam engine as a convenient and larger power source, and effectively ceased with the introduction of electric motors during the 1940s and 1950s.

The design and use of waterwheels as efficient and cost effective energy converters has received little written attention during the last century, and the inclusion of waterwheel design has been dropped by all modern mainstream hydraulics text books. During the last few decades however, a small amount of research, along with restoration and renewable-power projects has seen a small revival in waterwheel technology and use. There are now several companies within the USA and Germany which specialise in the manufacture of waterwheels. Reports such as Bacon (2004) and renewable energy books such as Giescke and Monsonyi (1998) now list waterwheels as an economic option for low head sites as they have been estimated to cost between 33% and 66% of equivalent turbines (Müller and Kauppert 2002).

3.1.2 Terminology

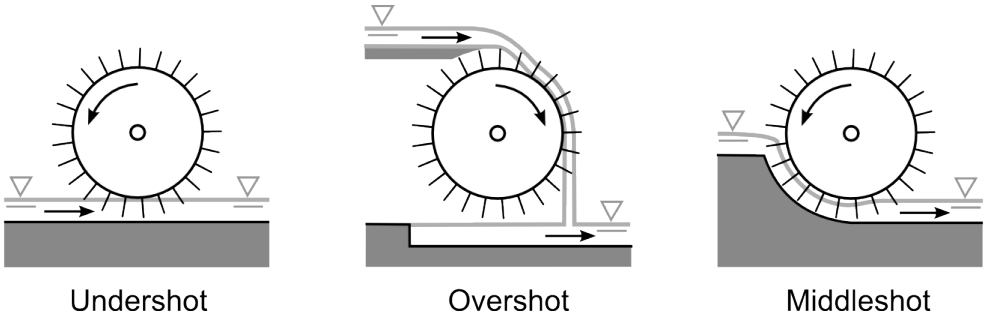

Figure 3.1: Waterwheel classification

Three forms of waterwheel are commonly defined along with *simple* explanations of their working principles. These are the *undershot*, *overshot* and *middleshot* (or *breast-shot*) waterwheels, which are depicted in Figure 3.1. The classification depends on the water entry mechanism as follows (Lal 1967):

Undershot: The water enters beneath the wheel, which is predominantly driven by impulse, resulting from a difference between the lower peripheral velocity of the wheel and the faster velocity of the water.

Overshot: The water enters from above the wheel, which rotates in the opposite direction to undershot and middleshot waterwheels. These are predominantly driven by the water's potential, resulting from gravity.

Middleshot: The water enters around the same height as the axle. These require a curved section of channel bed called a *breast* or *shroud*, and extract energy from the water through impulse and potential, lowering the water through a vertical distance under the influence of gravity.

The common explanations above are overly simple, as in practice a multitude of designs and approaches exist within each of the three classifications. These variations are discussed further in the following three subsections, following a brief introduction to the terminology used to describe the components and operating characteristics of waterwheels. The final subsection provides an overview of the head differences and flow rates which these waterwheels were suitable for exploiting.

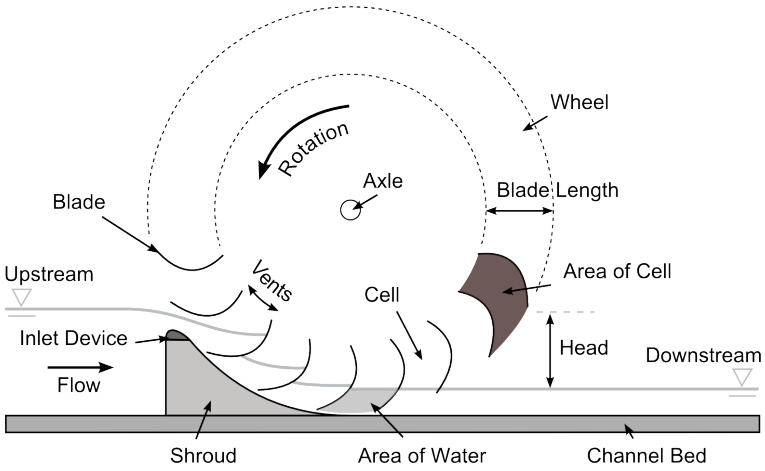

Figure 3.2: Generic waterwheel terminology

Figure 3.2 depicts a generic middleshot waterwheel to introduce the terminology used in this document to describe the components of waterwheels. This terminology is also common to undershot and overshot waterwheels. Water flows from the upstream to the downstream. It sometimes enters the wheel over an *inlet device* of which there are several forms, which provide the water with a suitable direction and velocity to enter the *cells*. These are the volumes between the *blades* of the wheel into which water flows. Some forms of waterwheel included *vents* or internal gaps between the blades, allowing air to ventilate the cells as they filled with, or drained of water. The wheel is partially surrounded by a curved section of channel bed called a *shroud*. The flow rate, Q, is a function of the frequency of rotation of the wheel, f, the volume of the cells, V, and the filling ratio, ε, as shown by Equation 3.1.

$$Q = V\,\varepsilon\,f \tag{3.1}$$

The volume of the cells is determined by the diameter of the wheel, the *blade length* and the width of the wheel. The *filling ratio* describes the proportion of the volume of the cells which is filled with water during rotation. It is the same as the ratio of the cross-sectional areas of the cell to the area of water as shown in Figure 3.2. The *flow capacity* or Q_{max} of a waterwheel describes the flow rate at which the maximum power, P_{max} is generated. In general, the greater the blade length, rotational speed and filling ratio, the greater the flow capacity of a waterwheel per unit width.

3.1.3 Undershot Waterwheels

Figure 3.3 includes original drawings demonstrating alternative designs of undershot waterwheels. In all cases the flow is from left to right and the waterwheels rotate anti-clockwise.

Early undershot waterwheel

The 'Early undershot waterwheel' in Figure 3.3 shows the original and most simplistic form of undershot waterwheel. Short blades protrude radially from the wheel into the flowing water. The water has a velocity greater than the peripheral velocity of the wheel, and imparts an impulse on the wheel, leaving with the same velocity as that of the blades. This process was described as a "shock and disturbance" by Bresse (1876, p.19) which described the accompanying turbulence generated in the water. As flow continuity applies, the relatively slow velocity downstream flow has a greater depth than the upstream. Recent analysis by Müller et al. (2007) has indentified that these waterwheels operated in shallow, supercritical flows generated within artifical channels. This means that the presence of the waterwheel does not have an impact on the depth of the upstream flow.

It is noteworthy that machines such as these, with filling ratios of less than one, do not have a fixed relationship between the flow rate and rotational speed. The rotational speed is determined by the load applied to the wheel, and undershot waterwheels which exploit impulse require good speed control so that they can be run with optimum efficiency. Smeaton conducted tests on such machines and found that the optimum ratio of blade to water velocity was 0.43, although theory would suggest that this value is 0.5 with the maximum efficiency being 50%. In reality efficiencies were generally measured to be between 25% and 35% (Bresse 1876, Meyers 1908, Fitz and Merriman 2004). These machines extract kinetic energy from the water and are inherently limited by their flat blades and by the channel design, which limits the reduction in horizontal water velocity that can be achieved whilst clearing the water from the wheel.

As discussed in the Section 3.1.1, prior to Smeaton's conclusive experimental testing, many engineers and millwrights believed that undershot waterwheels driven by impulse were more efficient than other forms driven partially or fully by potential. The result was that many sites with heads suitable for middleshot or overshot waterwheels were instead exploited with undershot waterwheels in conjunction with undershot weirs, which converted the potential energy of the water into kinetic energy. An example of such an installation is given in Figure 3.3. Although it is now accepted that these machines are less efficient than their middleshot and overshot coun-

terparts, it is not recorded whether such an arrangement could process a larger flow rate. This could potentially have been the case as the velocity of water generated beneath an undershot weir is greater than that over an overshot weir, as it is driven by a greater pressure head.

Later undershot waterwheel

The 'Later undershot waterwheel' in Figure 3.3 shows that slightly curved blades were adopted. These converted some of the kinetic energy into potential energy within the wheel as the water would run up the blade slightly upon impact, gaining potential. This resulted in less turbulence and a slightly improved efficiency. The curved blades would also lift from the downstream water with greater ease than flat blades. Unlike the 'Early undershot waterwheel', these operated in subcritical water flows, meaning the operation of the wheel could directly influence the depth of the upstream water. The low flow velocities and flow rates exploited using this type of undershot waterwheel meant that the power output of such installations was relatively low, when compared to the undershot waterwheels which operated in supercritical flows (Müller et al. 2007).

Of great significance is that the source of the picture (Brockhaus 1903) describes how the wheel was also partially driven by *pressure* and that this effect was most useful at low flow rates. This observation was also made by Müller (1939, p.162), who concluded an example of a 'city work canal' installation with an interesting observation. He describes how at very low flow rates, such an undershot waterwheel can be operated at a significantly reduced speed of rotation so as to not operate in impulse conditions. Instead it would work 'as if by an overshot inlet' [indicating a raised upstream water level], and operate with an efficiency slightly greater than expected for a traditional impulse operated undershot waterwheel. Indeed it is visible in Figure 3.3 that the first blade entering the water has a level change across it, and that the depth of water within the wheel is greater than in the downstream following the last submerged blade. The generation of this level drop is also resulting from a small shroud to the left of the wheel. This undershot waterwheel combines kinetic energy extraction as the blades enter the water, along with being partially driven by a pressure difference caused by dissimilar water depths across the blades on exit. Unfortunately neither source conducts theoretical analysis of the role played by pressure, nor provide data.

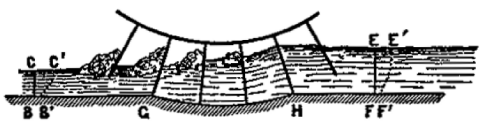

Early undershot waterwheel [1]

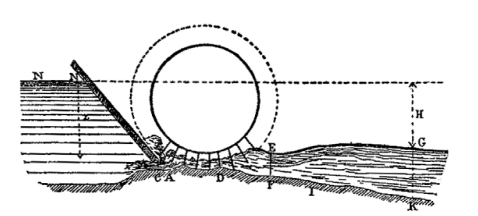

Early undershot waterwheel with undershot weir [1]

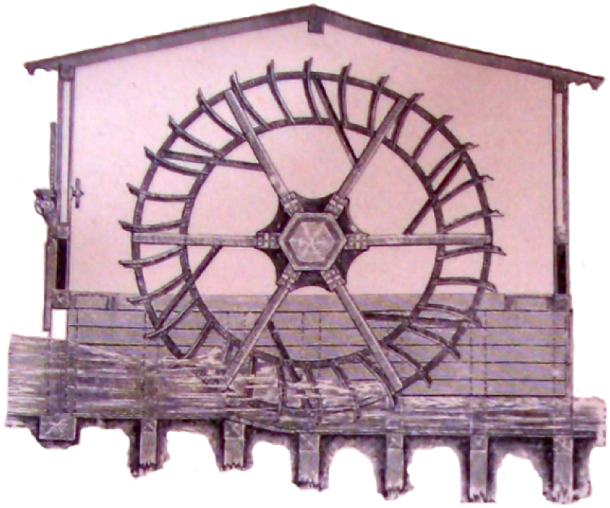

Later undershot waterwheel [2]

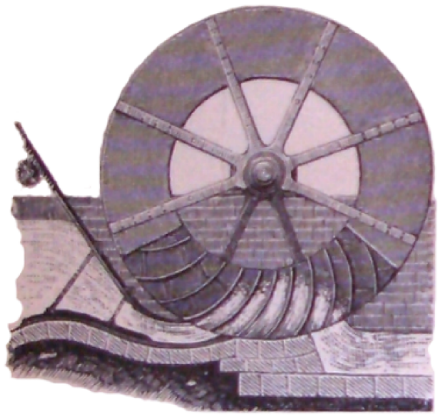

Poncelet waterwheel [2]

1: Bresse 1849, 2: Brockhaus 1903

Figure 3.3: Undershot waterwheels

Poncelet undershot waterwheel

The most developed form of undershot waterwheel was the *Poncelet* waterwheel. Several renowned engineers including Bossut, Smeaton and Carnot observed the original undershot waterwheel's faults and concluded that the water had to enter the wheel "without shock or percussion", and "exit without velocity" (Smith 1976). In simpler terms this means that the water must not impact on the blades as this wastes energy. Instead the water should ideally run onto the blades so that it is the water's weight alone that acts on the blades. The second point, although difficult to achieve, intends that the water should not decelerate after the blades providing a retarding force, or accelerate away from them.

Referring to Figure 3.3, Poncelet achieved this using a specially designed channel bed, shroud and curved blades. Initially, the potential energy of the upstream was converted to kinetic energy using an undershot weir. The water then ran up the blades, reverting to potential energy whilst effectively leaning on one side of the near-vertical blades. It was this 'dynamic pressure' acting across the blades which drove the wheel (Fitz and Merriman 2004, Encyclopaedia Brittanica 1911). The channel bed is also designed so the the water would then fall out of the cells with ease and reduced horizontal velocity; lower than in the upstream. It is often claimed this wheel had an efficiency of up to between 60% and 70% (Encyclopaedia Brittanica 1911, Meyers 1908, Bresse 1876), unfortunately no additional data or examples could be found.

3.1.4 Overshot Waterwheels

Overshot waterwheels such as those depicted in Figure 3.4 exploit potential energy, lowering the water within cells from the upstream to the downstream. The blades of the cells are designed so that their curvature initially matches that of the water as it falls from the upstream channel into the wheel. The fall that occurs as the water drops into the cells is one source of loss, constituting unexploited head. The most efficient overshot waterwheels minimise this loss by minimising the radial depth of the cells. It has also been found that the kinetic energy of the water generated by the entry fall can be partially recovered by controlling the load on the wheel, such that the peripheral velocity is roughly half the velocity of the water stream as it enters the cells. The second and most significant source of loss is the unexploited head resulting as the water spills from the cells before the downstream is reached. This occurs as the open cells rotate as they retreat beneath the wheel, and is related to the filling ratio and the design of the blades. In practice, overshot waterwheels were designed to have filling ratios between 0.3 and 0.5 (Bach 1899), and achieved efficiencies between 65% and 89% (Lal 1967, Müller and Kauppert 2004).

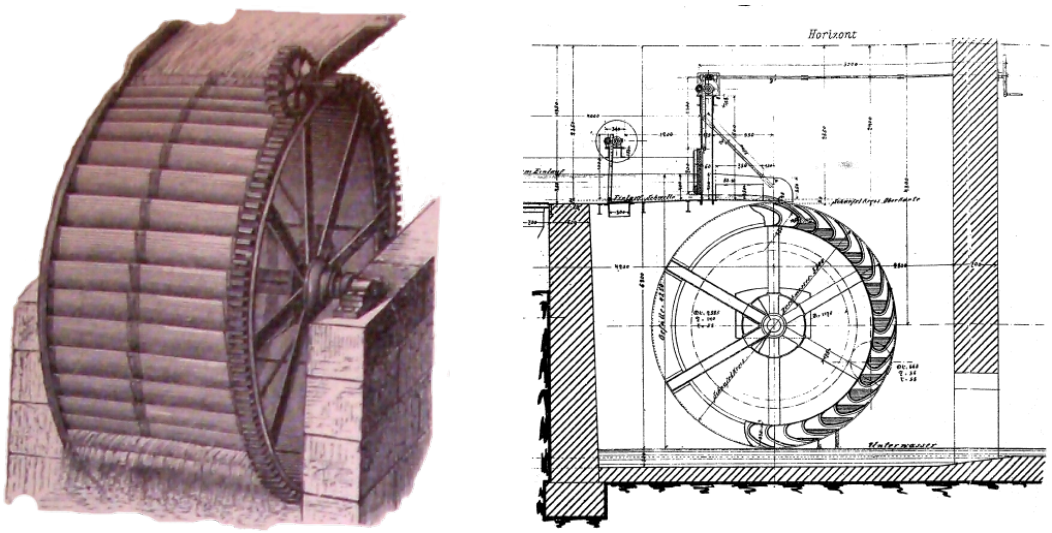

Figure 3.4: Overshot waterwheels: a) Brockhaus 1903, b) Müller 1899b

3.1.5 Middleshot Waterwheels

The common feature of all middleshot waterwheels is the curved section of channel bed called the shroud, which partially extends around them towards the upstream. The intended purpose of this structure is that the water is lowered down within the cells of the wheel through a vertical distance under the influence of gravity, allowing the potential energy of the water to be exploited. The accuracy of this analysis is discussed further in Section 4.1.2.

Figure 3.6 depicts the commonly built middleshot waterwheels, which operated with partially filled cells. These waterwheels with filling ratios less than one do not have a fixed relationship between the flow rate and the rotational speed. This property is exploited by modern middleshot waterwheel installations, where the load of the grid connected generators is varied with the hydraulic power being exploited, such that the rotational speed remains constant. The filling ratio therefore becomes a function of the flow rate.

Middleshot waterwheels appear to have come in two forms: from those with large cells and high filling ratios but low rotational speeds, to those with smaller cells and lower filling ratios but higher rotational speeds. For both forms, an important consideration for efficiency was the relationship between the inflowing water and the blades. Ideally the water would enter the cells without impact, instead running onto the blades as demonstrated by Figure 3.5. This would depend on the angle and velocity of the water and the blades, and could be manipulated with the use of inlet devices such as crested overshot weirs and guide vanes.

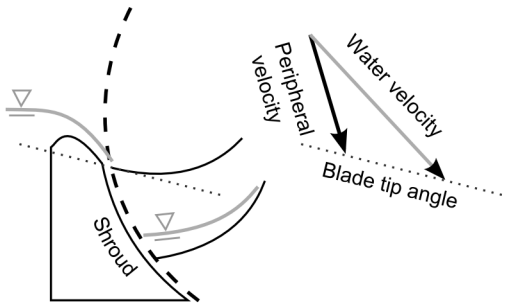

Figure 3.5: Inlet vector for middleshot waterwheel with overshot weir inlet

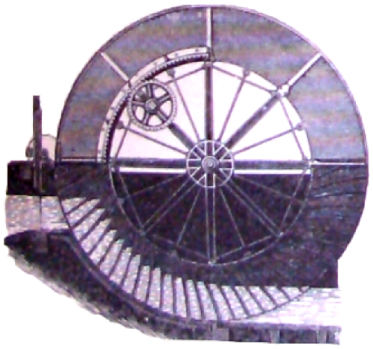

Sagebien waterwheel [1]

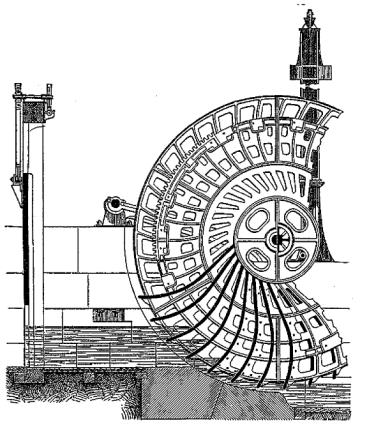

Zuppinger waterwheel [2]

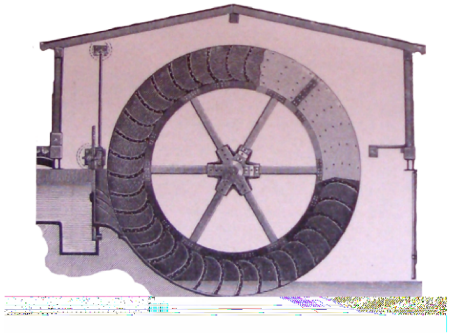

Middleshot waterheel
with Coulisse inlet [1]

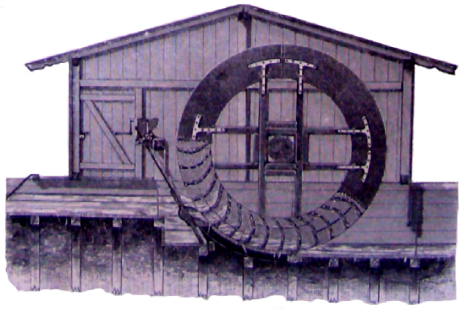

Middleshot waterwheel
with overshot weir inlet [1]

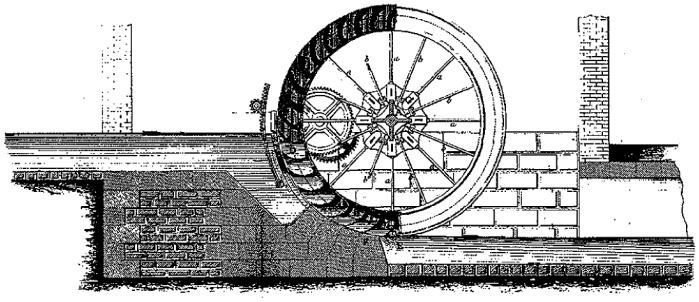

Middleshot waterwheel to Fairbairn's design [3]

1: Brockhaus 1903, 2: Meyers 1908, 3: Fairbairn 1849

Figure 3.6: Middleshot waterwheels

For slowly rotating wheels such as the *Sagebien* waterwheel, which rotated at around 2rpm (Sagebien 2007), the water could enter the wheel effectively horizontal as the blade was angled downwards to achieve smooth entry. The difficulty for wheels with large flat blades such as the *Sagebien* waterwheel, is not raising or pushing excessive water at the downstream as they exit. This would especially be a problem if the downstream water level was raised in high flow conditions. The solution came with wheels such as the *Zuppinger* middleshot waterwheel, which had curved tips to the blades which would exit the water more vertically and cleanly. These machines had efficiencies up to 77% (Müller and Kauppert 2004). For the faster revving machines (up to 10 rpm) with very curved blades such as those in the centre of Figure 3.6, either a *Coulisse* inlet (angled guide vanes) or an overshot weir would be required to give the water a sufficiently steep angle of entry to run onto the blades cleanly. The second purpose of the curved blades was that during entry over the inlet device, the water would drop a vertical distance and gain kinetic energy. This kinetic energy could be partially recovered as the water initially ran up the blades within the wheel regaining potential energy as shown in Figure 3.5, centre right. These waterwheels had efficiencies as high as 85% (Müller and Wolter 2004). In some cases the curved blades served simply to regain the kinetic energy gained on entry and were not required for clean exit from the downstream water. Examples include the middleshot waterwheels built by Fairbairn, which were constructed with the base of the wheel raised above the downstream water level. The water would simply fall out of the cells, sacrificing some of the head in favour of good performance in high downstream water level conditions.

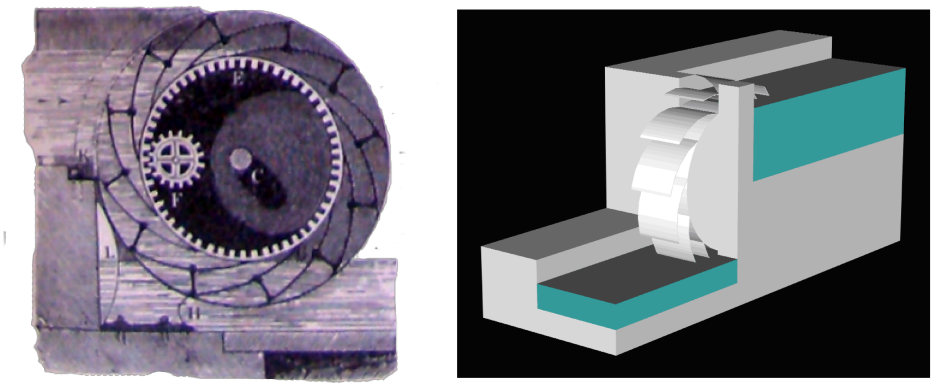

Figure 3.7: *Zuppingerrad* waterwheel: a) Brockhaus 1903 b) impression

There exists one example in the literature of a waterwheel where the filling ratio is one; i.e. the cells fill entirely with water. Although the water enters significantly above axle height, it seems appropriate to classify it as a middleshot waterwheel and not an overshot waterwheel as the water enters laterally and exits underneath. Figure 3.7a shows the only known depiction of the *Zuppingerrad* found in a German encyclopaedia from 1903 (Brockhaus 1903). A brief description within the text indicates that the upstream channel is wider than the wheel. The cells have open sides allowing the water to enter and air to ventilate from the sides, as well as the front of the wheel. This allows for the unusually steep blade angle, which in connection with a downstream channel that is also wider than the wheel, lowers the water completely down to the lowest level and lifts out of the water almost vertically. An impression of this is shown in Figure 3.7b. No indication of size or efficiency is given. As the original shows the headrace level well above axle height, this would indicate that such a machine could operate from very low heads all the way up to overshot waterwheel levels, possibly 1-10m.

It is interesting to note that the *Zuppingerrad* was presented in Brockhaus along with other well known designs; specifically overshot, undershot, *Poncelet*, *Sagebien*, and two forms of middleshot waterwheel. To be included in such a list would suggest that the *Zuppingerrad* was built, and an operational success. However, no reference is made to an actual installation and none are known to be in existence. Also interesting is that this is the earliest reference to the 'dam effect', whereby a central hub or cylinder retains a head difference. With a filling ratio of one, the flow rate would be directly related to the rotational speed of the wheel.

3.1.6 Waterwheel Overview

Waterwheel type	Head, m	Flow, m^3/s per m width	Power, kW per m width (deduced)
Overshot	2.5 - 10	0.1 - 0.2	2.0 - 18.0
Middleshot	1.5 - 4.0	0.35 - 0.65	4.0 - 20.0
Undershot	0.5 - 2.5	0.5 - 1.2	0.7 - 5.0

Table 3.1: Waterwheel operational ranges (Müller and Kauppert 2004, Müller 1939)

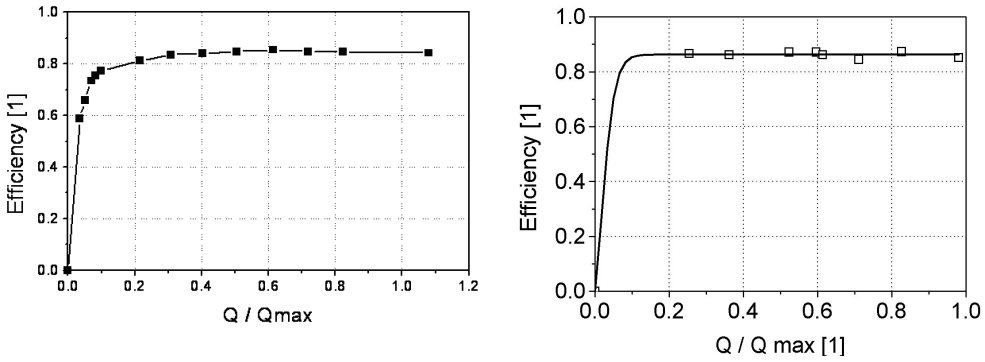

Figure 3.8: Waterwheel efficiency profiles: a) Overshot (Müller and Kauppert 2004), b) Middleshot (Müller and Wolter 2004)

Relative to one another, undershot and middleshot waterwheels can be thought of as high volume but low head, and overshot wheels as high head but low volume. Great difficulty can be experienced in comparing the flow capacities of these machines as most sources fail to consider the width of the wheels to which they refer. There are examples of waterwheels as wide as 22ft or 7m (Fairbairn 1849). Only two sources attempt to provide an overview of the heads and flow capacities of the traditional waterwheels with the flow given *per metre width of wheel* (Müller 1939, Müller and Kauppert 2004). The values are given in Table 3.1. It should be noted that Müller and Kauppert's head values for undershot wheels, as provided, are quite large when compared to other sources such as Meyers (1908) which gives the range 0.2 - 0.7m. This is because because the former included the *Zuppinger* waterwheel as an undershot waterwheel, whereas within this document it is considered to be a middleshot waterwheel, although borderline examples do exist. Also, at a time when undershot wheels were thought to be the most efficient form of waterwheel, undershot weirs were used to convert larger heads into fast streams to drive undershot waterwheels.

Whilst the peak efficiency has been measured or estimated for most of the forms of waterwheel, the efficiency profile over a range of flows has only been determined for some of the later overshot and midleshot waterwheels. Examples of these are provided in 3.8, and demonstrate how such waterwheels had a very flat efficiency profile, meaning that they operated with good efficiency over a wide range of flow rates. Importantly this characteristic could be achieved using a fixed blade and inlet geometry. This is in contrast to modern turbines which require active control mechanisms to adjust physical components, such as guide vanes, in order to maintain a good efficiency over a range of flow rates.

The traditional design waterwheel most commonly built today is the *Zuppinger* middleshot waterwheel, built in conjunction with an overshot-weir type inlet device such as that shown in Figure 3.6. Müller (1939), states that the upper flow capacity of such waterwheels is 0.95 m^3/s per metre width. He also gives an example of an especially large and slow revving *Zuppinger* waterwheel where the flow entered horizontally without an inlet device, with a maximum flow capacity of 1.2 m^3/s per metre width. This is considered to be the maximum flow capacity for a traditional type waterwheel. It is interesting to note the existence of the *Zuppingerrad* with the unusual side filling and ventilation, and the filling ratio of one. Although the literature does not indicate the performance of this machine, it may represent the direction that waterwheel technology would have taken had attention not been entirely diverted towards turbine development.

3.2 Established Technologies: Turbines

Turbine design and utilisation superseded the traditional waterwheel, being relatively compact, efficient and having the capability to process large flow rates and generate large power outputs. They are relatively complex, highly developed, and often require extensive civil engineering works. Whilst turbines do exist that can operate at very low head differences, the power outputs are limited and the economics of such installations become unattractive, as discussed in Chapter 2. Referring to Figure 2.2, page 23, the Crossflow and Axial/Kaplan hydropower machines are the only turbines suitable for exploiting very low head differences.

3.2.1 Crossflow Turbines

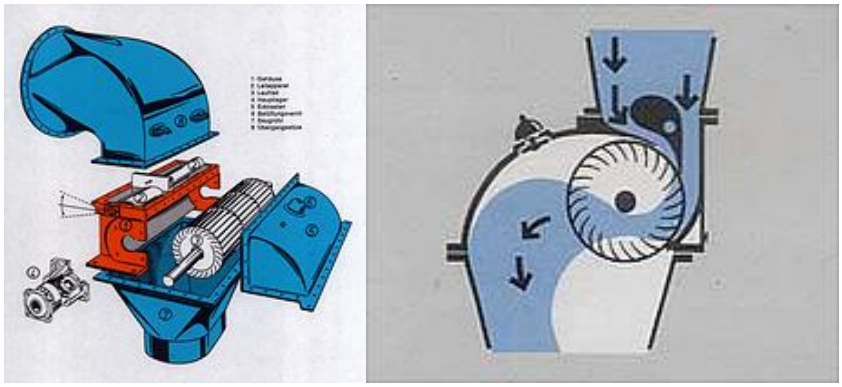

Figure 3.9: Crossflow turbine: a) expanded view b) cross-section (Ossberger 2008)

The *Crossflow* turbine is a form of *impulse* turbine, and was first patented in 1903. These operate by converting potential energy delivered via a high pressure supply pipe, to kinetic energy. This occurs as the water enters the turbine, which is air filled at atmospheric pressure, via a constriction thus accelerating the flow. Referring to Figure 3.9, the inflowing water is guided via an adjustable guide vane against a cylindrical rotor. The water is deflected by the vanes of the rotor through the rotor itself, acting on the vanes a second time on exit. The deflection process is one of momentum exchange through impulse. The leading manufacturer of Crossflow turbines is Ossberger from Germany. The manufacturer claims hydraulic efficiencies up to 86%, and that this efficiency can be extended over a wide range of flow rates by dividing the rotor into multiple cells which can be selected on the basis of flow rate, as demonstrated by

Figure 3.10 a. The Crossflow turbine is suitable for head differences between 2m and 200m. For very low head differences below 5m, the Crossflow turbine has a flow capacity of $10m^3/s$ per unit (Ossberger 2008).

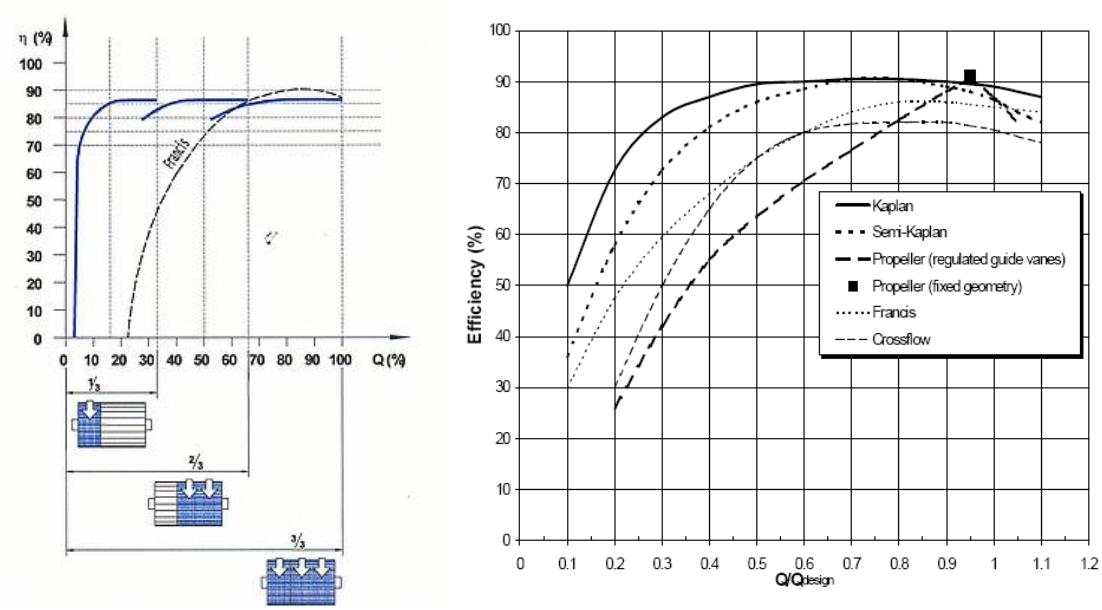

Figure 3.10: Turbine efficiency curves: a) Crossflow turbine (Ossberger 2008) b) Kaplan turbine efficiency curves (Bacon 2004)

3.2.2 Kaplan Turbines

The *Kaplan* turbine is form of *reaction* turbine, and was developed around 1913. It is a propeller type turbine, an example of which is shown in Figure 3.11. The turbine is housed within a fully submersed channel, of which many forms exist ranging from vertical to horizontal installations as shown in Figure 3.12. As the water flows past the propeller, a pressure difference is generated across the blades applying a torque. Many Kaplan turbines include variable pitch blades and guide vanes prior to the propeller to give optimum efficiency over a range of flow rates. Hydraulic efficiencies can reach 90% as shown in Figure 3.10 b. Besides the turbine itself, an essential component of a Kaplan installation is the *draft tube*, which is a specially designed channel exiting the turbine. This extensive structure is required to maintain a fully submersed turbine, delivering the water into the downstream without air entrapment. It is also required to recover some of the kinetic energy generated as the water is accelerated into the installation. This is achieved by decelerating the flow in a controlled manner without separation from the channel walls, resulting in a beneficial back pressure which acts upon the turbine (Giescke and Monsonyi

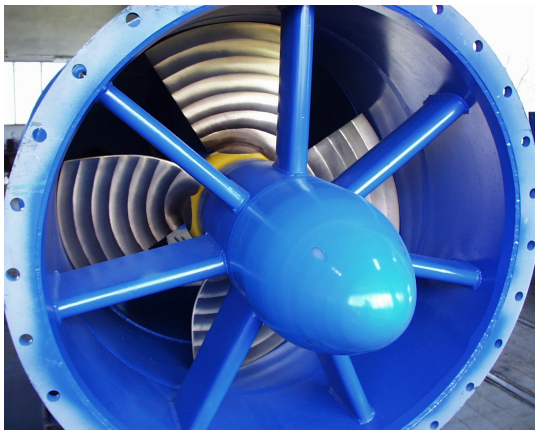

Figure 3.11: Kaplan propeller (Hydrolink 2008)

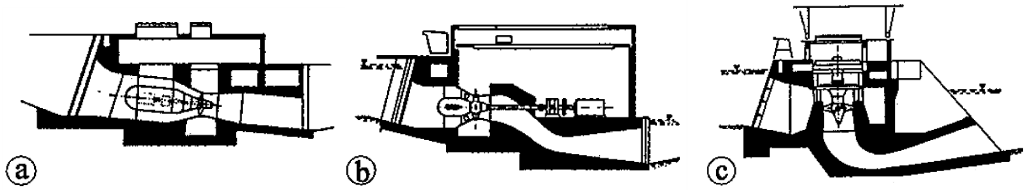

Figure 3.12: Kaplan turbine installations (Giescke and Monsonyi 1998, p.445)

1998, p.444).

In the field of Small Hydropower, several manufacturers offer Kaplan turbines which are claimed to be suitable for head differences as low as 1.5m (Hydrolink 2008), and even 1.0m, with flow rates between 0.25 and 35 m^3/s (Ossberger 2008). These suppliers do not provide efficiency curves or case studies of examples exploiting such low head differences. Whilst they may be feasible, it is not known if such installations are actually realised due to economic considerations. For larger flows which are present at low head sites, the power of the turbine increases with the square of the diameter of the propeller. The weight and size of the required infrastructure however increases with the cube of the diameter of the runner, and this is why low head machines with larger flows have a higher specific cost than large head, smaller flow installations (Bacon 2004). The commonly quoted lower limit for kaplan installations is over 2.0m (Giescke and Monsonyi 1998), and investigations into low head technologies such as Krompholz (2008) do not provide case studies of Kaplan turbine installations below 2.0m head.

3.3 Contemporary Very Low Head Technologies

This section introduces the contemporary very low head hydropower technologies developed within the last few decades. Difficulties in conducting this review arise as the vast majority of sources of information are commercial, only publishing favourable or optimistic data and predictions. Whilst magazine articles and internet blogs discussing most of the technologies exist, they do not present independently verified data.

Many novel hydropower machines exist ranging from patented ideas, operational prototypes, and in the case of just one machine at this time, a commercially established product. What is presented is a selection of the concepts which are considered to potentially be technically and economicially viable, covering most of the approaches to exploiting very low head hydropower. Head, flow and efficiency values provided by the manufacturers are quoted but not verified. Claims regarding cost or environmental credentials are omitted. This review does not include large free stream kinetic energy converters designed for large scale tidal energy conversion, or ideas that are considered to be technically or economically unviable. Wiemann (2007), provides further reading on such machines.

Where manufacturers propose an operating principle for their machine, this is highlighted in italics. All of the operational principles mentioned are then discussed further in Chapter 4.

3.3.1 *A.U.R. Water Engine*

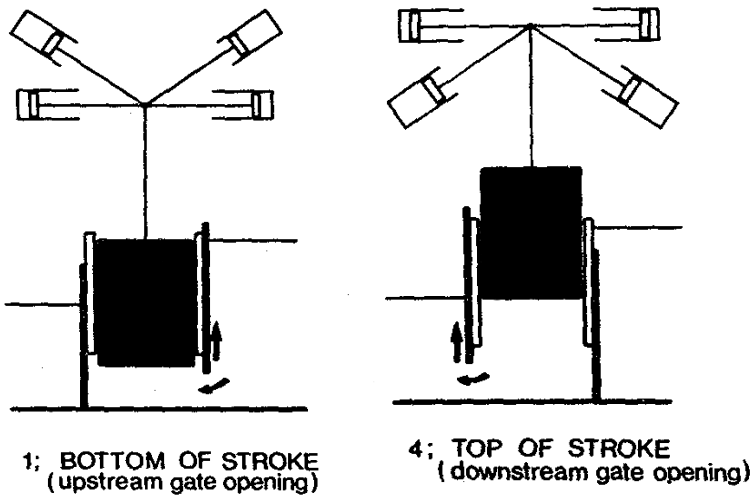

Figure 3.13: *A.U.R. Water Engine* (Wilson 1984)

The *A.U.R. Water Engine* (named after the inventor, Alister Ure Reid), was patented in 1975. Following model testing at the University of Salford, its design was published along with the *Salford Transverse Oscillator*, which follows (Wilson 1984). Referring to Figure 3.13, the basic principle which drove the machine was *buoyancy*; the upward lift on submerged volumes resulting from hydrostatic pressure. A pair of gates would alternately connect a central chamber to the deeper upstream water and the shallower downstream water. Within the chamber was a float, which was connected to hydraulic rams which formed the power take-off. On the upward motion, the power available would reduce with the stroke as the buoyancy force decreased with increased float height. On the downward stroke, the force would be provided by the weight of the float itself. Although buoyancy was identified as the driving force of the machine, no theoretical analysis has been published.

Four model tests were conducted and generalised performance curves produced. Deduced by the author from the scaled estimates provided for a full scale installation, the hydraulic efficiency of such a machine was in the 50% - 60% region. Despite 10kW to 200kW installations being envisaged, no evidence can be found of any commercial *A.U.R Water Engine* installations.

3.3.2 *Salford Transverse Oscillator*

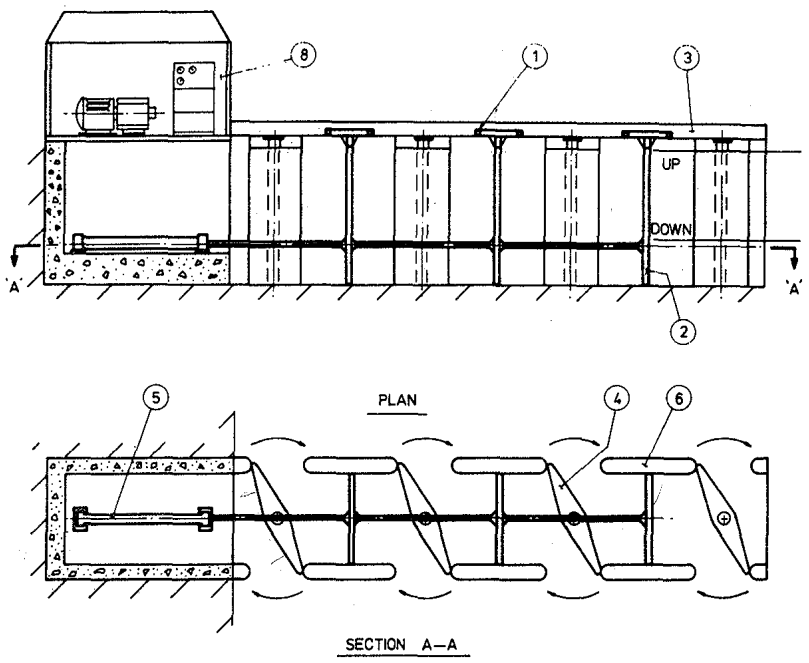

Figure 3.14: *Salford Transverse Oscillator* (Wilson 1984)

The *Salford Transverse Oscillator* is a positive displacement type machine designed for installation in river and tidal scenarios. It features in a paper by Wilson (1984) along with the *A.U.R. Water Engine*. Referring to Figure 3.14, the concept consisted of a parallel wall barrage which generated a *pressure differential*. This pressure differential was alternately applied to either side of 'paddles' shown as (2), by controlling multiple gates shown as (4). By switching the gates at the end of each paddle stroke, the paddles would oscillate in a transverse direction to the flow. The paddles would be attached to a hydraulic piston power take-off, (5). Although the pressure differential was credited with driving the machine, no theoretical analysis has been published.

The paper includes several case studies and cost estimates of the application of *Salford Transverse Oscillators* in different environments. However, it is not clear whether model testing was conducted, and although generalised performance curves were provided, no actual data was published from which the efficiency of such machines could be determined. Despite stated intentions to commercialise the machine, no evidence can be found that any full scale *Salford Transverse Ocillators* were installed.

3.3.3 *Sundermann Turbine*

The *Sundermann Turbine* is an Australian invention consisting of multiple vertical blades which which extend from the channel bed to the water surface and rotate about a common axis (Sundermann 2008). Figure 3.15 depicts the only prototype to date; the machine represents a constriction in the flow generating a head difference across it. The blades are controlled by a mechanism such that they present their full face to the flowing water on the power stroke, whilst being oriented sideways on the return stroke as depicted in Figure 3.16. The inventor provides no explanation for its operation except that it "extracts energy from the water *flow*". No theoretical analysis or data regarding flow rate, head differences or efficiencies are given.

Figure 3.15: *Sundermann Turbine* prototype (Sundermann 2008)

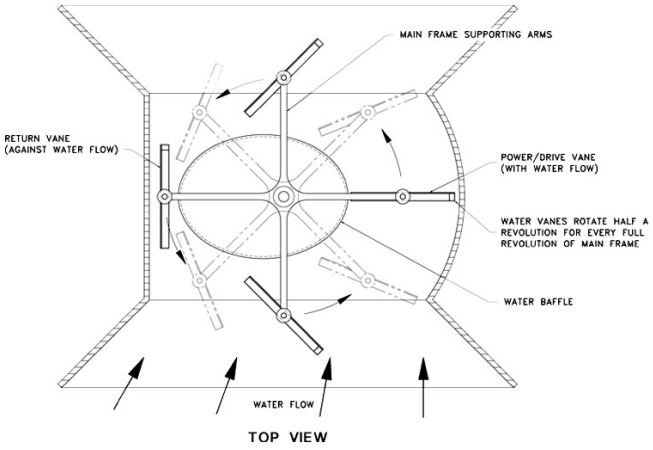

Figure 3.16: *Sundermann Turbine* plan view (Sundermann 2008)

3.3.4 *Archimedes Screw*

The *Archimedes Screw* is an ancient machine for pumping water from a lower level to a higher one. It is traditionally credited to Archimedes who lived between 287 B.C. and 212 B.C. (Rorres 2000). In recent years, the *Archimedes Screw* has been installed as a hydropower machine, instead lowering the water and generating power. This is depicted in Figure 3.17, consisting of a rotating screw supported within a trough by bearings at each end, with a gearbox and generator situated in the control house. The water is lowered within cells which form between the blades and the trough.

Analysis of the geometry and parameters including blade pitch have been conducted for the *Archimedes Screw*. This is mostly from the perspective of its utilisation as a pump, and its 'performance' is based upon the volume of water lifted per rotation (Rorres 2000). Limited investigation into the efficiency of the *Archimedes Screw* as a pump has been conducted by initially assuming 100% efficiency from which losses, including leakage, sources of friction and turbulence are deducted (Nagel and Radlik 1988). The only work investigating the *Archimedes Screw* operating as a hydropower machine is a recent Master's dissertation by Harkin (2007). This work was conducted to investigate the relationship between efficiency and angle of inclination. It was conducted using scale model testing, and secondly a mathematical analysis was conducted, resulting in the power output equation given in Appendix A. Whilst this equation is lengthy, and not instantly accessible in its significance, it is important to note that it has been derived based on an analysis of hydrostatic pressure acting upon the *Archimedes Screw*. The equation has been derived as an initial attempt to estimate the power output of *Archimedes Screws*, however the author concludes that whilst the results are of the correct magnitude, the equation requires further development.

To date, the *Archimedes Screw* is becoming the most commercially successful of the contemporary low head hydropower machines. Dozens of units have been installed in recent times, the main manufacturer being Ritz-Atro, a German manufacturer from which the following information is sourced (Atro 2006). Referring to Figure 3.18, their *Archimedes Screws* are claimed to be suitable for flow rates up to 5.5 m^3/s per unit, and heads between 1m and 10m. Efficiencies are claimed to be up to 90% for the largest diameter machines. Similar to traditional waterwheels, the filling ratio of the cells is less than one. The machines on the market are currently run at constant speed, the filling ratio increasing with flow rate. The manufacturer claims that the *Archimedes Screw* is driven by the *potential* of the water.

Figure 3.17: *Archimedes Screw* installation (Atro 2006)

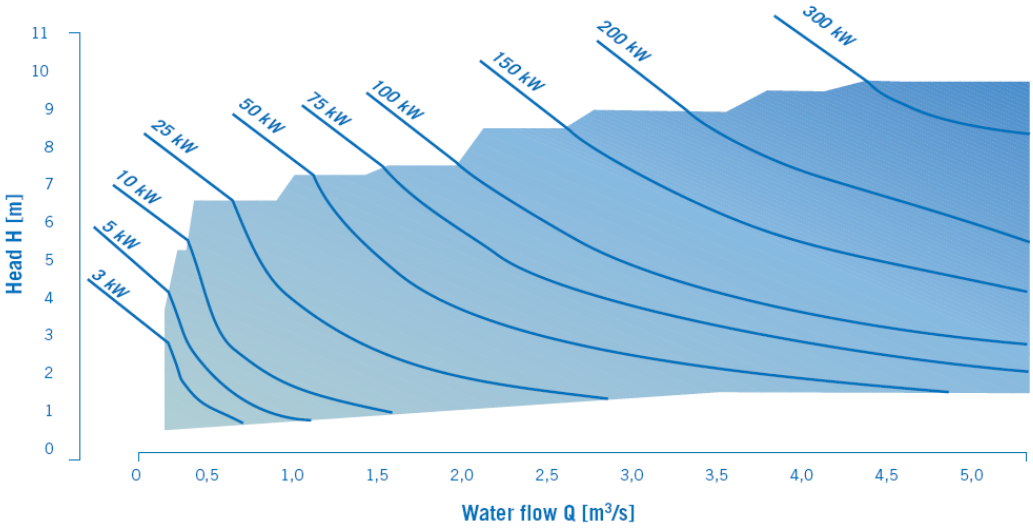

Figure 3.18: *Archimedes Screw* operating range (Atro 2006)

3.3.5 *Aqualienne*

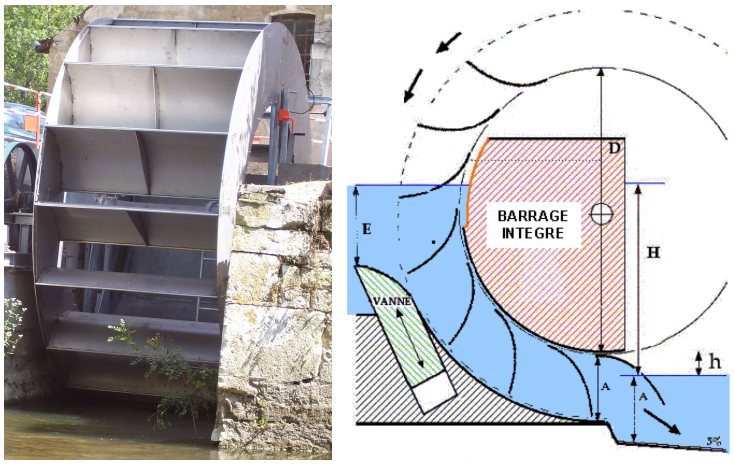

Figure 3.19: *Aqualienne* (Fonfrede 2008a)

The *Aqualienne* is the design of French Engineer Michael Fonfrede, and was patented in 2004 (Fonfrede 2004). It is a development from his studies on the *Sagebien* waterwheel. This hydropower machine utilises a shroud on the channel bed like many middleshot waterwheels, lowering the water from the upstream into the downstream in cells which form between the blades of the wheel and the shroud itself. What is novel is the manner in which the cells manage to fill and ventilate with relative ease. Central to the design of the *Aqualienne* is a stationary internal shroud within the wheel itself. This internal shroud is only present between the upstream and downstream water levels, forming the inside of the cells, closing the large internal gaps between the blades. The internal gaps are not bridged by the internal shroud above the upstream water level, or beyond the point where the blades lift from the downstream. In these regions the gaps are open allowing air to freely flow into and out of the cells. This design feature allows the *Aqualienne* to have a filling ratio of one like the *Zuppingerrad*, page 48, fully utilising the volume of the cells and maximising the flow capacity.

The inventor has completed two *Aqualienne* installations, and claims the peak hydraulic efficiency to be in the region of 80%. He claims that this machine could be used to exploit head differences between 1m and 5m, and flow rates up to 50 m^3/s (Fonfrede 2008a) . This upper flow rate appears optimistic when it is noted however that the larger of the two machines constructed to date has a width of 5.5m and a flow capacity of $10m^3/s$, indicating a flow capacity per metre width of 1.8 m^3/s (Fonfrede 2008b). This would suggest a 30m wide waterwheel, being the largest waterwheel ever constructed, potentially susceptable to weight and torsional issues.

3.3.6 *Staudruckmaschine*

3.3.6.1 Manufacturers claims

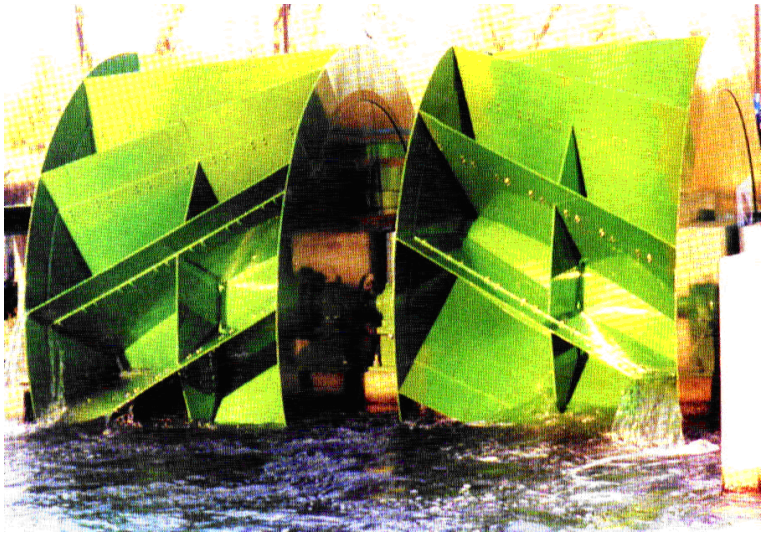

Figure 3.20: *Staudruckmachine* prototype (Brinnich 2008)

The original *Staudruckmaschine*, meaning 'dam-effect machine', was patented in 2001 (Brinnich 2001) as an attempt to exploit hydropower sites with head differences between 1m and 3m, and flow rates between 5 m^3/s and 15 m^3/s (assuming a 5m wide wheel). The only prototype of this design is shown in in Figure 3.20, comprising two symmetrical units, and was decommissioned following trials. Referring to Figure 3.21, the *Staudruckmaschine* has a central hub the same diameter as the head drop between the upstream and downstream water levels. This is similar to the *Zuppingerrad*, and like this machine and also the *Aqualienne*, has a filling ratio of one. Where this machine differs is that the channel bed is flat, resulting in a less tortuous route for the water to enter, and it has a relatively large blade length, roughly two thirds of the radius of the waterwheel. This means that the volume of the cells that fill with water is relatively large, and the flow capacity per metre width, per revolution, is relatively large. The speed of rotation will depend on the ease with which the large blades can enter and exit the water. This will also have implications for the efficiency. It is here that the *Staudruckmaschine* has a unique feature. Its diagonally mounted blades enter and exit the water gradually across the width of the wheel as it rotates, instead of at an instant as with traditional waterwheel blades. This allows the water to run into and out of the cells more gradually and with less impulse. The blades are supported between two outer disks.

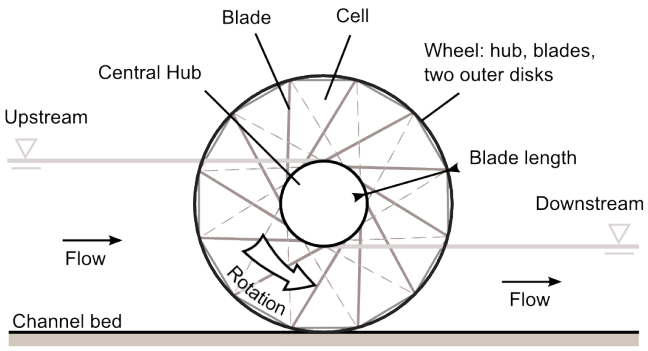

Figure 3.21: *Staudruckmaschine* description

The inventor claimed that the efficiency of the *Staudruckmaschine* would never drop beneath 90%, even when operating at partial flow, as the only source of loss was leakage through air gaps. This only loss was quantified as being 2% to 3% of the maximum flow rate, which was stated to be 3 m^3/s per m width. The explanation provided indicated that the *Staudruckmaschine* exploited the energy of the *"current"*, similar to a "classic stream wheel" - i.e. 100% impulse (Brinnich 2001). There are several points within these claims worth analysing. A constant efficiency based upon one source of loss is unrealistic. Most losses such as friction and turbulence increase with speed. Also the large depth of the upstream channel would result in such low velocities that there would be little kinetic energy to extract. When it is observed that the downstream water is roughly half the depth and has accordingly twice the velocity of the upstream (i.e. it departs the installation with greater kinetic energy), the impulse explanation appears to be false. This conclusion was also reached in a study by Killer (2003), who found that no data was available from the pilot program and access was not granted. He concluded that the claims did not seem reasonable and that the true efficiency was not known. Killer also proposed his own theory of operation for the *Staudruckmaschine* which is given in section 3.3.6.2. For the same reasons, a scale model was independently constructed and tested to determine the true performance of the *Staudruckmaschine* (Senior 2007). The findings of this study are given in Section 3.3.6.3.

A second prototype was patented and constructed in 2006 which addressed some of the design faults observed with the original *Staudruckmaschine* (Brinnich 2006). Part of the new design involved significantly reducing the blade length, thus eliminating the large cell volume that distinguished the original *Staudruckmaschine* from alternative waterwheel designs. Further reference to the *Staudruckmaschine* in this document relates only to the original prototype discussed.

3.3.6.2 Independent theoretical analysis

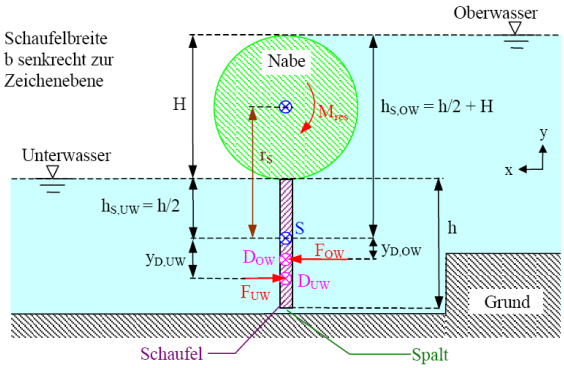

Figure 3.22: Analysis of *Staudruckmaschine* by Killer (2003)

One alternative theory of operation has been proposed for the *Staudruckmaschine*, and was included as part of a Master's thesis on low head hydropower machinery (Killer 2003). This research was conducted in partnership with a German energy company from which the document was obtained. The theory has not otherwise been published and analysis of this theory, by the author of this thesis, suggests that there is a critical error and that it is incomplete. Despite this, the theory is significant as it proposes that the *Staudruckmaschine* is driven primarily by the *hydrostatic pressure* resulting from the depth of water acting on a vertical blade when beneath the hub.

The theory analyses the upstream and downstream separately in two stages ('Oberwasser' and 'Unterwasser'). The moments (or torque) are calculated for each in the static scenario as shown in Figure 3.22. It is worth noting that the step in the ground is not indicated by Brinnich (Brinnich a), although it does not feature in Killer's calculations. The second moments of area are calculated resulting in points D_{ow} and D_{uw} at which the average pressure acting on the blade is calculated. The force is then calculated by multiplying the pressure by an area equal to the blade depth multiplied by the wheel width. The resulting moment from this force is then calculated by multiplying by the radius to points D_{ow} and D_{uw}. Although this part of the theory is correct, it is also unnecessarily complicated. The need to calculate the second moment of areas and the location of points D_{ow} and D_{uw} can be eliminated when it is observed that the pressure *difference* between the upstream and downstream acting on the blade itself is constant for the entire length of the submerged blade. The error occurs when Killer calculates

the power by multiplying the moment, calculated in the *static* scenario, by the angular speed. For angular speed values other than zero, the moment must be calculated in the *dynamic* scenario where Bernoulli's equation applied to open channel flows would suggest that the surface levels and pressures would reduce with increasing flow rate. Killer also fails to take into account the reaction of the installation as a whole to the acceleration of the water between the upstream and downstream. These points are addressed in Chapter 5, which proposes an alternative theoretical analysis of machines such as the *Staudruckmaschine*.

3.3.6.3 Independent physical testing

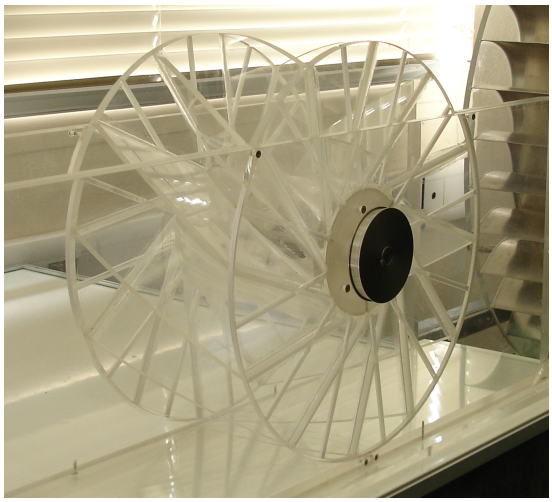

Figure 3.23: 1:10 scale *Staudruckmachine* model

In 2006, a 1:10 scale model of the *Staudruckmaschine* was built and hydraulically tested at the University of Southampton. The model is shown in Figure 3.23, and the results of these tests were presented as a paper at the 2007 I.A.H.R. conference (Senior et al. 2007), which are provided as Appendix D. The peak efficiency of the machine was determined to be just 40%, whilst the maximum flow rate through the machine when running at freewheel without load was just 12 l/s. The scaled equivalent of this flow rate is 1.6 m^3/s per metre width for a machine with the dimensions of the prototype *Staudruckmaschine*, for which a flow capacity of 3 m^3/s per metre width was claimed. Despite this, it was concluded that the *Staudruckmaschine* had development potential as two solvable design flaws were identified, which resulted in decreased efficiency and flow capacity.

- Stated briefly, the first design flaw was the large gaps which formed between the diagonally mounted blades and flat channel bed, as shown in Figure 3.24. Significant leakage of water between the upstream and the downstream occurred through these gaps and reduced the efficiency of the machine.

- The second design flaw was the mounting of the diagonally mounted flat blades between solid outer disks. Referring to Figure 3.25, which depicts the wheel from both sides, this arrangement resulted in several problems. The filling and ventilation of the cells was governed by the arrival of the outside tips of the blades reaching the water surfaces of the upstream and downstream. This resulted in the displacement of water, volume i on entry, and the raising of water o on exit. On the other side of the wheel, a small quantity of water would fail to exit the cells as the blades exited the downstream, whilst at the upstream, air would be energetically ejected from the cell on blade entry. The poor design of the blades and blade mounting not only reduced efficiency, but acted as a brake to the rotation of the wheel, reducing the flow capacity and resulting in significant pulsation and wave generation.

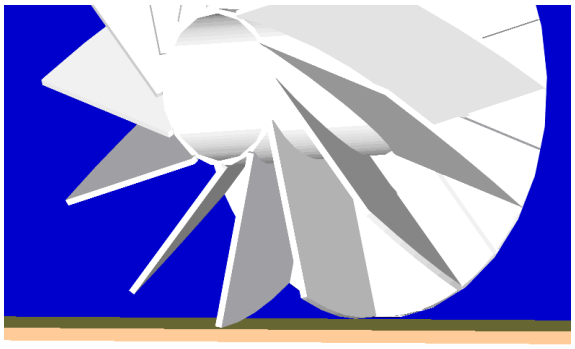

Figure 3.24: *Staudruckmaschine* leakage gaps

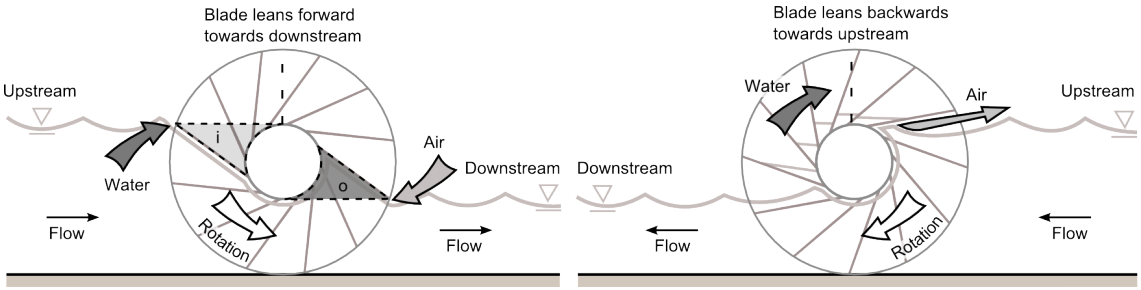

Figure 3.25: *Stadruckmachine* losses resulting from poor design

3.3.7 *Very Low Head Turbine*

Figure 3.26: *Very Low Head Turbine*: a) runner b) installed (Leclerc 2009)

The *Very Low head Turbine* is a novel form of *Kaplan* turbine that operates without complex inlet and outlet structures. Referring to Figures 3.26a and 3.26b, it consists of a large diameter runner installed at 45 degrees to the vertical within a concrete shroud, extending from the channel bed up to the free water surface. The runner is directly connected to a submerged permanent magnet generator, and operates at variable speed to maximise its operational efficiency at a given flow. Trials of the first prototype turbine commenced in March 2007 and were presented at the 2008 Hidroenergia Conference (Leclerc 2008). The grid connected and fully commissioned turbine consists of a 4.5m diameter runner, and operates with a nominal head, flow, and electrical power output of 2.5m, $22.5m^3/s$ and 438kW respectively. It operates with a hydraulic efficiency of 85% at nominal flow, reducing to 50% at 20% of nominal flow.

The stated intention of the manufacturer is to provide five standardised designs with runner diameters between 3.55m and 5.6m, suitable for head differences between 1.4m and 2.8m, and flow rates between $10m^3/s$ and $30m^3/s$. The manufacturer claims that the *Very Low Head Turbine* would only become economical for installations above 100kW (Leclerc 2009).

3.3.8 *Gravitational Vortex Machine*

The *Gravitational Vortex Machine* has been designed and built by Austrian engineer Franz Zotlöterer. Depicted in Figure 3.27, a concrete structure generates a vortex between the upstream and downstream. The velocity at the centre of the vortex is high and is exploited through reaction by a vertically mounted central impeller shown in Figure 3.28. In 2006, a prototype was constructed utilising a 1.2m head and a flow rate of 1 m^3/s. The electrical power output was 6.2kW, indicating a total efficiency 50%. Assuming a gearbox and generator efficiency of 82% and 80% respectively, the inventor claims a turbine efficiency of 80%, although he believes 88% could be achieved (Zotlöterer 2006). The data provided for the prototype is limited, not including performance at reduced flow rates. No developed theoretical analysis of the vortex or power conversion has been published. It is anticipated by the inventor that the *Gravitational Vortex Machine* could be constructed to exploit heads between 1m and 3m, and flow rates between 1 m^3/s and 40 m^3/s (Zotlöterer 2009).

Figure 3.27: *Gravitational Vortex Machine* prototype (Zotlöterer 2006)

Figure 3.28: *Gravitational Vortex Machine* impeller (Zotlöterer 2006)

Chapter 4

Discussion on Operational Principles

In the literature review, several terms were used by manufacturers and inventors to describe the operational principles of the hydropower machines discussed. Some of the proposed operational principles are supported by well developed scientific theory whilst others are not. This section reviews the terminology encountered in the literature. It concludes by identifying a proposed operational principle which is not currently supported by detailed scientific theory, but appears to have significant development potential.

4.1 Review of Terminology

Impulse: This is a commonly used scientific term and describes a force multiplied by the amount of time it acts over. In the context of hydropower machines, it is equivalent to a momentum exchange process, when a jet or stream of water impacts upon a relatively slow moving bucket or blade. Examples of such hydropower machines include highly efficient Pelton turbines, and some basic forms of undershot waterwheel. Importantly, the multiple blades or vanes of these machines are not being continuously acted upon, instead rotating about an axle, being sequentially introduced into, and then removed from the jet or stream of water.

Reaction: This term describes the force resulting from a change in velocity and pressure of flowing water. In the case of a reaction turbine, such as a Kaplan turbine, a torque is exerted as the water flows through the propeller, as a pressure difference is generated across the curved blades. Importantly, the water flows over the surfaces of the blades with relatively high velocity. It does not push directly against them with a common velocity. The blades are continuously submersed, being acted upon at all times.

Potential: This term is used to describe machines where the weight of water contained within cells is exploited to drive hydropower machinery by lowering the cells through the available head difference, reducing their potential. The most prominent example of a potential machine is the overshot waterwheel. The concept of potential machines is quite intuitive, the driving force at any point being analogous to the weight experienced when holding a bucket of water. This understanding is however overly simplistic and the fundamental properties of such machines are not recognised in the literature. As a result several machines, such as middleshot waterwheels and Archimedes Screws are at times inaccurately, or at least over simplistically, referred to as being driven by weight or potential. To clarify these points, the fundamental properties of potential machines and the mis-application of this term are investigated in the following subsection, 4.1.1.

Buoyancy: This term was used to describe the operational principle behind the *AUR Water Engine*. Buoyancy is the vertical lift experienced by a submersed body resulting from the hydrostatic pressure of the water acting on its surfaces. Archimedes' law states that the lift is equal to the volume of the water displaced by the submersed object. As observed by the inventor, the lift experienced by the float of the *AUR water engine* reduced as it ascended through each stroke. As such, machines which exploit the principles of buoyancy do not exploit the available pressure, which is a function of the head differential, effectively over a complete cycle.

Hydraulic Pressure Differential: This term was used to describe the *Salford Transverse Oscillator*. A simpler term, *Pressure*, was also used to describe the undershot waterwheel operating in non-impulse conditions. In both cases, these terms were used to describe the situation where a depth of water in the upstream acts directly upon a vertical paddle or blade. The water does not impact upon or flow over the blades. In such scenarios, which are neither impulse, reaction, nor potential, these terms do indicate a plausible operational principle. Their use however was brief and vague, not being supported by a developed scientific proof or theory.

Flow and Current. These final terms were used in the description of machines such as the *Staudruckmaschine* and the *Sundermann* turbine. They are abstract terms and do not indicate a operational principle through which the flow or current acts upon the machines. They are proposed when the manufacturer or inventors of the machines have little or no scientific understanding of hydraulics or energy exchange. Interestingly, both of these machines have strong similarities to the *Salford Transverse Oscillator* and the undershot waterwheel acting in non-impulse conditions. The flowing water does not impact upon or flow over the blades, but acts directly upon them. These similarities, and the work by Killer on the *Staudruckmaschine*, indicate that such machines could also be driven by hydrostatic pressure, for which no scientific proof or theory has been developed.

4.1.1 Theory of Potential Machines

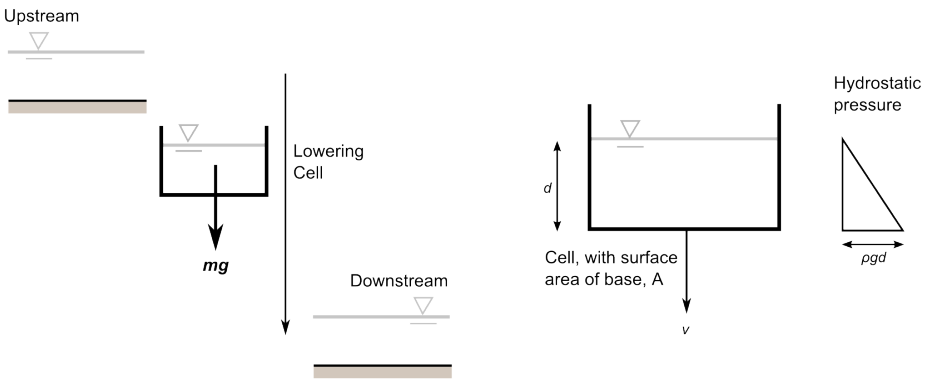

Figure 4.1: Representation of Potential machines: a) weight based analysis b) hydrostatic pressure based analysis

An ideal model of a potential machine is given in Figure 4.1a, showing an individual cell with a horizontal base and vertical walls, containing water, and descending vertically from the upstream to the downstream. Referring to the lowering cell, this is the most intuitive analysis of *weight*, where the downward force of the water is simply the product of the mass of the water multiplied by the acceleration due to gravity. Although correct, this analysis does not readily make the fundamental properties of such machines clear.

Referring to Figure 4.1b, the weight of the water exerts a force on the cell as a result of the *hydrostatic pressure* it generates. Hydrostatic pressure is defined as the pressure at a point in a fluid due to the weight of the fluid above it. This is calculated using Equation 5.1, where the hydrostatic pressure is p, the depth of the water in the cell is d, ρ is the density of the fluid and g is the acceleration due to gravity. The hydrostatic pressure is zero at the water's surface and increases linearly to its maximum, $\rho g d$, at the cell's base. The downward force of the water within the cell, F, is the product of the pressure acting on the base of the cell, multiplied by the area of the base. As the cell lowers, and force is exerted over a distance, it is said to do *work*. The amount of work done per second is the *power*, P, of the moving cell. This is calculated by multiplying the force by the velocity of the cell, shown by Equation 4.2.

$$p = \rho\, g\, d \tag{4.1}$$

$$P = F\, v = (\rho\, g\, h\, A)\, v \tag{4.2}$$

An understanding of the role of hydrostatic pressure and Newton's laws allows the following fundamental properties of true potential machines such as overshot waterwheels to be recognised:

- Potential machines are designed so that the water is contained entirely within cells, not requiring stationary shrouds or casings to retain the water between moving blades. The hydrostatic pressure of the water within the cell acts on *all submerged surfaces*. Forces exerted by the pressure acting *laterally* on the opposing sides of the cells cancel. The net force is downwards, resulting from the pressure acting on the *base* of the cell.

- As the base of the cell is directly beneath the water contained, it is subjected to the maximum hydrostatic pressure that can be generated over its entire surface area. Therefore for a given depth of water, the force exerted on the base of the cell is the maximum available force.

- For a net force downwards to exist, the underside of each cell is surrounded by air at atmospheric pressure. Therefore there is a pressure difference across the base of the cell resulting from the weight of the water on its top surface.

- *The movement of the cells of potential machines is vertical, or rather the direction in which work is done is parallel to gravitational acceleration.*

4.1.2 Limitations of the Potential Analysis

The fundamental properties of true potential machines such as the overshot waterwheel have been identified in the previous subsection. Using these as a reference, the departure of machines such middleshot waterwheels and the *Archimedes Screw* from the potential machine analysis can be analysed. These departures are demonstrated using Figure 4.2 which represents a generic middleshot waterwheel. Initially, a blade at position 'A' does represent a cell exploiting the potential of the water it contains. The cell is horizontal, moves vertically, and the working surface is situated beneath the water and is subjected to the maximum pressure for the given depth.

However, as the blade rotates about the axle, the situation no longer matches the criteria identified for a true potential machine.

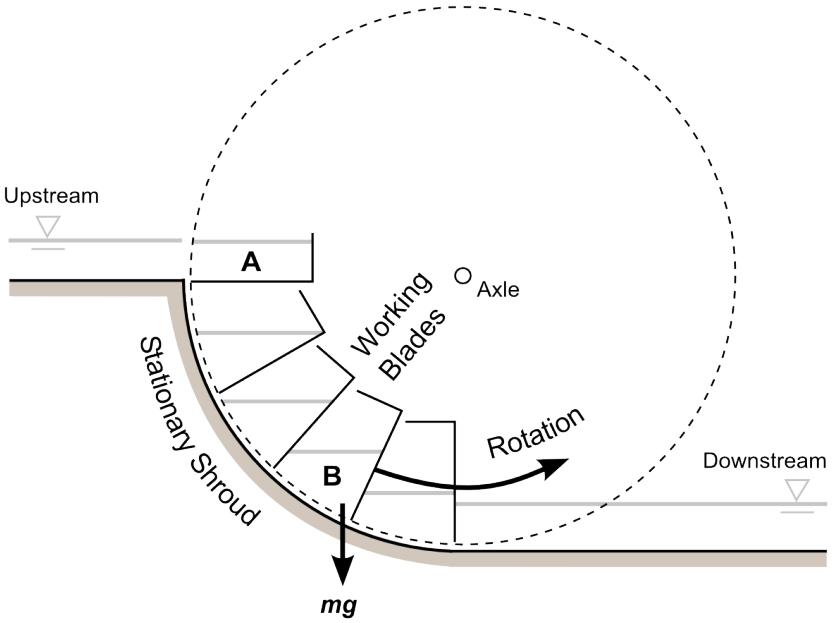

Figure 4.2: Representation of changing operational principle within a middleshot waterwheel

Considering the scenario when the blade is at position 'B':

- The water is contained between the shroud and the blade, both of which are subjected to hydrostatic pressure. The blade is mobile and is therefore a *working* surface which generates power. The shroud however is stationary, so the hydrostatic pressure acting on it does no work, and generates no power.

- The direction of work is not vertical, parallel with gravity, but tangential to the axle of the machine. 'Weight' describes the *vertical* component of a force exerted by mass as a result of gravity. As the blade rotates beneath the axle and tends towards the vertical, the *lateral* component of the force exerted by the hydrostatic pressure on the blades becomes dominant.

- The pressure acting on the working surface is not constant as the blade is *beside* and not *beneath* the water. It increases with depth from zero at the water's surface, and therefore the maximum force available from a given depth of water is not exerted on the blade.

- The combination of blades and a shroud is not the same as the cells employed by potential machines. The reverse side of the blade becomes partially submersed by the water con-

tained in the previous cell. This creates a counteracting pressure. In the extreme case of middleshot waterwheels with filling ratios of one such as the *Aqualienne* and *Zuppingerrad*, this means that the pressure difference across the blades whilst within the shroud is zero as there are no free water surfaces *within* the cells.

The analysis of a blade at position 'B' on a middleshot waterwheel, where a non-horizontal working surface moves with a lateral component relative to a stationary shroud, applies equally to the blades of an *Archimedes screw*. It can be appreciated that the generation of pressure, force and power for these machines is significantly more complex than for a true potential machine.

In conclusion, it would be more thorough and exact to describe such machines as being driven by *Hydrostatic Pressure*, which acts in all directions on all submerged surfaces, as opposed to *Potential*, which acts only in a vertical direction.

4.2 Opportunity for Research and Development

The operation of modern turbines and the overshot waterwheel by *impulse, reaction,* and *potential*, are sufficiently understood and supported by scientific theory. There are however other machines where the water and the blade speed are matched (excluding impulse and reaction as plausible operational mechanisms), whilst the working surfaces are non-horizontal and move non-vertically (excluding potential as a plausible operational mechanism). These machines include the undershot waterwheel operating in non-impulse conditions, middleshot waterwheels during part of their operation, the *Salford Transverse Oscillator*, the *Staudruckmaschine*, the *Archimedes screw* and more. Although in some cases the operation of these machines was attributed to weight, current or flow within the literature, it is proposed that they are best described as driven by *Hydrostatic Pressure*. As of yet, no detailed scientific theory describing this operational principle has been published.

To demonstrate the opportunity presented by hydropower machines driven by hydrostatic pressure, consider Figure 4.3. On the left is depicted a traditional middleshot waterwheel and in the centre, the *Staudruckmaschine*. Both machines can be described as driven by hydrostatic pressure, however the first was designed with the intention to exploit the hydrostatic pressure in the vertical direction (*weight*), whilst the second allows the hydrostatic pressure to be exploited, *but predominantly in the horizontal direction.* This difference in approach greatly simplifies the

flow path on entry into, and passing through the machine, as demonstrated by the corresponding graphs in Figure 4.3. This simple design, with its filling ratio of one and relatively large cells, demonstrates how such machines could potentially process significantly larger flow rates than traditional low head technologies such as waterwheels. Also, when compared to the depiction of a turbine on the right of Figure 4.3, they operate situated with free water surfaces, and do not require inlet or outlet structures to accelerate or decelerate the flow. This means that unlike most turbines, they could operate at very low head differences under 3m.

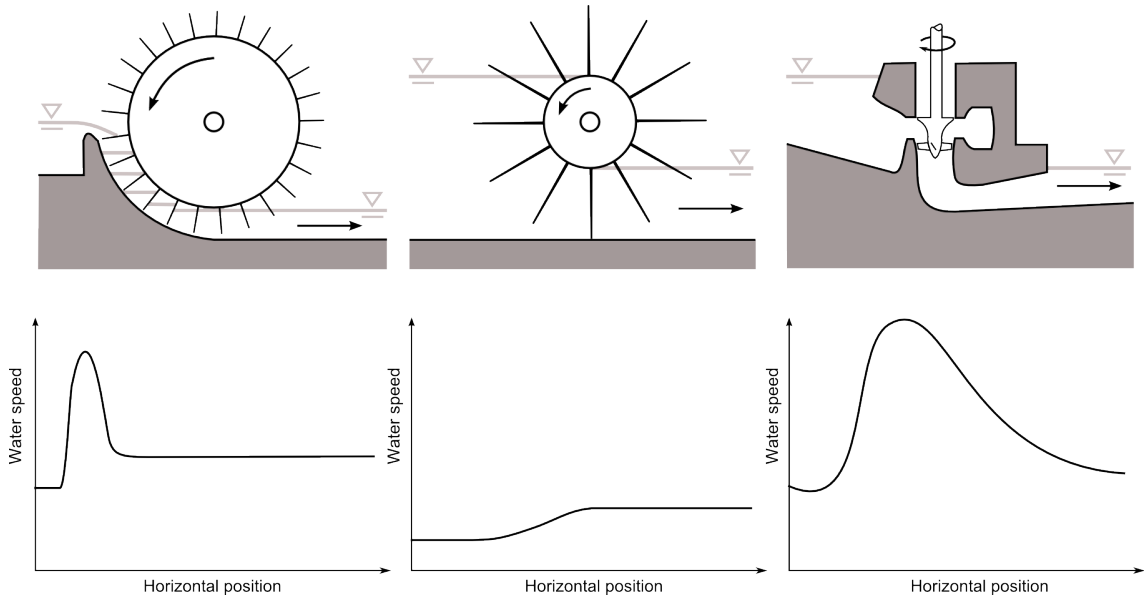

Figure 4.3: Comparison between the traditional waterwheel, a hydrostatic pressure driven machine and a turbine

- In conclusion, it can be stated that it is possible to use the hydrostatic pressure generated by a depth of water to drive hydropower machines. Several machines reviewed in the literature appear to use this principle, however a working, scientific theory has not, to the author's knowledge, been published. Importantly, exploiting the horizontal component of hydrostatic pressure in a free surface environment has the potential to create hydropower machines with increased flow capacities and power outputs, which operate at very low head differences.

Chapter 5

Theory of Hydrostatic Pressure Converters

The previous section indicated that hydropower machines may exist which are predominantly driven by hydrostatic pressure acting on a non-horizontal working surface, moving with a horizontal component. Such an operational mechanism has not been analysed theoretically. This Chapter commences by demonstrating how hydrostatic pressure can be converted into power using a simplified representation of such a hydropower machine. These machines are being named *Hydrostatic Pressure Converters* (HPCs). With an understanding of this basic principle, the hydropower machines from the literature review are re-considered and it is identified that two types of pressure machines exist. The fundamental properties of these two types of hydrostatic pressure converter are defined, and full theories are developed for each. These theories are ideal, being based on the defining geometry of the machines whilst being independent from non-ideal design factors such as manufacturing tolerances, gaps between moving and non-moving surfaces, and number of blades. The theories given here are referred to as 'ideal theory' in the subsequent chapters, as design related factors such as leakage and turbulent losses are introduced in those chapters.

5.1 Demonstration of the Basic Principle

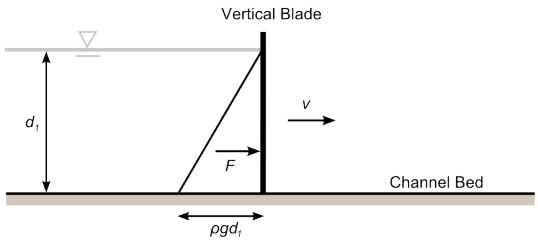

Figure 5.1: Basic representation of the hydrostatic pressure principle

Hydrostatic pressure is defined as the pressure at a point in a fluid due to the weight of the fluid above it. This is shown by Equation 5.1; the pressure, p, increases linearly with depth, d, where ρ is the density of the fluid and g is the acceleration due to gravity.

$$p = \rho\, g\, d_1 \tag{5.1}$$

Referring to Figure 5.1, consider a simple vertical blade which extends from a channel bed and retains a depth of water, d, to one side. This blade is shown as the thick vertical line, and extends into the page. The diagonal line represents the hydrostatic pressure acting on the vertical blade, which is zero at the water's surface and increases to a maximum of $\rho g d$ at the channel bed. The force acting on the blade, F, is a product of the *hydrostatic pressure multiplied by the area* of the blade. This is shown by Equation 5.2 where W is the width of blade into the page:

$$F = \rho\, g\, \frac{d_1^2}{2}\, W \tag{5.2}$$

If the vertical plate moves laterally with velocity, v, whilst the water is replenished to maintain a constant depth such as in a flow scenario, then a power, P, is generated on the moving blade as shown by Equation 5.3:

$$P = F\, v = \rho\, g\, \frac{d_1^2}{2}\, W\, v \tag{5.3}$$

5.2 Identification of two forms of Hydrostatic Pressure Converter

The literature review and discussion on operational principles indicated that there are several forms of machine which may predominantly be driven by hydrostatic pressure. These included the Undershot waterwheel operating in non-impulse conditions, the *Zuppingerrad*, the *Sundermann Turbine*, the *Staudruckmaschine* and the *Salford Transverse Oscillator*. It has been identified that these machines can be categorised into two groups, depending on how the working surfaces or blades of the machines are exposed to and driven by the hydrostatic pressure. This is significant as the theories developed in the following sections suggest that the two forms of hydrostatic pressure converter develop force and generate power in significantly different ways. In this document, the two forms are defined as:

'Type One' HPCs: Hydropower machines where the working surface extends from the channel bed to the ***upstream*** water surface. Such machines include the Undershot waterwheel operating in non-impulse conditions, the *Salford Transverse Oscillator*, the *Sundermann Turbine* and the *Archimedes Screw*, all of which are represented in Figure 5.2. It is interesting to note that the *Archimedes Screw* is the only machine reviewed in the literature where the total head differential is segmented into multiple cells. As the sprial blade enters and exits the water in the trough with each thread, it is modelled as multiple working blades. Each machine representation includes a lesser depth of water acting on the downstream sides of the working surface. This depth is included in the following theory, and can have a value from zero upwards depending on the designed operational conditions.

'Type Two' HPCs: Hydropower machines where the working surface extends from the channel bed only up to the ***downstream*** water surface. This is possible by mounting or rotating the working surfaces or blades beneath a central hub or dam like structure which retains the head differential. Such machines include the *Zuppingerrad*, the *Aqualienne* and the *Staudruckmaschine*, also represented in Figure 5.2.

The following two sections present theories developed to describe how 'type one' and 'type two' HPCs generate power from the hydrostatic pressure of water. These theories also aknowledge and account for the change in kinetic energy observed between the upstream and downstream of actual machines. This change in velocity was not present in the simple demonstration of the basic principle, Section 5.1.

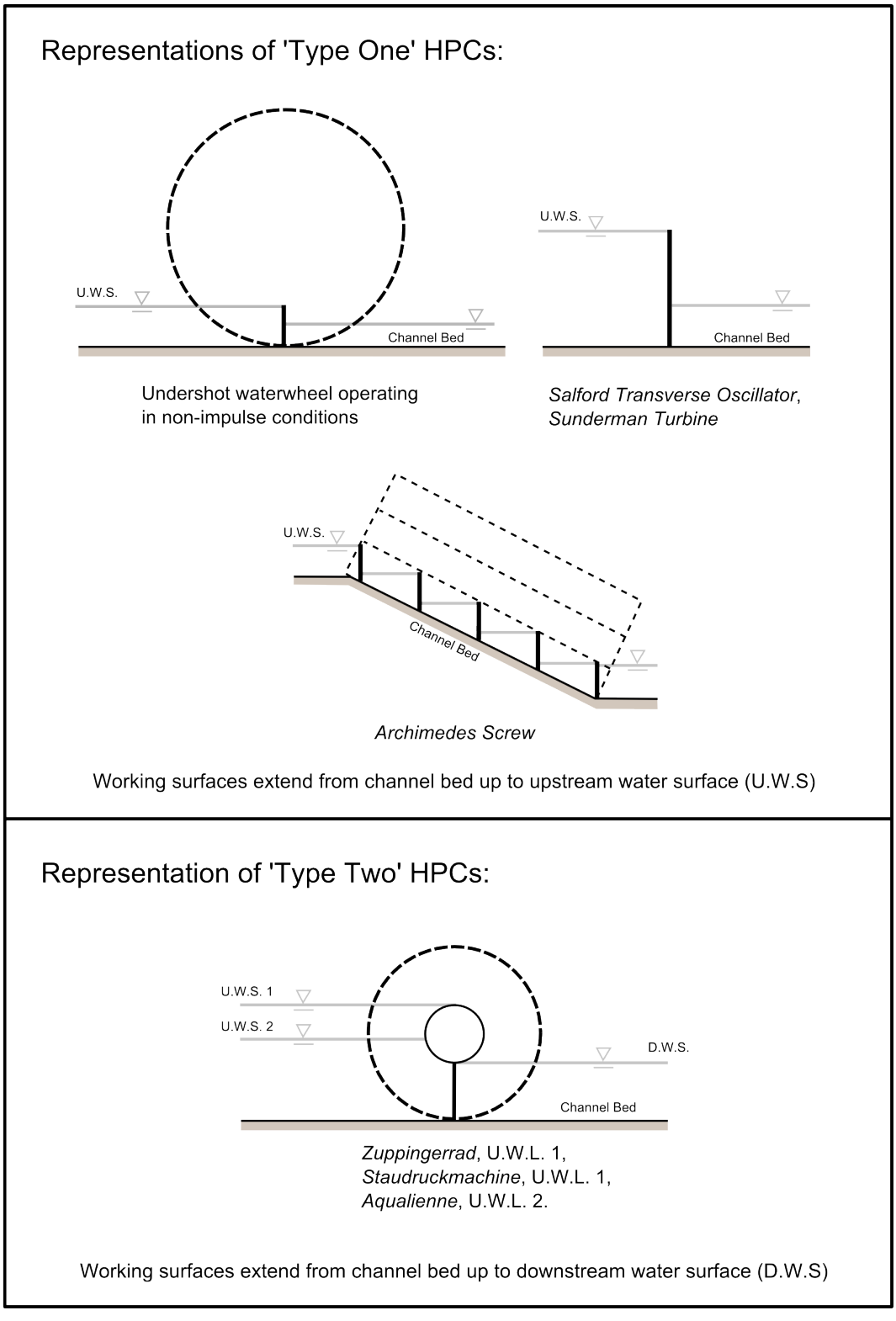

Figure 5.2: Representations of 'type one' and 'type two' HPCs

5.3 'Type One' HPCs

Section 5.2 introduced 'type one' HPCs as hydropower machines where the working surface extends from the channel bed to the *upstream* water surface. This section develops a theory which covers how the hydrostatic pressure exerts force on the working surfaces of these machines and generates power during flow conditions. The theory is ideal, being based on the fundamental geometry of such machines, whilst assuming no design related losses such as leakage or turbulence. The ideal models used in this theory do not account for the change in kinetic energy observed between the upstream and downstream of actual 'type one' HPCs such as the *Salford Transverse Oscillator*. This increase in kinetic energy is assummed to be the result of a process which does not directly contribute to the power output of 'type one' HPCs, and is analysed in Section 5.3.3. In Chapter 9, the implications of the ideal theory and the model testing which follow are discussed with regards to the hydropower machines seen in the literature review.

5.3.1 Force calculations

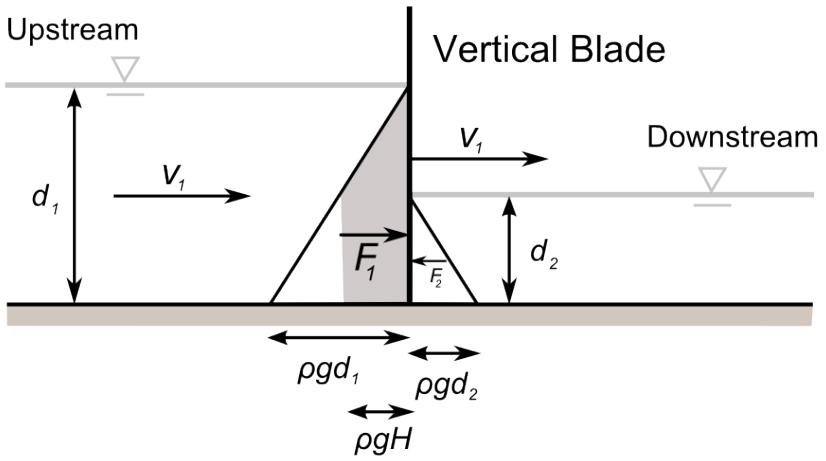

Figure 5.3: 'Type one' HPC nomenclature

Figure 5.3 depicts a simple vertical blade which extends from the channel bed to slightly beyond the upstream water surface. This blade is the working surface on which the hydrostatic pressure of the water acts, and has width W into the page. The blade is shown to be partially submerged in the downstream, the depth of which, d_2, is between zero and the upstream depth, d_1. On both the upstream and downstream sides of the blade, the hydrostatic pressure is represented

by the diagonal lines and increases from zero at the water's surface up to a maximum of $\rho g d_1$ and $\rho g d_2$ respectively. Importantly the grey shaded area represents the effective pressure. This increases with depth until the downstream water level is reached, beyond which it does not exceed $\rho g H$ where H is the head difference and equals d_1 minus d_2. This is because the increase in pressure on the upstream side of the blade is counteracted by the increasing pressure on the downstream side of the blade. The force exerted by the hydrostatic pressures on the upstream and downstream sides of the blade are F_1 and F_2 respectively. The total force acting on the blade, F, is accordingly the result of the upstream force minus the downstream force, equation 5.4:

$$F_1 = \rho\, g\, \frac{d_1^2}{2}\, W$$

$$F_2 = \rho\, g\, \frac{d_2^2}{2}\, W$$

$$F = \rho\, g\, \frac{d_1^2 - d_2^2}{2}\, W \tag{5.4}$$

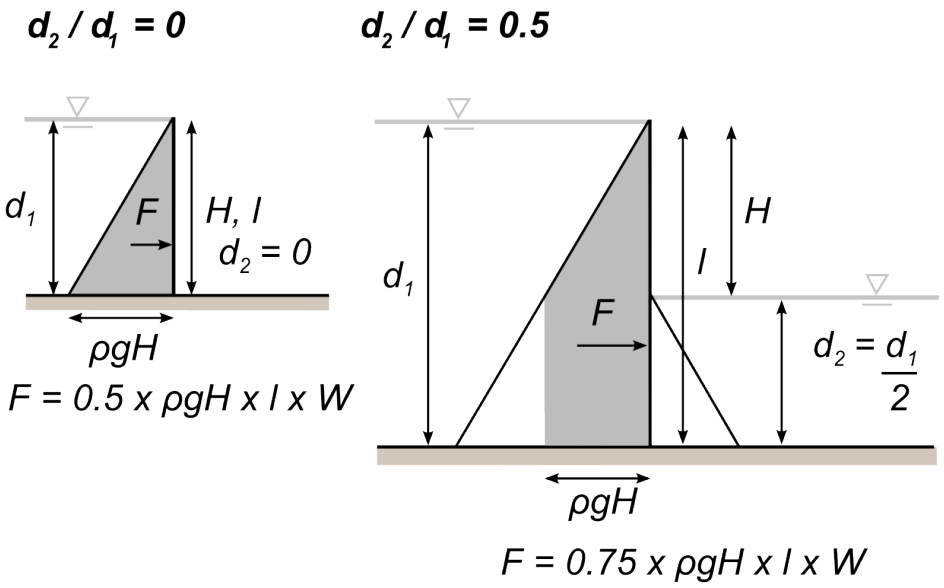

Figure 5.4: 'Type one' HPC, demonstration of relationship between force and the ratio d_2/d_1

The most significant outcome from Figure 5.3 and equation 5.4, is that the total force exerted on the blade is not dependent only the the head difference, equal to d_1 minus d_2, but also the ratio of the submerged depths of the blade in the upstream and downstream, d_2/d_1. This relationship is demonstrated graphically by Figure 5.4, where the total force is written as a function of the head difference, H, and the blade length, l.

The scenario on the left applies hydrostatic pressure only from the upstream side of the blade. The downstream depth d_2 is zero, as is the ratio d_2/d_1. The total force exerted on the blade is equal to just *half* of that associated with the maximum pressure ρgH acting upon the area of the blade. In contrast, the scenario on the right has the same head, however the ratio d_2/d_1 is 0.5. The force exerted on the blade is equal to *three quarters* of that associated with the maximum pressure ρgH acting upon the area of the blade.

The relationship between the ratio d_2/d_1 and the force applied to the blade is thus critical. As the ratio d_2/d_1 tends towards a value of 1, the maximum pressure ρgH is applied to an increasing proportion of the blade area. Technically, the maximum pressure will be applied over the entire length of blade when d_2/d_1 equals 1, however this is trivial as the head and thus the pressure differential at this point would equal zero.

5.3.2 Power and efficiency calculations

In accordance with Equation 2.1 given in the literature review, the input hydraulic power at an HPC installation, P_{in}, is a function of the total head and flow rate, as shown by equation 5.5. Section 5.1 introduced the basic concept behind HPCs and indicated how power could be developed if a blade subjected to a force moved laterally in the direction of the flow. If the blade upon which the force is exerted extends from the channel bed to the upstream water surface and the upstream depth is to be maintained, then the blade must move with the same velocity as the upstream water, v_1. Accordingly the output power, P_{out}, of a 'type one' HPC is shown in Equation 5.6.

$$P_{in} = \rho\, g\, (d_1 - d_2)\, (v_1\, d_1\, W) \tag{5.5}$$

$$P_{out} = F\, v_1 = \rho\, g\, \frac{d_1^2 - d_2^2}{2}\, W\, v_1 \tag{5.6}$$

$$\eta = \frac{P_{out}}{P_{in}} = \frac{1}{2}\left(1 + \frac{d_2}{d_1}\right) \tag{5.7}$$

The efficiency, η, of a 'type one' HPC is shown in Equation 5.7. This equation shows that the efficiency, just like like the force and output power equations, is a function of the ratio d_2/d_1. Significantly, in the ideal analysis which assumes no leakage or turbulent losses, the efficiency is independent of the blade and upstream water velocity, v_1. The implications of this are shown in the following two graphs:

- Figure 5.5 plots power and efficiency versus the ratio d_2/d_1, where the flow rate and the head is constant. The ratio d_2/d_1 has been increased from 0.0 to 1.0 by increasing the values of d_1 and d_2 whilst retaining their difference in value (the head). This is similar to Figure 5.4, of which both examples have a common head difference. It can be seen that the efficiency value increases linearly from 0.5 to 1.0 as the ratio d_2/d_1 tends towards 1.0. When designing a 'type one' HPC installation, this relationship must be understood in context of installation size versus the head being exploited, which economically is equivalent to cost versus return. To demonstrate this, a second line and axis is plotted indicating how the size of the machine, which is a function of d_1, increases relative to the head as the ratio d_2/d_1 increases. This value increases exponentially and would result in an upper efficiency boundary limited by the size of the machine, and therefore economics.

- Figure 5.6, in contrast, plots power and efficiency versus increasing flow rate, where the head is constant and the ratio d_2/d_1 arbitrarily fixed at 0.75. As equation 5.7 is a function of d_2/d_1 and independent of the blade and flow velocity, v_1, it can be seen that the efficiency has a constant value of 0.88. In this ideal analysis, the P_{out} increases linearly with the flow rate.

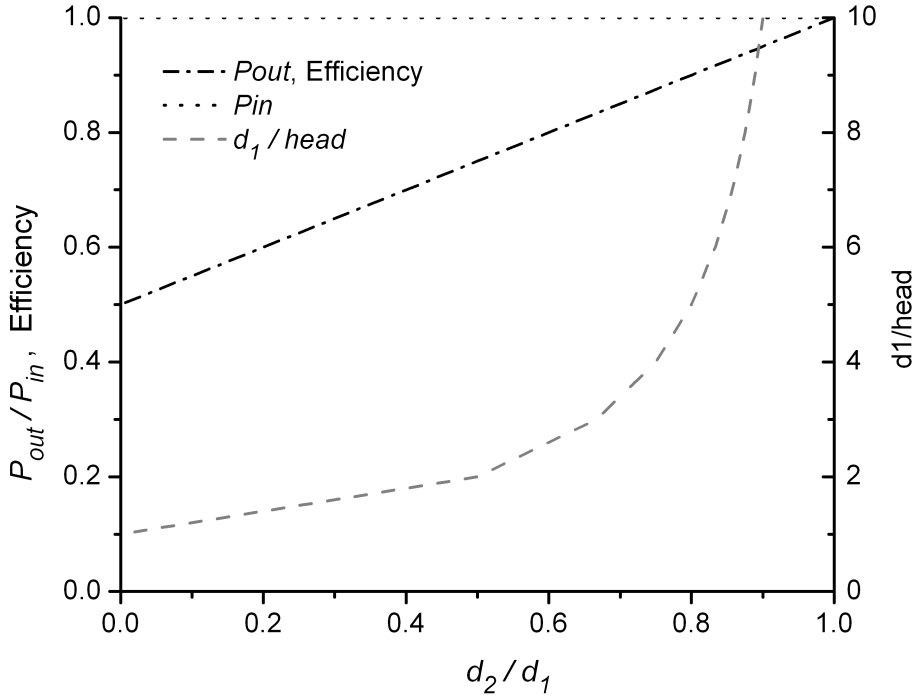

Figure 5.5: 'Type one' HPC theory with constant head and flow rate, but variable d_2/d_1 ratio

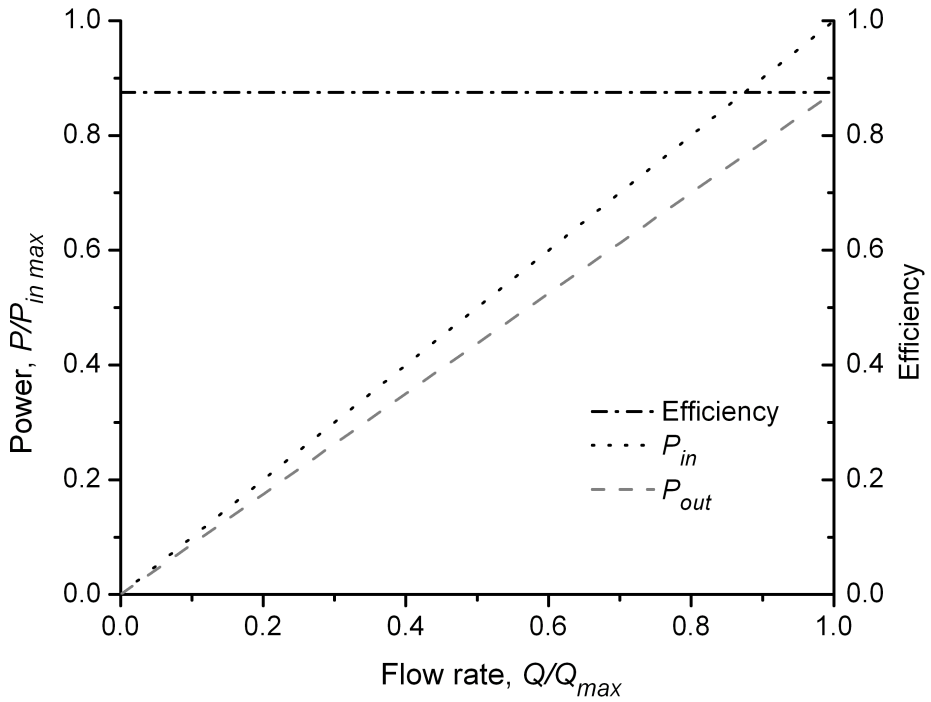

Figure 5.6: 'Type one' HPC theory with ratio d_2/d_1= 0.75, constant head and variable flow rate

5.3.3 'Evacuation' and the resulting kinetic energy change

When considering actual 'type one' HPCs such the *Salford Transverse Oscillator*, the velocity of the downstream flow, v_2, would be greater than that of the upstream, v_1, as the downstream water depth is less than the upstream, whilst the flow rate is common. This is demonstrated by equation 5.8.

$$v_2 = \frac{d_1}{d_2} v_1 \tag{5.8}$$

This increase in kinetic energy, and its generation, is not considered by the ideal model in the proposed theory. This was because the ideal model included a single working blade which moved laterally and with the same velocity as the upstream flow, v_1, and no water crosses the working blade.

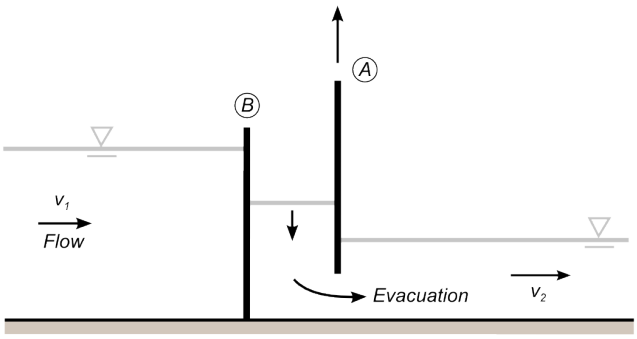

Figure 5.7: Depiction of 'evacuation' process

In practice it is not achievable to have a single blade move laterally and indefinitely with the flowing water. Instead, water must flow from the upstream to the downstream, being processed by a stationary hydropower installation which either uses multiple blades which rotate about an axle, such as with the Undershot waterwheel, or reciprocating blades controlled by gates as with the *Salford Transverse Oscialltor*. In order for the water to depart the machine once work has been done on a blade, a process termed 'evacuation' must take place. This process is represented in Figure 5.7, where 'A' represents either a blade being removed from the flow or an opening gate, and 'B', the following blade on which work will be done. As 'A' is removed or opened, the water surface between 'A' and 'B' drops from the upstream level to the downstream level and departs the machine.

It is during the 'evacuation' process that the head or pressure differential is generated across the blades. This process occurs with the passing or rotation of each blade, following the power extraction of the previous blade. As the water which is initally above the downstream level 'evacuates' the cell, its potential energy is converted to kinetic energy, accounting for the increase in velocity from v_1 to v_2. The acceleration occurs normal to the motion of the working blades. *It is therefore assumed that the 'evacuation' process does not contribute to the power oytput of the 'type one' HPC.*

The power associated with the evacuation process per unit width, P_{evac}, is shown as Equation 5.9. When plotted along with the P_{out} estimate from the ideal theory against the ratio d_2/d_1 as in Figure 5.8, it can be seen that the P_{evac} accounts for the remaining input power, P_{in}, which was not exploited by the 'type one' HPC.

$$P_{evac} = \rho\, g \left(\frac{d_1 - d_2}{2}\right)\left(\frac{d_1 - d_2}{d_1}\, v_1\, d_1\right) \tag{5.9}$$

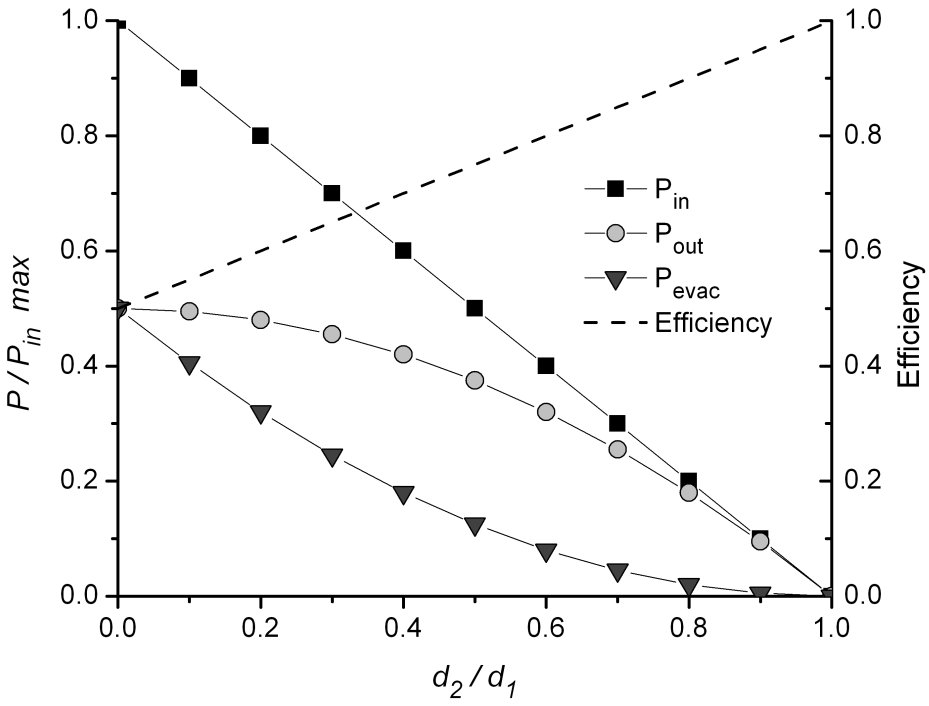

Figure 5.8: Power associated with 'evacuation' resulting in increased flow velocity

5.4 'Type Two' HPCs

Section 5.2 introduced 'type two' HPCs as hydropower machines where the working surface extends from the channel bed only up to the *downstream* water surface. This section develops a theory which covers how the hydrostatic pressure exerts force on the working surfaces of these machines and generates power during flow conditions. The theory is ideal, being based on the fundamental geometry of such machines, whilst assuming no design related losses such as leakage or turbulence. In Chapter 9, the implications of the theory and the model testing which follow are discussed with regards to the hydropower machines seen in the literature review.

5.4.1 Force calculations

HPCs can be designed such that the blade or working surface upon which the pressure acts extends from the channel bed only up to the downstream water surface. This is possible when the blades are mounted on a rotating submerged central hub, or revolve around a stationary dam like structure, which act to retain the head difference between the upstream and the downstream. The axle around which the blades rotate is between the upstream and downstream water levels. This approach has been employed by the *Zuppingerrad*, the *Staudruckmaschine* and the *Aqualienne*, a representation of which was given in figure 5.9. For the purposes of the ideal theory, the 'type two' HPC is represented as a single blade mounted beneath a central hub, and the upstream and downstream water levels are fixed, coinciding with the upper and lower surfaces of the central hub. It is also assumed that the machine and the channel in which it is situated share a common width.

Comparing Figure 5.9 ('type two' HPC) with Figure 5.4 ('type one' HPC), it can be seen that the central hub has a significant impact on the force exerted on the blade. It allows the maximum pressure at the wheel, ρgH, to be applied over the entire length of the blade, and for head values greater than zero. This means that for a given head difference, the force exerted on the blade is maximised. The pressure acting on the hub results in a force which acts normal to its surface, directed towards the axle. This force does not however result in any work being done on the central hub, as there is no movement of water across the volume occupied by the central hub. Only the force acting upon the blade attached to the central hub has significance, as it moves with the water and thus does work, generating power.

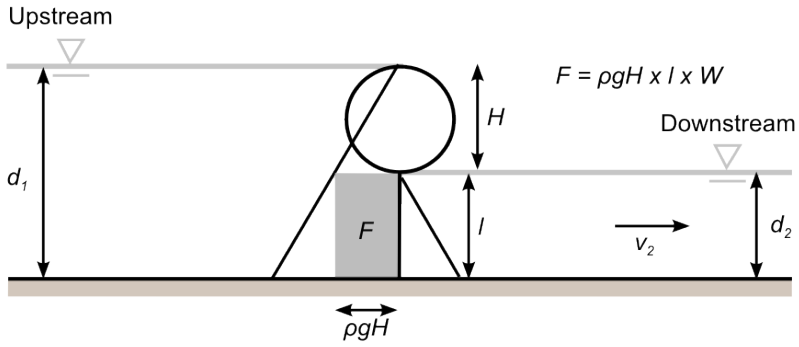

Figure 5.9: 'Type two' HPC: demonstration of force generation

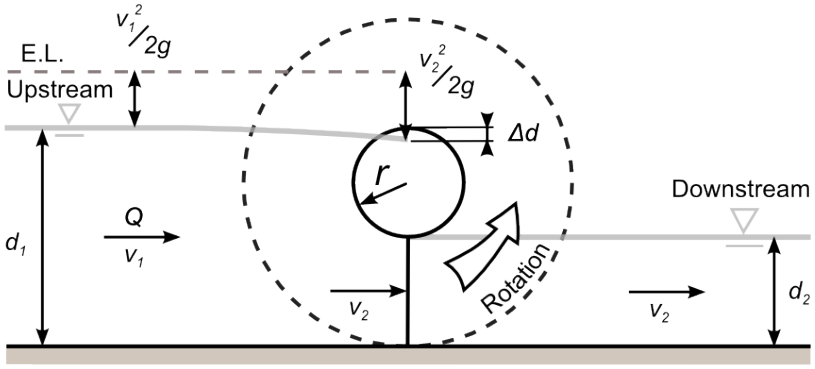

Figure 5.10: 'Type two' HPC dynamic nomenclature

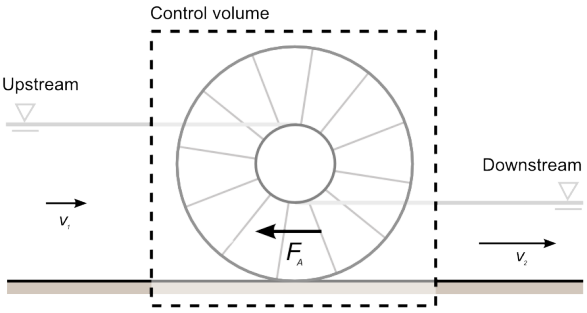

Figure 5.11: 'Type two' HPC installation reaction force

It has been ascertained that the maximum pressure difference, $\rho g H$, is applied along the entire length of the blade. This pressure however is a function of the head difference *at* the machine, and and for 'Type two' HPCs this is not constant, even if the upstream and downstream depths d_1 and d_2 are. Referring to Figure 5.10 and assuming that flow continuity holds, for non zero flow rates the downstream velocity, v_2, must be greater than the upstream velocity, v_1:

$$v_2 = \frac{d_1}{d_2} v_1 \tag{5.10}$$

Application of the Energy Equation indicates that the acceleration from v_1 to v_2 is accompanied by a drop in the water surface level, Δd, relative to the energy line, *EL*, also shown in Figure 5.10. Although the maximum pressure $\rho g H$ continues to apply over the entire length of the blade, l, the magnitude of the head, H, is reduced by Δd . Therefore the force exerted on a blade of width W resulting from the hydrostatic pressure becomes F_P, given in Equation 5.12.

$$\Delta d = \frac{v_2^2 - v_1^2}{2g} \tag{5.11}$$

$$F_P = \rho\, g\, (d_1 - d_2 - \Delta d)\, l\, W \tag{5.12}$$

The acceleration of water through the machine has a secondary influence besides the reduction in head and pressure at the wheel. Referring to Figure 5.11, consider an installation holistically within a control volume. Whilst passing through the installation, a mass of water is accelerated from a lower speed, v_1, to a higher speed, v_2. In accordance with Newton's second and third laws, this acceleration must result in a force to which a reaction force exists, provided by the installation itself. This 'inertial reaction force' to the acceleration, F_A, is quantified by calculating the momentum change of the water, equal to the mass flow rate multiplied by the velocity change, and is shown by Equation 5.13.

$$F_A = \rho\, v_1\, d_1\, W\, (v_2 - v_1) \tag{5.13}$$

5.4.2 Power and efficiency calculations

The input power at a 'type two' HPC installation is a function of head and flow rates, similar to a 'type one' HPC installation, and is shown in Equation 5.14.

In the ideal analysis, the working surface of 'type two' HPCs, the blade, is mounted vertically beneath a central hub or dam. Referring to Figure 5.10, in this position both the blade and the downstream velocity will be v_2. It is this velocity which is used to multiply the total force acting upon the blade and calculate the output power of the machine, as shown in Equation 5.15. In this calculation it is assumed for simplicity that the entire inertial reaction force, F_A, acts upon the blade.

$$P_{in} = \rho\, g\, (d_2 - d_1)\, (v_1\, d_1\, W) \tag{5.14}$$

$$P_{out} = (F_P - F_A)\, v_2 \tag{5.15}$$

$$\eta = \frac{P_{out}}{P_{in}} = \frac{(F_P - F_A)\, v_2}{\rho\, g\, (d_2 - d_1)\, (v_1\, d_1\, W)} \tag{5.16}$$

It has been shown that the head difference across the machine reduces with increasing flow rate resulting from the acceleration of the water beneath the hub, which also results in a inertial reaction force. As a result the efficiency of these machines is related to the flow rate, as shown by Equation 5.16. This decreasing efficiency is plotted along with P_{in} and P_{out} versus increasing flow rate in Figure 5.12, for a 'type two' HPC operating with a constant head difference between the upstream and downstream.

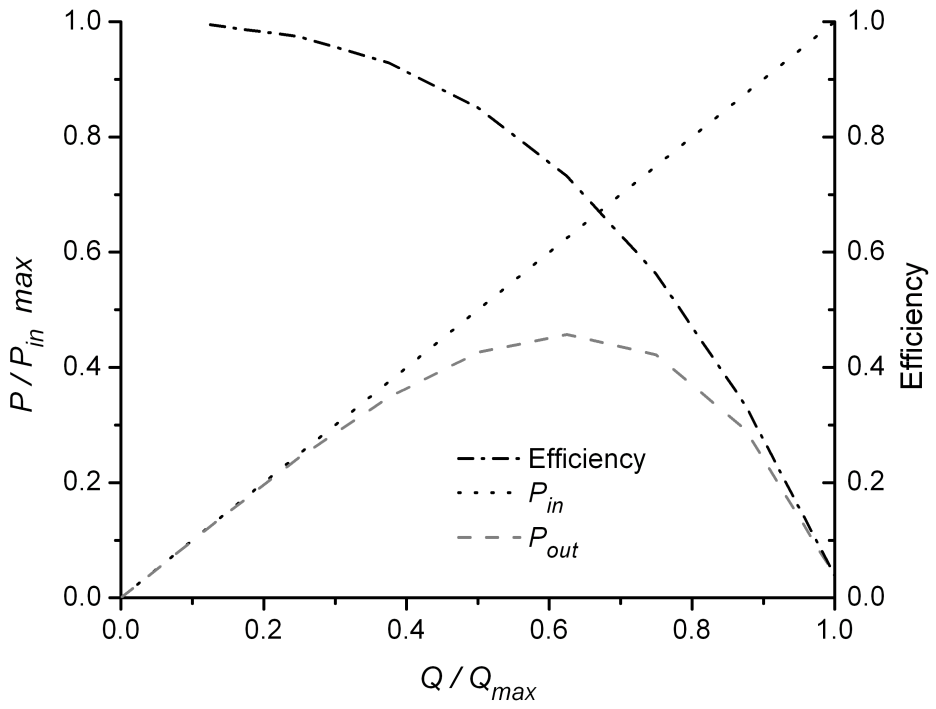

Figure 5.12: 'Type two' HPC theory: performance versus increasing flow rate

5.5 Limitations of the Ideal Analysis

The aim of the proposed theories was to clearly identify the main principles which govern the operation of the two types of HPC. To achieve this, simplistic generic models were analysed which were not complicated by the specific dimensions or geometry of individual designs. As with any ideal model, if a comparison were made with actual machines, minor differences would be expected as common assumptions such as uniform flow velocities with depth do not hold.

There are however two assumptions in the theory, the fairness of which depends heavily on the quality of the design and manufacture of the machines in question, which are anticipated could result in significant differences in the efficiency response of the practical machine versus the ideal theory. These assumptions were that the machines suffered no leakage flow or turbulent losses. Machines which rotate or reciprocate whilst submerged in water will require gaps between the stationary and non stationary components. Water will leak through these gaps, reducing the efficiency significantly at low flow rates where the leakage flow will account for a large proportion of the total flow. Similarly, the action of blades entering and exiting the water is anticipated to result in turbulent losses. The magnitude of the leakage and turbulent losses will depend entirely on the design and dimensions of the machine in question, and their influence on the efficiency response calculated by the ideal theories is investigated in Chapter 8; the Results and Analysis of the scale model testing.

5.6 Summary

A general outline of the proposed theory is that hydrostatic pressure differences, present where there are head differences in flowing water, can be used to exert force on a working surface and thus generate power. Such hydropower machines are being termed *Hydrostatic Pressure Converters* (HPCs). It has been identified that this operational mechanism can be implemented in two different ways:

- The first approach, termed 'type one' HPCs has a working surface which extends from the channel bed up to the *upstream* water surface. This working surface, or blade, moves with the velocity of the upstream flow. In the ideal analysis used to describe such machines, the hydraulic efficiency is related only to the ratio of upstream and downstream submerged depths of the blade, d_2/d_1, and varies between 0.5 and 1.0.

- The second approach, termed 'type two' HPCs has a working surface which extends from the channel bed only up to the *downstream* water surface. For these machines, the working surface, or blade, moves with the velocity of the downstream flow. In the ideal analysis, the hydraulic efficiency is related to the flow rate, and varies between 1.0 and 0.0.

In practice it is anticipated that the efficiency profiles of actual machines will vary from those of the ideal theory because of leakage and turbulent losses. These factors are related to the quality of design and manufacture of actual machines. They were not included in the theories so that clarity in demonstrating the basic principles behind the two forms of HPC could be retained. They are however considered further in the Results and Analysis of the scale model testing, Chapter 8.

Chapter 6

Experimental Concepts

The aim of this work is to develop a new technology for exploiting very low head hydropower. It has been identified through the literature review that hydrostatic pressure may be the driving force behind some hydropower machines. A scientific analysis of this operational principle has been proposed, and identified that there are two ways of approaching the exploitation of hydrostatic pressure. Accordingly two concepts have been developed:

- The Undershot - Hydrostatic Pressure Converter represents a 'type one' HPC, as the submerged portion of the working blade extends from the channel bed to the *upstream* water surface.
- The Middleshot - Hydrostatic Pressure Converter represents a 'type two' HPC, as the submerged portion of the working blade extends from the channel bed only up to the *downstream* surface.

These concepts have been designed so that scale models could be hydraulically tested and used to assess the validity of the proposed theories, and to indicate the potential performance of hydropower machines purposefully designed with the intention of exploiting hydrostatic pressure. It should be noted however that they are prototypes, and do not represent optimised designs.

6.1 Undershot - Hydraulic Pressure Converter

The Undershot - Hydraulic Pressure Converter (U-HPC) represents the 'type one' HPC, however for practical reasons its design differs from the ideal model used in the theory chapter. These design 'compromises' were required as it is not possible to construct a vertical blade which moves laterally and indefinitely.

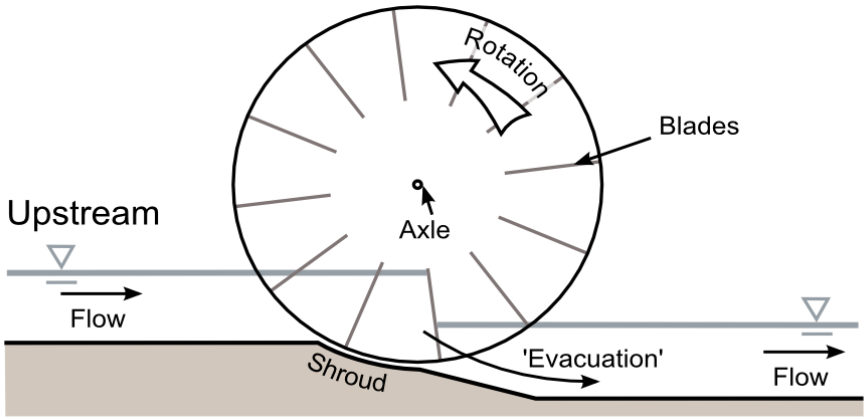

Figure 6.1: Depiction of the U-HPC concept

Referring to Figure 6.1, the U-HPC consists of multiple blades rotating about a common axle, similar to a traditional waterwheel. As such, the channel bed includes a shroud to prevent the opening of leakage gaps as the cells pass the channel bed. The arc length of the shroud is equal to that between the blade tips. It is not equivalent to a large shroud as used by traditional middleshot waterwheels, such as those in Figure 3.6, which were required to generate a height over which the water flows, presenting a constriction to the flow. The blades could either be held between two outer disks, or supported on a spoked frame.

Unlike a traditional undershot waterwheel, the intention is to exploit hydrostatic pressure and not impulse. As such, the blades are simple flat plates. In principle, only one working blade is required at any moment and as such, fewer blades are required. For good operation, it was chosen to have twelve blades; roughly one third as many as a traditional waterwheel. Whilst fewer blades could have been employed, this would have required a larger shroud to enclose the resulting larger cells. This would not have been desirable as the arc length of the shroud increases, the flow path through the installation and operation becomes increasingly similar to that of a traditional waterwheel. Equally, more blades were not employed as they would have unneccesarily added complexity and turbulent losses to the machine without aiding its operatoin

as a 'type one' HPC. It can be seen that head a difference exists across a single blade positioned beneath the axle, due to the two different water depths from the upstream and the downstream.

As the working blade rotates out of the flow, the water contained withing the following cell 'evacuates' under the influence of gravity into the downstream, thus creating the head difference across the subsequent working blade. So that the evacuation could commence at the earliest convenience, the shroud was designed to be asymmetrical, positioned on the upstream side of the wheel. It was felt that a symmetrical shroud would delay the start of the evacuation process, and potentially limit the flow capacity of the wheel. The asymmetrical shroud does however represent a compromise in the design, as the water depth is marginally less upstream of the wheel than within the wheel. The implications of this are discussed further in Section 8.1.5. To aid the evacuation process, the channel bed was designed to initially slope down from the shroud, resulting in a downstream more similar in depth to that of the upstream.

6.2 Middleshot - Hydraulic Pressure Converter

The Middleshot - Hydrostatic Pressure Converter (M-HPC) represents the 'type two' HPC, where the working blade extends only up to the level of the downstream water surface, being mounted on a central hub which is equal in diameter to the head difference. To be consistent with the design of the U-HPC, is was designed to have twelve working blades.

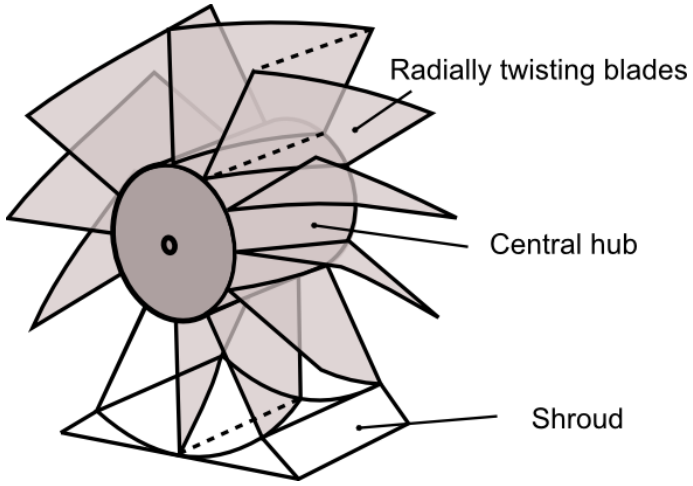

Figure 6.2: M-HPC concept: depiction of wheel and shroud

The design of the M-HPC combines three features from three different machines. Initially inspired by the *Staudruckmaschine*, the cells of this machine are relatively large, with a length

equal to the diameter of the hub. Model testing of the *Staudruckmaschine*, reviewed in section 3.3.6.3, identified that poor design resulted in significant leakage and turbulent losses associated with blade entry and exit. Referring to Figure 6.2, these issues have been addressed in the design of the M-HPC. The periodic opening of gaps as the cells pass the channel bed are prevented by the construction of a small shroud, similar to that used with traditional undershot waterwheels. This has an arc length sufficient to fully enclose one cell. The blades extend radially from the central hub at all points, twisting around the hub along its width to do so. This means the interaction of the blade as it enters and exits the water will be consistent along the width of the wheel. The trailing edge of each blade coincides with the leading edge of the subsequent blade. The intention of the blade design is to provide continual blade tip entry and exit from the water, minimising the potential sources of pulsation in the M-HPC's rotation.

Most significant in the design of the M-HPC, is that the blades are mounted only to the central hub, and the sides of the cells remain open. Referring to Figures 6.3 and 6.4, the combination of the open sides and a suitably designed support structure for the wheel allows the passage of water and air though through the sides of the cells as well as from the front and back, similar to the *Zuppingerrad*. This allows them to commence filling on blade entry upstream and commence ventilation on blade exit downstream as soon as the *inside* edges of the blades, at the central hub, reach the water surfaces, as opposed to the outside blade tips. This design is intended to allow the relatively large blades to enter and exit the water without pushing or lifting water as encountered by the *Staudruckmaschine* (see Figure 3.25). This process is referred to as *side filling and ventilation* in the remainder of the document.

Referring to figure 6.3, the support structure consists of side walls which have length 'x' beside the central hub, increasing to the length of the shroud at the channel bed. This design leaves the cells of the wheel open sided, except in the region where the blade is within the shroud. This is to prevent leakage occurring diagonally though the wheel through the sides of the cells. For the side filling and ventillation to occur, the overall width of the channel must be greater than the wheel itself. This characteristic could lend the M-HPC to installation in the bays of weirs in rivers. Once the water departs the cells of the M-HPC, it has already passed beneath the central hub, descending through the head difference between the upstream and downstream water levels. As a result, the water does not experience an 'evacuation' like the U-HPC, but is simply released into the downstream.

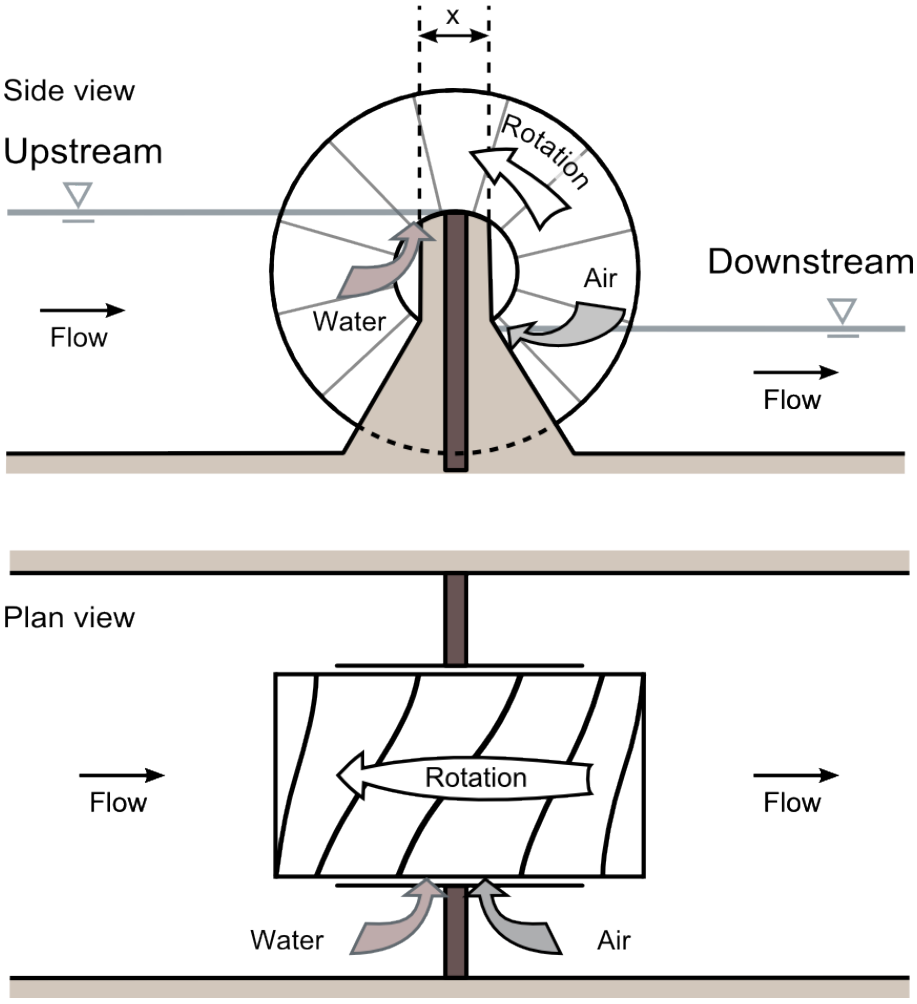

Figure 6.3: M-HPC concept: depiction of support structure and resulting side filling and ventilation

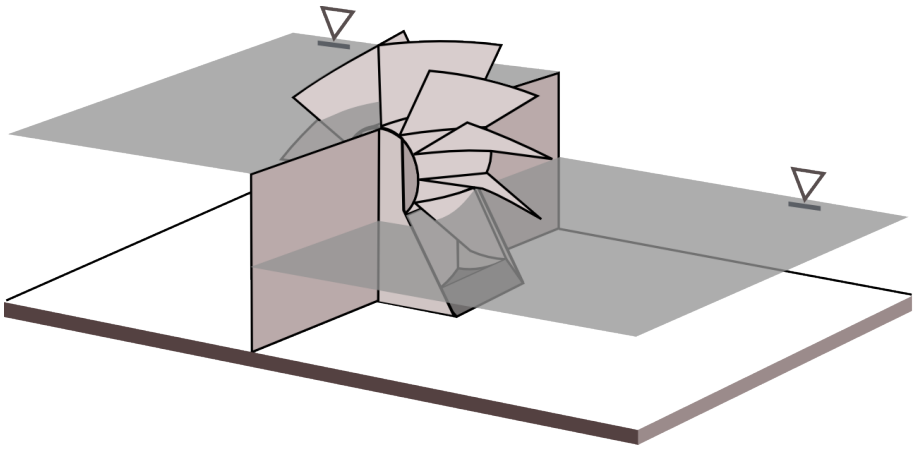

Figure 6.4: M-HPC concept: installation overview

Chapter 7

Experimental Testing

7.1 Summary

A series of scale hydraulic model tests were devised to verify the proposed 'type one' and 'type two' HPC theories, and determine the performance of the U-HPC and M-HPC concepts. These were conducted using two scale models of the U-HPC, referred to as *small scale* and *large scale*, and one model of the M-HPC. The tests can be sumarised as follows:

- The small scale U-HPC was tested to determine the hydraulic efficiency at a range of rotational speeds, flow rates and head differences. The purpose of this testing was to verify whether or not the relationship between the d_2/d_1 ratio and the efficiency proposed by the 'type one' HPC theory holds. Due to the nature in which these tests were conducted, they are referred to as *self-levelling* tests.

- The small scale U-HPC model was also tested to determine the hydraulic efficiency at a range of rotational speeds and flow rates, but with a constant head difference, representing a river installation. These tests are referred to as *constant level* tests. These tests were devised to be used in conjunction with the Froude scaling laws, outlined in Appendix B, providing an indication of the performance of full scale U-HPCs.

- The large scale U-HPC model was tested at a bigger test facility, in a repeat of the small scale U-HPC *self-levelling* tests. This was done so that it could be ascertained whether or not *scale effects* were present during the small scale tests, potentially distorting the full scale estimates. Scale effects are discussed further in Appendix B.

- The M-HPC model was tested to determine its efficiency at a range of rotational speeds and flow rates but with a constant head difference, equal to the diameter of the central hub as intended. Once again, these tests represented a river installation and are referred to as *constant level* tests. The data from these tests was also used in conjunction with the Froude scaling laws, to indicate the performance of larger, full scale scale M-HPC installations. The conclusions from the large scale U-HPC tests with regards to scale effects were applied equally to the scale estimates of the M-HPC data.

The following sections in this chapter describe the scale models constructed of the U-HPC and M-HPC concepts, and the hydraulic flumes in which they were tested. This is followed by a general overview of the measurement equipment, techniques, and equations used. The final sections, 7.3 and 7.4, describe the experimental procedure for each of the four test series summarised above. The four test series are also summarised as a test matrix in Appendix C, along with some comments on the actual testing.

7.2 Equipment and Measurement Techniques

7.2.1 Models and flumes

7.2.1.1 *Small scale* U-HPC

The small scale U-HPC model and its critical dimensions are shown in Figure 7.1 and Table 7.1. Its construction consisted of twelve perspex blades mounted between two, one metre diameter perspex disks. The model was mounted on a stainless steel axle, running in two sets of pillow block mounted ball bearings. Keyed directly into the axle was a pulley, forming part of the power take-off system, described in Subsection 7.2.2.3. The shroud was cut from engineering foam, with the upstream channel bed artificially raised within the hydraulic flume. This model was designed to be tested in a hydraulic flume with a cross sectional area of 0.3m x 0.4m (width x height) and a maximum flow rate of 20 l/sec, as shown in Figure 7.2.

7.2.1.2 *Large scale* U-HPC

The large scale U-HPC model and its critical dimensions are shown in Figure 7.3 and Table 7.2. Its cross section was geometrically similar to the small scale U-HPC, but 160% larger. The width of the model was determined by the flume in which it was tested, and was four and a half times wider than the small scale U-HPC. The model consisted of twelve pvc blades mounted on a spoked frame constructed from mild steel angle section. This was bolted to three central disks mounted on a steel axle, running in two pillow block mounted ball bearings. The pulley required by the power take-off was not directly attached to the wheel's axle. As greater torques were anticipated at the larger scale, a single synchronous belt gear phase was installed between the wheel and the pulley, stepping up the rotational speed by a ratio of 1:8.8. The efficiency of this gearing was assumed to be 95% as indicated by the manufacturer. The shroud was constructed from four pre-cast concrete sections, with the upstream channel bed artificially raised within the hydraulic flume. This model was designed to be tested in a hydraulic flume with a cross sectional area of 1.4m x 0.6m and a maximum flow rate of 300 l/sec, as shown in Figure 7.4.

7.2.1.3 M-HPC

The M-HPC model and its critical dimensions are shown in Figure 7.5 and Table 7.3. It was constructed from twelve hand formed aluminium blades, which were slotted into aluminium spokes mounted onto the ends of a perspex central hub. A stainless steel axle and power take-off pulley were designed to be submerged in the upstream, and the model ran in two wetted plain bearings machined from nylon. The M-HPC model was tested in a *specially constructed* flume, with a cross sectional area of 0.75m x 0.4m and a maximum flow rate of 25 l/sec, as shown in Figure 7.6. Although this flume has similar height and flow to that used for the small scale U-HPC tests, it had more than twice the width, allowing the M-HPC to have sufficient width and operate with side filling and ventilation as intended.

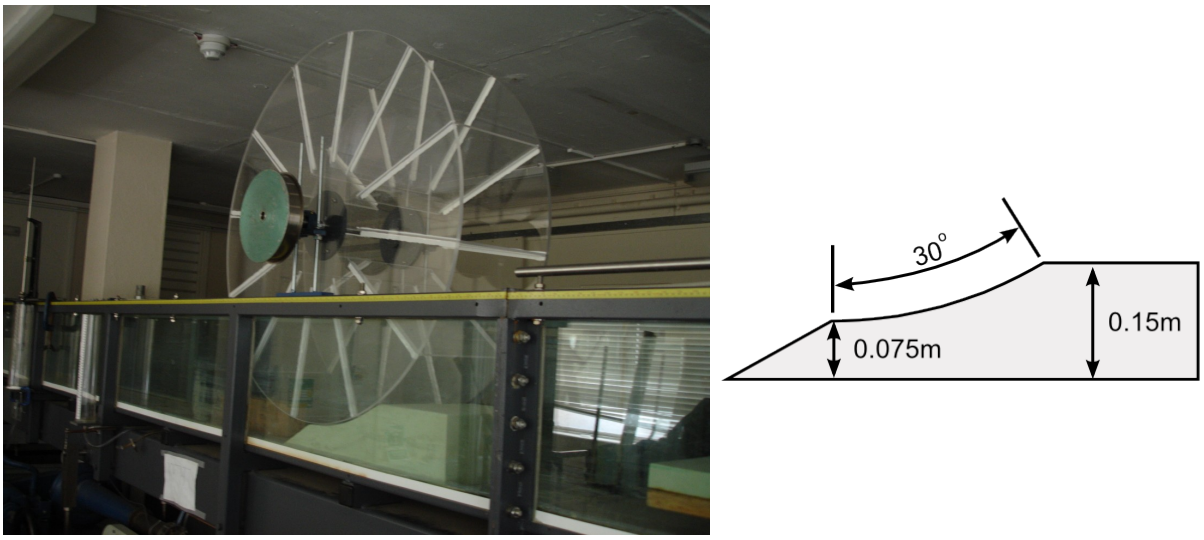

Figure 7.1: a) Image of small scale U-HPC model, b) Dimensions of the shroud

Dimension	mm, where appropriate	Dimension	mm
Outside diameter	1000	Blade length	350
Internal Width (between disks)	275	Gap width at sides, g_s	2
Disk thickness	8	Gap width beneath wheel, g_b	2
Number of blades, n	12	Pulley diameter	216
Blade thickness	6		

Table 7.1: Dimensions of small scale U-HPC model

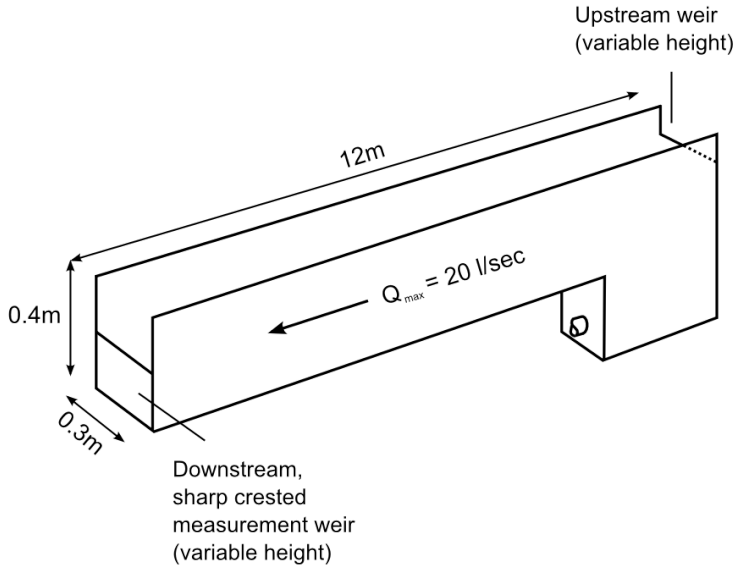

Figure 7.2: Depiction of hydraulic flume used for the small scale U-HPC testing

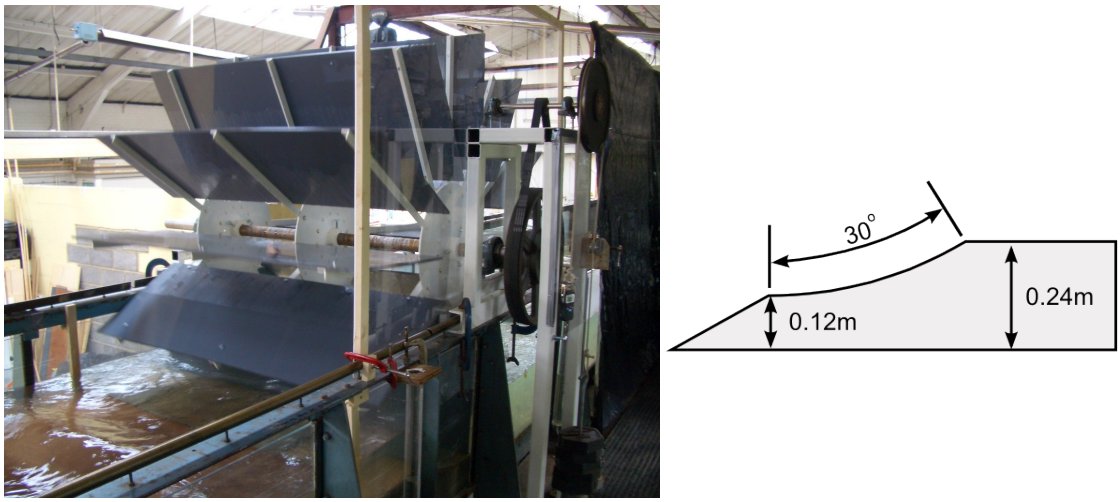

Figure 7.3: a) Image of large scale U-HPC model, b) Dimensions of the shroud

Dimension	mm, where appropriate	Dimension	mm
Outside diameter	1600	Gap width at sides, g_s	8
Wheel width	1360	Gap width beneath wheel, g_b	5
Number of blades, n	12	Pulley diameter	295
Blade thickness	9	Gear ratio	1:8.8
Blade length	550		

Table 7.2: Dimensions of large scale U-HPC model

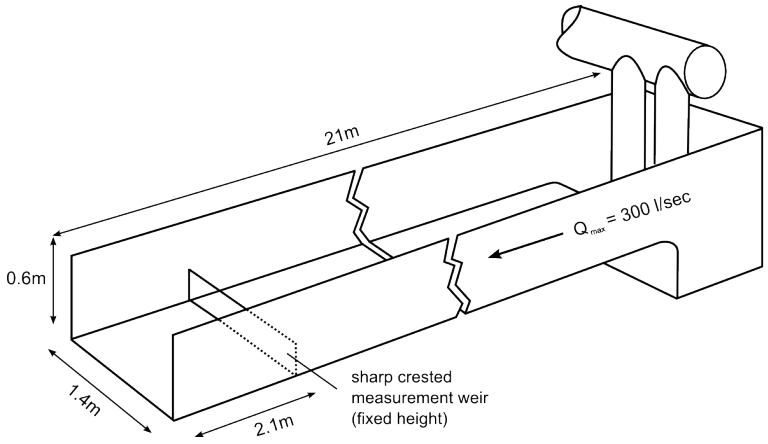

Figure 7.4: Depiction of hydraulic flume used for the large scale U-HPC testing

Figure 7.5: Image of M-HPC model

Dimension	mm, where appropriate	Dimension	mm
Outside diameter	450	Blade thickness	1
Hub diameter	150	Blade length	150
Wheel width	235	Gap width at sides, g_s	4
Channel width (flume)	750	Gap width beneath wheel, g_b	3.5
Number of blades, n	12	Pulley diameter	100

Table 7.3: Dimensions of M-HPC model

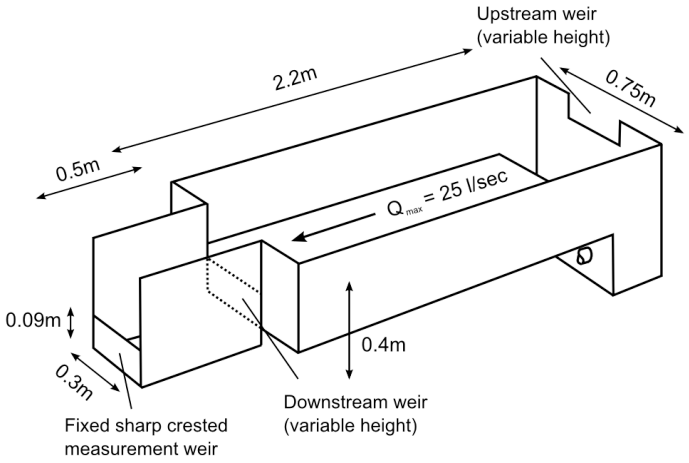

Figure 7.6: Depiction of hydraulic flume used for the M-HPC testing

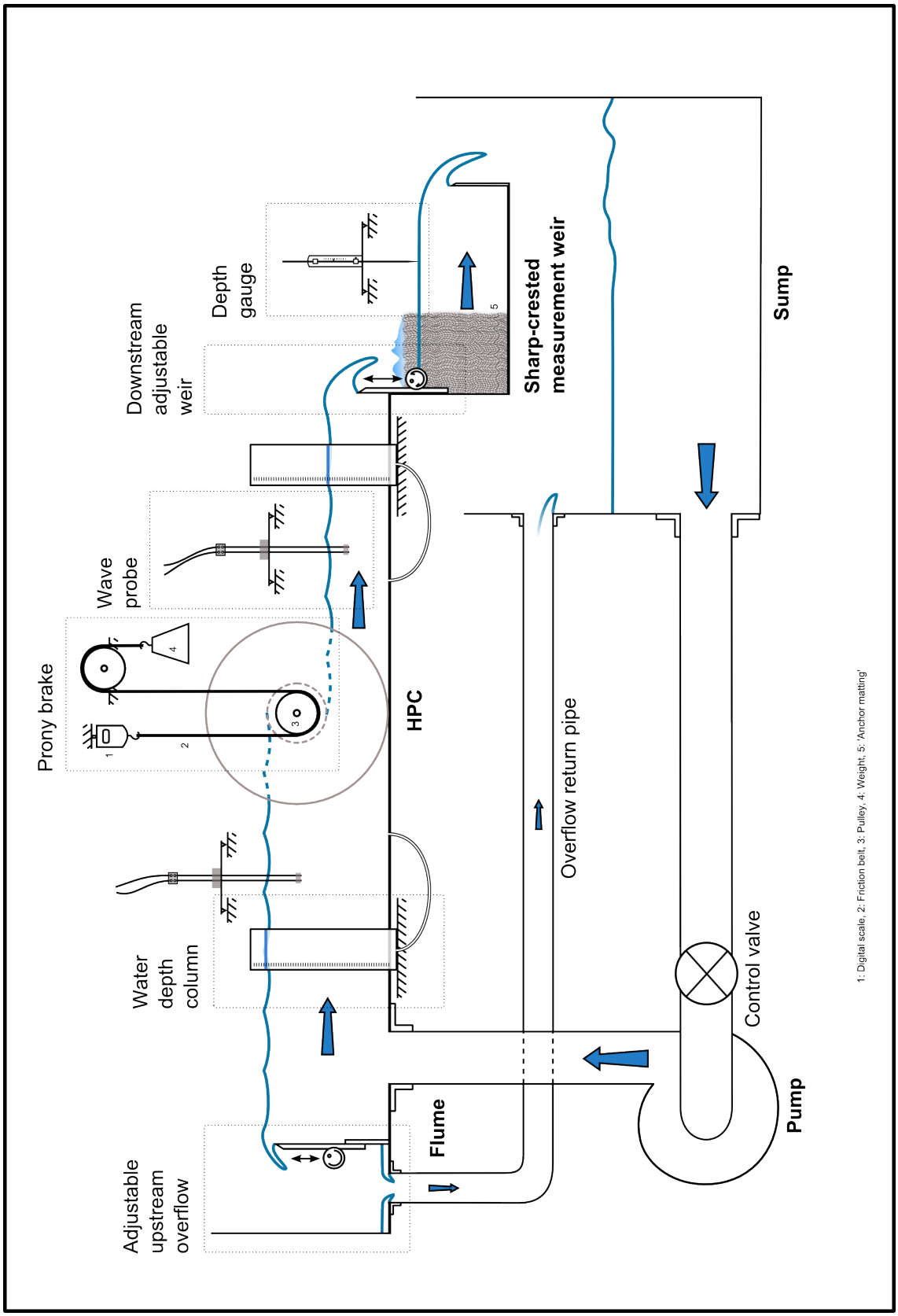

Figure 7.7: Representation of experimental equipment and arrangement

7.2.2 Equipment, setting up and measurement

The general setup of the hydraulic tests conducted is depicted in Figure 7.7, using the M-HPC model and its purpose built flume as an example. The main components of the experimental setup are indicated with regards to adjusting and recording the water levels, the flow rate, and the load being driven by the HPC being tested.

During testing, raw data such as depths, weights and speeds would be recorded. The accuracy of these direct measurements are summarised in Subsection 7.2.2.7. Variables of interest, such as power and efficiency, were calculated from the raw data using purpose written spreadsheets. The following Subsections discuss the adjustment of the experimental setup, the measurement and accuracy of the raw data, and the calculation of the remaining variables.

7.2.2.1 Water levels

The upstream and downstream water levels were measured to within ±1mm with the aid of damped water columns. Referring to Figure 7.7, these consisted of transparent perspex tubes with a diameter of 100mm being positioned externally from the flume, connected to the flume bed via 4mm diameter tubing. The principle behind this arrangement is that the water level within the column will equalise with the average water level within the flume at the location of the pipe, whilst any short term fluctuation in the depth resulting from waves or turbulence are damped. The level could then be read directly from the column, which had depth markings. These markings were calibrated by partially filling the flume channel, terminating the flow of water and retaining the water within the flume by raising weirs and closing valves. The depth within the flume would then be measured accurately with the aid of a depth gauge, and the corresponding value marked onto the water column. A ruler marked in millimetres was then adhered to the column as appropriate.

The testing of the U-HPC in self-levelling conditions did not require the fine adjustment of the upstream and downstream water levels. In contrast, the constant level tests of both concepts did. It was determined in preliminary tests of the small scale U-HPC that the upstream and downstream levels, the rotational speed of the wheel, and the flow rate were all inter-dependent. Alteration of any one would affect the others. Despite this, the speed of rotation and flow rate could be altered primarily through manipulation of the load applied to the wheel and the supply

from the flume pump. Similarly, the downstream level could be altered through the adjustment of the downstream weir. The problem during these preliminary tests arose as conventional flumes do not provide any control of the water level *upstream* from any object placed within the flume. Instead the upstream level was dependent on obtaining the precise corresponding flow, head and rotational speed of the remaining variables. A slight adjustment to any one of these was found to result in a large alteration in the upstream water level, of many millimetres. Following any adjustment, it could take up to thirty minutes for the variables to find their new steady-state equilibrium. Once this was obtained, further alterations could be made once the steady-state error in levels was determined. Overall this process meant that obtaining a single data point could take several hours. What was required was a direct method of controlling the upstream water level which had a reduced influence on the remaining variables. What was devised was an 'adjustable upstream overflow'. Depicted in Figure 7.7, this device consisted of an adjustable height weir positioned upstream from the HPC model being tested. The supply of water to the flume channel would be set marginally higher than required, and the excess water would overtop the overflow. It was then piped directly to the sump of the flume, bypassing the model and not being included in the flow measurement, which occurred at the sharp crested weir located in the downstream. With this arrangement, any adjustment to the other three variables would result in only very slight upstream level changes. Precise adjustments of fractions of millimetres could then be made, and the new steady-state equilibrium obtained within two minutes. The adjustable upstream weir was retrofitted to the 0.3m wide flume used for the small scale U-HPC tests, and included within the design of the purpose built 0.75m wide flume for the M-HPC tests. It was an essential component for conducting constant level tests within acceptable time frames. It was not possible to retrofit the 1.4m wide flume, this being why 'constant level' tests were not repeated using the large scale U-HPC model.

7.2.2.2 Flow rate

The flow rate was measured using a sharp crested measurement weir placed downstream of the model being tested, being the final structure the water must negotiate before returning to the flume sump. This location was essential as it measured only the flow which went through the model, and not the excess flow from the pump which went over the upstream overflow. Standard equations were used in conjunction with the sharp crested weirs to calculate the flow rate (Chanson 2001). These are shown as Equations 7.1 and 7.2, where t_1 and $\triangle Z$ are the water depth and weir height as indicated in Figure 7.8. Essential to the correct operation of a sharp crested weir is that the reverse side of the weir, marked 'x', is aerated and subject to atmospheric pressure. The small scale U-HPC and M-HPC experimental setups used 'anchor matting', a form of plastic mesh, to remove waves and turbulence from the water departing the model, as shown in Figure 7.7. This resulted in a smooth laminar flow on approach to the measurement weir, the depth of which was measured to an accuracy of ±0.2mm using a depth gauge. The large scale U-HPC experimental setup measured this depth to an accuracy of ±0.5mm using a damped water column. The position of measurement was upstream from the weir, a distance equal to 1.5 times the width of the measurement weir. The heights of the measurement weirs were measured directly with an accuracy of ±0.5mm.

$$q = \frac{2}{3} C \sqrt{2\,g(t_1 - \Delta Z)^3} \tag{7.1}$$

$$C = 0.611 + 0.08 \frac{t_1 - \Delta Z}{\Delta Z} \tag{7.2}$$

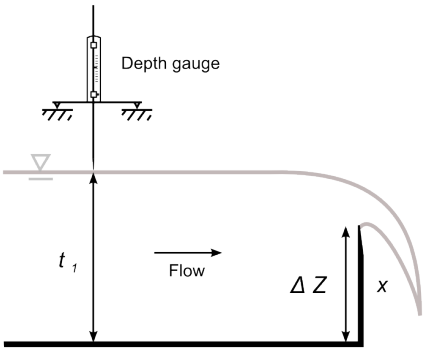

Figure 7.8: Sharp crested weir

7.2.2.3 Rotational speed control and power output

The speed control and power output of all three models was controlled and measured with the use of a *Prony Brake*. The Prony Brake is a traditional method of of applying a controlled and measurable load to a rotating axle. Shown in the centre of Figure 7.7 in its inverted form on the M-HPC model, a stationary friction belt slips on the surface of a pulley on the rotating axle. A 'weight' attached to this belt applies tension to it which creates friction against the pulley. The resulting torque reduces the weight transmitted through the belt to the 'counterweight', which takes the form of a securely fixed digital scale. The resulting power of the rotating axle is the torque multiplied by the angular speed giving Equation 7.3, where m_{weight} and $m_{counterweight}$ are the mass of the weight and counterweight in kg, r is the radius of the pulley in metres, and f is the frequency of rotation (s^{-1}). The weights and digital scale used were accurate to $\pm$0.005kg. The frequency of rotation was recorded by timing five or more complete revolutions (more at higher speeds) and using Equation 7.4. For the purposes of calculating error bars it was taken as accurate to $\pm$0.3 rpm.

$$P_{out\,measured} = (m_{weight} - m_{counterweight})g \times r \times 2\,\pi \times f \tag{7.3}$$

$$f = \frac{number\ of\ revolutions}{time,\ s} \tag{7.4}$$

Both the small and large scale U-HPC models ran in lubricated ball bearings above water level. The friction of these units was considered to be negligible and the power output was taken as that calculated using the Prony Brake, with the efficiency of the synchronous belt drive being taken into account for the large scale U-HPC.

In contrast the M-HPC model ran in submersed plain nylon bearings. These were considered to not give a scaled equivalent of the sealed roller bearings which would be used for a full scale M-HPC, instead providing greater friction and thus reducing the power output reading in the scaled test environment. Therefore the relationship between friction and the rotational speed was quantified as the 'power lost to friction', $P_{friction}$, and the power output of the M-HPC model was calculated using Equation 7.5.

$$P_{out\,M-HPC} = P_{out\,measured} + P_{friction} \tag{7.5}$$

The relationship between friction and rotational speed was ascertained by wrapping a chord around the pulley and attaching weights to the chord. The weights would drop under the influence of gravity, accelerating the wheel from zero rpm up to a steady-state speed where the force of the friction was in equilibrium with that of the weight, falling under gravity. The machine as a whole would be tested dry, without water providing resistance to the blades. However, as the bearings would be submersed in the test environment, these friction measurements were conducted with the bearings alone made wet. The steady-state speed was measured by marking 30 degree radial lines on the wheel and recording its rotation using a digital camera with a frame rate of 25 frames per second. The 'power lost to friction' at this speed was calculated using equation 7.3 with the counterweight value set to zero. The speed would be measured 5 times for each weight, and tests would be conducted with three separate weights giving three steady-state speeds of rotation. A graph of speed versus power lost to friction would be plotted and a linear line would be added, intersecting the axes at (0,0). The gradient of this line would be recorded and added to the data spreadsheet in the form of $y = mx$. Thus the power lost to friction could be calculated in the spreadsheet based upon the speed of rotation. Friction tests were conducted when the M-HPC model was first installed, halfway through testing and again on completion of testing. This allowed the running in of the bearings to be recorded, accounted and compensated for.

7.2.2.4 Hydraulic power input and efficiency

The hydraulic power input, required so that the hydraulic efficiency of the model being tested could be calculated, is a function of the head difference being exploited and the flow rate. The power input and hydraulic efficiency were calculated using equations 7.6 and 7.7.

$$P_{in} = (d_1 - d_2)\,\rho\,g\,Q \tag{7.6}$$

$$\eta = \frac{P_{out}}{P_{in}} \tag{7.7}$$

7.2.2.5 Wave generation

The generation of waves by the small scale U-HPC and M-HPC models was recorded with the use of wave probes. Referring to figure 7.7, these consisted of two electrically isolated 2.0 mm diameter stainless steel rods separated by 10 mm, partially submersed in the water. An amplifier measured the potential difference across the two rods, which increased with the length of submersion. The output from the amplifier, varying with the wave profile, was recorded using a PC in real time. The wave probe arrangement was calibrated by submersing the rods into stationary water with roughly the same depth as the average expected during testing. The output, recorded in mV would be noted at this height, and also with the probes raised by 10mm. The difference in output would thus correspond to 10mm change in water level relative to the probe, and this relationship could be applied to the test data with the use of a suitably constructed spreadsheet.

7.2.2.6 Rotational quality

The 'rotational quality' describes how consistently the wheels turn during each rotation. Pulsation is considered to be an undesirable property. Whilst the manual measurement of the average frequency of rotation was sufficient for the power output calculation, a device was required with sufficient resolution to observe variation with the passing of individual blades. To record the rotational quality a device was sought which did not apply additional load to the models, as any additional load would not be accounted for by the Prony Brake measurement. This ruled out any form of mechanical reader, so a non-contact optical system was required.

The solution was a computer optical mouse positioned beside the rotating pulley, used in conjunction with purpose written java software (see acknowledgements). As the pulley of the M-HPC model was submersed, the mouse was hydraulically sealed. When a computer mouse detects movement, the in-built processor sends data to the computer. As Microsoft Windows automatically connects the mouse for its original intended purpose, the software written would re-position the cursor to the centre of the monitor after each recording event. The frequency at which the data was recorded was adjustable, a form of resolution control. The output from the software included the number of pixels moved in the x and y coordinates and the computer time stamp at which they were recorded. This information could then be processed using spreadsheets to plot velocity in pixels per millisecond versus time. The result would then be calibrated, comparing the average velocity in pixels per second against the average frequency of rotation, measured manually with a stop watch. The relationship between velocity and rotational speed was assumed to be linear, and the data recorded could thus be processed to output the frequency of rotation recorded in real time.

7.2.2.7 Measurement accuracy

As described in Subsection 7.2.2, raw data such as water depths, weights and speeds would be recorded during experimental tests. The accuracy of these measurments is summarised in table 7.4. Variables of interest, such as power and efficiency, were then calculated from the raw data using purpose written spreadsheets. The spreadsheets also performed sensitivity analysis of the data, shown as error bars in the Results and Analysis Chapter. This was done by performing each calculation using the measured data, and also the same data adjusted to upper and lower boundaries as appropriate, based on the accuracy with which they were measured. As such the error bars plotted in the Results and Analysis Chapter represent the absoulte maximum and minimum values which the corresponding data point could have held.

Parameter	Description	Measurement accuracy
d_1 and d_2	Upstream and downstream water depths	$\pm$1 mm
t_1, for Small scale U-HPC and M-HPC testing	Water depth upstream from sharp crested measurment weir	$\pm$0.2 mm
t_1, for large scale U-HPC testing	Water depth upstream from sharp crested measurment weir	$\pm$0.5 mm
$\triangle Z$	Depth of sharp crested measurement weir	$\pm$0.5 mm
m_{weight} and $m_{counterweight}$	Mass of the Prony Brake weight and counterweight	$\pm$0.005 kg
rpm	Speed of rotation	$\pm$0.3 rpm

Table 7.4: Measurement accuracy of raw data

7.3 U-HPC Test Procedure

7.3.1 Self-levelling tests at the small scale

The first tests of the small scale U-HPC model were devised to measure the hydraulic efficiency of the model at a range of d_2/d_1 ratios, and thus determine whether the proposed theory could be supported or not. It was anticipated that the water levels were a function of three variables. The upstream level would be a function of the flow rate and the rotational speed of the wheel, whilst the downstream level would be a function of the flow rate and the downstream conditions, determined by the height of the weir.

Five downstream weir heights were chosen; 30mm, 80mm, 130mm, 180mm, and 230mm. For each of these weir settings, a preliminary test would be conducted to determine the maximum, medium and minimum flow rates at which the wheel was judged to run acceptably. This is discussed further in Subsection 8.1.6. The flow rate would be determined by the pump speed and control valve of the flume, being independent of the model. With the minimum flow rate and weir setting selected, the Prony Brake would be loaded until the limit was reached, beyond which the wheel could not rotate continuously or the upstream level would overflow the flume walls. The speed of rotation and the water depths would self-regulate to find a steady-state equilibrium where all of the variables would remain steady. This is the reasoning for referring to these tests as 'self-levelling'. At this point all the data would be recorded as described in Section 7.2. The weight on the Prony Brake would then be reduced in five further steps, allowing the speed of the wheel to increase, concluding with no load, allowing the wheel to freewheel. The data would be collected at each speed. The whole procedure would then be repeated at the medium and maximum flow rates, and also with the downstream weir set at the four remaining, pre-determined heights.

7.3.2 Constant level tests at the small scale

The small scale U-HPC was also tested with the upstream and downstream levels being held constant, whilst the speed of the wheel and the flow rate were increased. This was achieved in conjunction with adjustment of the downstream weir and purpose-devised upstream overflow. The levels at which the upstream and downstream were to be held were selected based on the results of the self-levelling tests, the criteria being levels at which the U-HPC operated with acceptable hydraulic efficiency.

The tests would commence by determining the minimum flow and maximum load on the Prony brake at which the target upstream and downstream water levels could be maintained, whilst the wheel would run as slowly as possible, but continuously. The required data would then be recorded, and the load on the Prony Brake would be reduced in six steps, allowing the speed of the wheel to increase until the final data set would be freewheel at no load. Each time the load was altered, the flow rate from the flume pump and the adjustable weirs would have to be adjusted to maintain the target water levels, before data could be collected. The constant level tests were conducted a total of five times.

7.3.3 Self -levelling tests at the large scale

The large scale U-HPC model was tested in the same manner as the small scale self-levelling tests. These tests were devised to verify whether or not scale effects had been present at the smaller scale, and whether the constant level test data could be used in conjunction with the Froude scaling laws to indicate the full scale performance of the U-HPC design. The Froude scaling laws and scale effects are discussed in Appendix B. As the large scale U-HPC model was 1.6 times larger than the small scale model, the downstream weir heights chosen were: 48mm, 128mm, 208mm, 288mm and 368mm. Constant level tests were not conducted using the large scale U-HPC due to limited availability of the 1.4m wide flume, and because it was not feasible to modify this flume to include an adjustable upstream overflow as required.

7.4 M-HPC Test Procedure

7.4.1 Constant level tests

The M-HPC design is different to the U-HPC in that it is designed to exploit a specific head difference, equal to the diameter of the central hub. Therefore the M-HPC model only underwent 'constant level' testing. The upstream level would coincide with the top of the central hub, whilst the downstream level would coincide with the bottom of the central hub.

The tests would commence by determining the minimum flow rate and maximum load that could be applied to the Prony Brake such that the target levels could be obtained whilst the wheel ran at a slow but continuous speed. The relevant data would then be recorded, as described in Section 7.2. The load on the Prony Brake would then be reduced in five steps, allowing the speed of the wheel to increase, with the final measurements taken when the wheel ran at freewheel with no load. The pump and weirs would require adjustment so that the target water levels could be maintained for each speed of rotation of the wheel. These constant level tests were also conducted a total of five times.

Chapter 8

Results and Analysis

This Chapter gives the results of the scale model testing of the Undershot and Middleshot Hydrostatic Pressure Converters (U-HPC and M-HPC). These two concept machines where detailed in Chapter 6 and designed to represent the 'type one' and 'type two' HPCs identified in the theory, Chapter 5. The analysis of these machines includes:

- Comparison with the ideal theories they were designed to represent.
- Investigation into the effects of leakage and turbulent losses on the machines, and the impact this has on the efficiency profiles.
- Indication of the potential full scale performance of the two machines.
- A description of the observed operational characteristics of the machines, such as wave generation and the quality of rotation.

8.1 Undershot - Hydrostatic Pressure Converter

The U-HPC concept was designed to test the principle of 'Type one' HPCs as described in the theory, Chapter 5. The results and analysis of this machine are broken down into the following sections:

- Section 8.1.1 covers the 'self-levelling' tests which were designed to verify whether the relationship between the ratio d_2/d_1 and efficiency proposed in the theory holds.
- Section 8.1.2 covers the 'constant level' tests which investigate the efficiency and power output characteristics of the U-HPC in a river scenario where the water levels need to be maintained. A brief comparison is made with the ideal theory, and the influence of both leakage and turbulent losses is observed, both of which are design related factors. These factors are then investigated in greater detail in the following section.
- Section 8.1.3 investigates the influence of leakage and then turbulence on the U-HPCs hydraulic efficiency profile. The leakage analysis is confirmed using the experimental data, and utilised in the following section on scale effect analysis.
- Section 8.1.4 analyses whether or not any significant scale effects were present during the testing of the U-HPC model. The results are then used to indicate the potential full scale performance performance of the U-HPC concept.
- Section 8.1.5 analyses the accuracy with which the U-HPC represents the ideal 'type one' HPC model used in the theory. Deviations in the concept's design resulted from the practicalities of designing a working machine, and the significance of these 'compromises' are assessed.
- Section 8.1.6 details the operational characteristics of the U-HPC observed. These included the generation of waves and the quality of rotation.

8.1.1 Operation with variable water depths

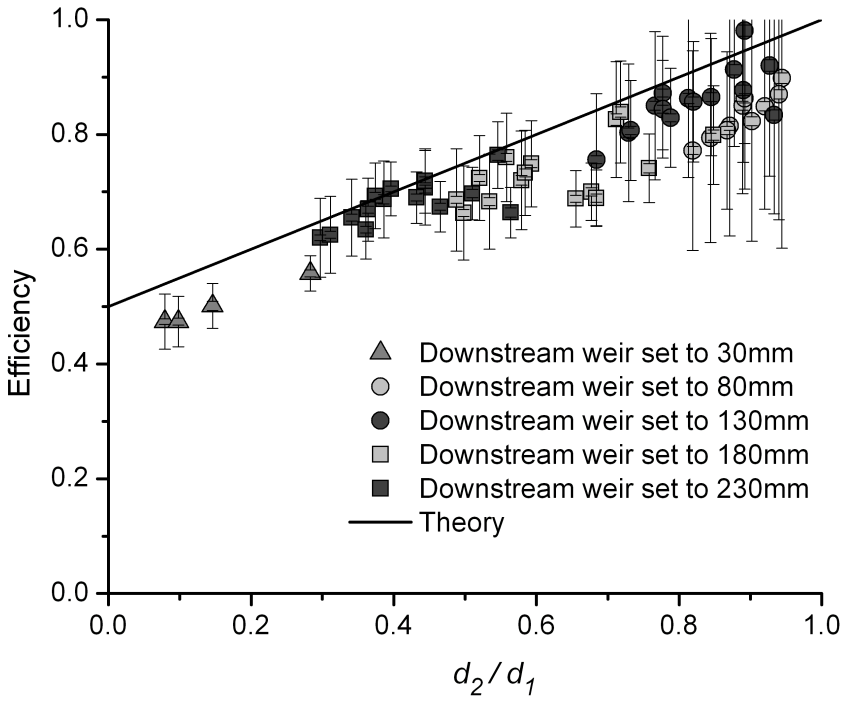

Figure 8.1: Results of U-HPC 'self-levelling' tests (error bars representing the extent of the possible values)

The small scale, 1.0 m diameter model of the U-HPC machine underwent 'self-levelling' tests, as described in Section 7.3. The results of these experiments are given in Figure 8.1, along with the theoretical efficiency line calculated using the ideal 'type one' HPC theory.

- Overall, Figure 8.1 indicates that there is a linear trend in the relationship between the ratio d_2/d_1 and the efficiency. This is consistent with the fundamental relationship identified in the 'type one' HPC theory, although at higher d_2/d_1 ratios there is some discrepancy, as discussed below.

As the water depths and rotational speed of the wheel were self-regulating, it is assumed that the U-HPC would adopt an operational condition at which losses were minimised. This would suggest that each data point represents the maximum possible efficiency of the machine in the given flow scenario. For each d_2/d_1 value, a vertical spread of experimental data can be observed. This is because several flow rates were tested over each measurement weir, resulting in different

Weir height, mm	Q, l/sec	d_1, mm	d_2, mm	d_2/d_1	rpm	η
130	23.4	197	167	0.84	11.6	0.80
180	16.1	232	196	0.84	6.5	0.87

Table 8.1: Comparison between two data points with same d_2/d_1 ratio

d_1 and d_2 depth values with the same d_2/d_1 ratio. For example consider the two data points shown in Table 8.1. Despite the d_2/d_1 ratio being equal, these points have different flow rates and water depths. The resulting difference in rotational speed of the wheel and flow velocities have an influence on the level of turbulent losses contributing to the 7% difference in efficiency. Turbulent losses were not considered in the ideal 'type one' HPC theory, but are discussed further in Section 8.1.3.

Less data was obtained at low d_2/d_1 values as only data where the U-HPC was judged to be operating in 'reasonable' conditions was recorded. This does not include flow rates where the resulting upstream and downstream levels resulted in extreme turbulence, or conditions where the machine was not able to generate a hydrostatic pressure differential as intended. These limitations are discussed in Section 8.1.6. As the head difference tends towards zero as the d_2/d_1 ratio tends towards one, the error bars increase significantly due to the accuracy at which the water depths were measured. However, the quantity and close proximity of the data at the high d_2/d_1 values provide confidence that the trend observed trend does exist.

8.1.2 Operation with constant water depths

The small scale U-HPC model was also tested in 'constant level' conditions as described in Section 7.3. The efficiency and output power of the model are plotted in Figure 8.2, and represent how such a machine would operate when subjected to a constant head difference but a varying flow rate. Following the 'self-levelling' tests, the depths d_1 and d_2 were chosen to be 235mm and 165mm respectively, giving a d_2/d_1 ratio of 0.7. The efficiency as calculated by the ideal 'type one' HPC theory for a d_2/d_1 ratio of 0.7 has also been plotted.

- The 'self-levelling' tests of section 8.1.1 suggested that the efficiency is fundamentally related to the ratio d_2/d_1, as indicated by the ideal 'type one' HPC theory. Referring to Figure 8.2, it is however clear that although the peak efficiency of the of the U-HPC model does coincide well with the theory, in practice the efficiency is also a function of

the flow rate. The difference is attributed to the presence of leakage and turbulent losses observed during the model testing, factors not considered by the ideal theory. The impact of leakage and turbulent losses are investigated further in Section 8.1.3. Despite these losses, the efficiency profile is quite flat; operating with an efficiency over 60% over a large range of flow rates from 5 l/s to 30 l/s.

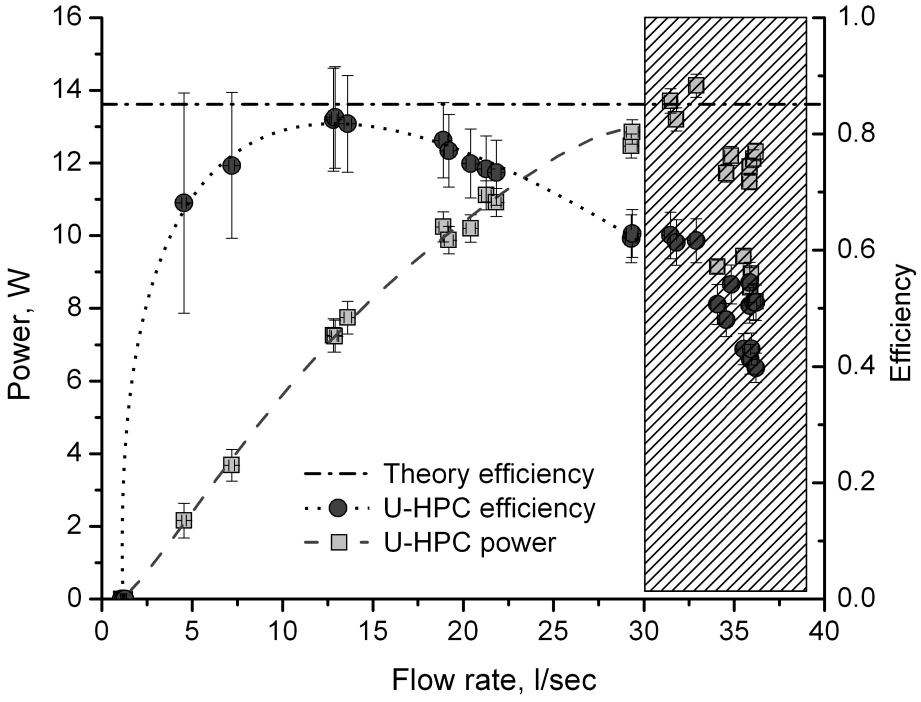

Figure 8.2: Results of the U-HPC 'constant level' tests

The data plotted in Figure 8.2 beyond 30 l/s has been hatched, as limitations in the hydraulic flume used for the testing meant that the upstream water depth, d_1, could not be maintained above this point. Despite this limitation, it is clear that by 30 l/s the efficiency of the U-HPC model was decreasing. For the purposes of the scaling exercise in Section 8.1.4, the peak efficiency is taken as ~80%, and the maximum output power and flow rate, P_{max} and Q_{max}, are conservatively taken to be ~13W and ~30 l/s. Q_{max} occurred when the rotational speed of the wheel was ~12 rpm.

8.1.3 Analysis of leakage and turbulent losses

This section analyses the influence of leakage and turbulent losses, which were observed during experimental testing, on the hydraulic efficiency of the U-HPC. The analysis is conducted by incorporating additional variables into the ideal 'type one' HPC theory. This allows an assessment to be made; as to whether or not the leakage and turbulent losses can account for the difference observed between the experimental data and ideal theory shown in Figure 8.2, and therefore whether the ideal theory holds.

8.1.3.1 Leakage analysis

The rotational speed and corresponding flow rate of the U-HPC model during the 'constant level' tests are plotted in Figure 8.3. It can be seen that there is a linear relationship between rotational speed and flow rate up to 12 rpm and 30 l/sec. Beyond 30 l/sec, the data is not valid as the limitations of the hydraulic flume meant that the upstream water level d_1 could not be maintained.

- Significantly, the minimum flow rate when the wheel was stationary is approximately 1.0 l/s and not zero l/sec. This flow rate is the result of leakage through gaps between the submerged portion of the machine (the blade) and the channel bed and walls in which the water flows. It is proposed that this leakage flow is related to the head difference across the machine, and a theory is developed below.

The leakage flow rate is dependent on the pressure differential across the blade and the gap size, and is estimated by calculating the velocity resulting from the pressure, and multiplying this by the cross sectional area through which the water flows. Referring to Figure 8.4, the blade has width W, whilst the width of the gap beside the blade is g_s and the depth of the gap beneath the blade is g_b. The leakage analysis is broken down into three components. Q_1 is the leakage beside the blade in the region extending between the upstream and downstream water surfaces, and is calculated by Equation 8.1. In this region, the pressure differential and accordingly the velocity of the leakage flow increase with depth. Q_2 is the region beside the blade beneath extending between the downstream level and the bottom of the blade, and is calculated by Equation 8.2. Q_3 is the final region beneath the blade and is calculated by Equation 8.3. In both regions Q_2 and Q_3, the pressure differential and velocity of leakage flow are constant with depth. The total

leakage flow, $Q_{leakage}$, is the sum of the leakage through two side gaps and one bottom gap. The flow rate through the wheel itself is estimated by Equation 8.5. This is the product of the total submersed volume of the cells of the wheel multiplied by the frequency of rotation, where r is the radius of the wheel, n is the number of blades and t is the thickness of the blades.

$$Q_{leakage} = velocity\,of\,flow \;\times\; area\,of\,gap$$

$$Q_1 = \left(\int_{d_2}^{d_1} \left(\sqrt{2gd} \right) dd \right) g_s = \frac{\sqrt{2g}\,(d_1 - d_2)^{1.5}}{1.5}\, g_s \tag{8.1}$$

$$Q_2 = \sqrt{2g\,(d_1 - d_2)}\,(d_2\, g_s) \tag{8.2}$$

$$Q_3 = \sqrt{2g\,(d_1 - d_2)}\,(g_b\,(W + 2\,g_s)) \tag{8.3}$$

$$Q_{leakage} = 2\,(Q_1 + Q_2) + Q_3 \tag{8.4}$$

$$Q_{wheel} = f\,W\,\left(\pi\,\left(r^2 - (r - d_1)^2 \right) - (n\,d_1\,t) \right) \tag{8.5}$$

The leakage flow through the gaps, $Q_{leakage}$, is plotted in Figure 8.3. It can be seen that the line coincides with the flow rate when the wheel was stationary, and in the constant head scenario tested, is constant versus rotational speed. A second line is also plotted which is the combination of the leakage flow and the flow through the wheel itself, called Q_{total}. This represents the complete flow rate and correlates well with the U-HPC data.

- It is concluded that the leakage flow rate through gaps between the blade and the channel is a function of the head difference across the wheel. This leakage flow rate is independent from the rotational speed of the wheel itself.

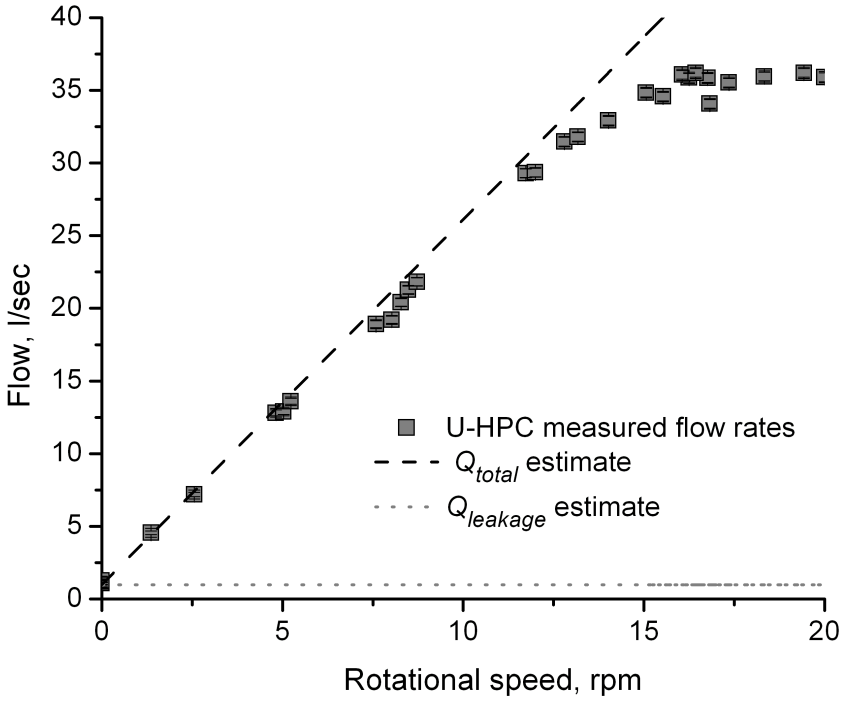

Figure 8.3: U-HPC: relationship between flow rate and rotational speed

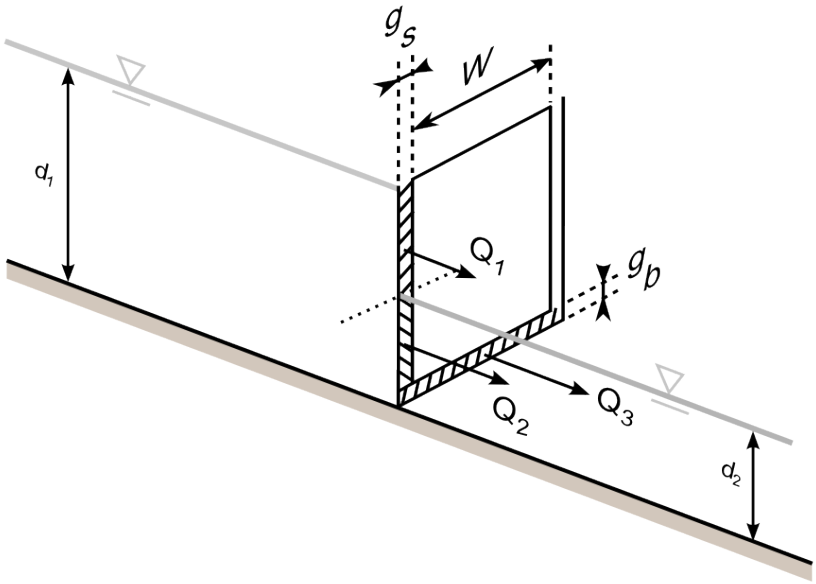

Figure 8.4: Representation of U-HPC leakage gaps

For any given 'type one' HPC, the leakage can be factored into the ideal theory. The leakage can either be calculated using Equation 8.4, or quantified by measuring the flow rate through an installation when the wheel or blade is stationary. The leakage flow is assumed to pass through the installation without contributing to the power output of the machine. In what is being termed the 'leakage adjusted theory', the velocity of the blade and the water acting on it is now not taken as v_1, the upstream water velocity, but a slightly lower value, v_b. This velocity is calculated using the area of the submerged blade and the flow rate through the wheel, Q_{wheel}, Equations 8.6 and 8.7. The leakage adjusted power output is then calculated by multiplying the force exerted on the blade by the hydrostatic pressure by the blade velocity, Equation 8.8.

$$Q_{wheel} = Q_{total} - Q_{leakage} \tag{8.6}$$

$$v_b = \frac{Q_{wheel}}{W d_1} \tag{8.7}$$

$$P_{out,\,leakage\,adjusted} = \rho\, g \frac{d_1^2 - d_2^2}{2}\, v_b \tag{8.8}$$

$$\eta_{leakage\,adjusted} = \frac{P_{out,\,leakage\,adjusted}}{P_{in}} \tag{8.9}$$

The leakage adjusted efficiency, calculated using equation 8.1.3.1 for the constant head scenario tested in Section 8.1.2, is plotted in Figure 8.5. This new efficiency estimate matches the experimental data convincingly at the lower flow rates. As the leakage flow rate is constant, it initially accounts for the entire flow rate when the wheel is stationary, and a decreasing proportion of the total flow rate as the rotational speed of the wheel increases.

- The effect of the leakage is to reduce the hydraulic efficiency of the U-HPC at low speeds of revolution and flow rates. The significance of the leakage on the efficiency decreases at the higher flow rates, where the higher output powers are generated, as the leakage flow accounts for a decreasing portion of the total flow.

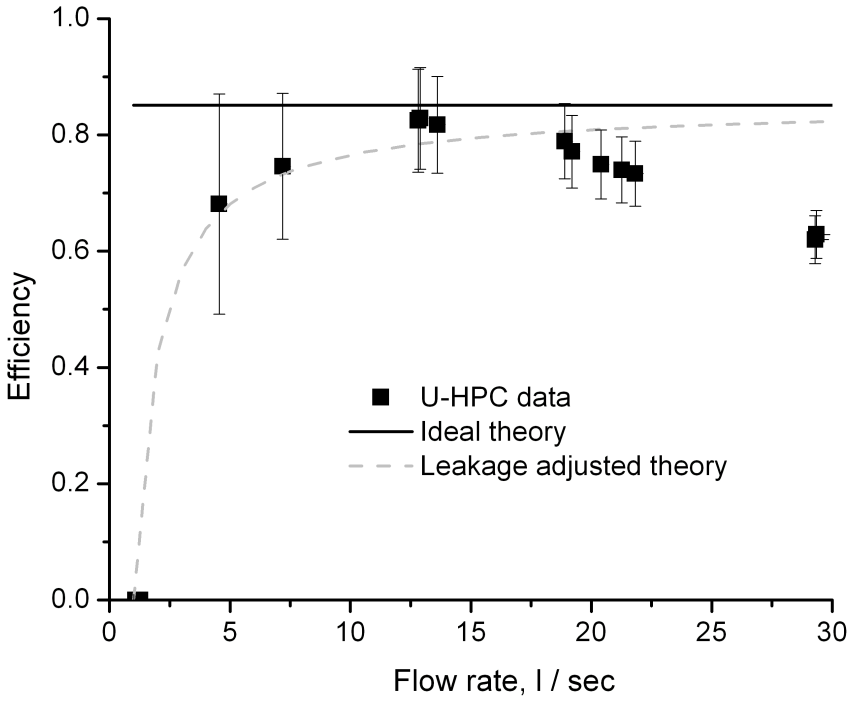

Figure 8.5: U-HPC leakage adjusted analysis

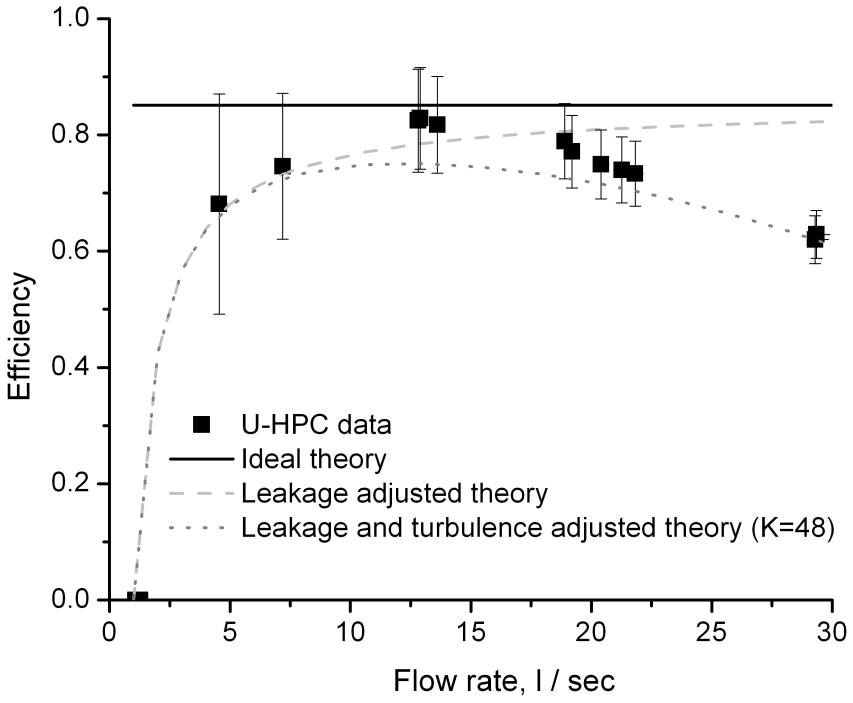

Figure 8.6: U-HPC leakage and turbulence adjusted analysis

8.1.3.2 Turbulent losses analysis

It has been shown that leakage flow through gaps can account for the difference between the efficiency profiles of the ideal 'type one' HPC theory and the experimental data at low flow rates. It is proposed that the remaining difference at higher flow rates can be accounted for by turbulent losses.

In the ideal model, a single vertical blade moved laterally with the exact velocity of the upstream water. In practice, the U-HPC consisted of multiple blades revolving about a central axle. The introduction of the blades into the upstream water flow and their progress through the water towards the downstream was the source of turbulent losses. This was primarily the result of the blade tip entering the water at an angle and with a velocity greater than the average velocity of the water.

The flow situation described above is highly complex, where the blade changes its relative angle and velocity during rotation, and is confined within a tight fitting channel. As such, it is not reasonable to attempt to estimate the turbulent losses using conventional techniques such as those applied to closed pipes or scenarios where objects within flow experience drag. This is because the coefficient values required by such calculations could not be selected with any confidence. What is common to these techniques however, is that turbulent losses are generally modelled as velocity squared losses (Chadwick et. al. 2004). In order to demonstrate the influence of turbulence, a turbulent force which detracts from the power output of the wheel, F_T, was calculated. This was done using Equation 8.32, where the velocity, v_b, is the average blade velocity, and K is a constant which was empirically determined, with a value of 48. This turbulent force was incorporated into Equation 8.8 to give equations 8.11 and 8.34, which estimate the power output and efficiency of the U-HPC with a leakage and turbulence adjustment. The latter is plotted in Figure 8.6.

$$F_T = K\, v_b^2 \tag{8.10}$$

$$P_{out,\, leakage\, and\, turbulence\, adjusted\, theory} = \left(W\, \rho\, g\, \frac{d_1^2 - d_2^2}{2} \; - \; F_T \right) v_b \tag{8.11}$$

$$\eta_{leakage\, and\, turbulence\, adjusted} = \frac{P_{out,\, leakage\, and\, turbulence\, adjusted\, theory}}{P_{in}} \tag{8.12}$$

- Figure 8.6 demonstrates that turbulence, modelled as a velocity squared loss, can account for the difference between the ideal 'type one' HPC theory and the U-HPC experimental data at higher flow rates.

8.1.4 Scale analysis and estimates

One of the stated aims of this work is to indicate the potential full scale performance of any concepts developed. A conventional methodology to achieve this is the application of the Froude scaling laws, which are detailed in Appendix B. As explained in the experimental procedure section, prior to applying these laws, it needs to be determined whether or not the small scale experimental data being scaled exhibited 'scale effects', leading to errors in the scaled estimates. This section analyses the results of the large scale U-HPC model tests and compares them with the smaller scale U-HPC model tests to assess whether scale effects were present. Following this assessment, indications of potential full scale performance are calculated.

8.1.4.1 Large scale U-HPC testing

The large scale, 1.6m diameter U-HPC model was tested in 'self-levelling' conditions in a similar manner to the 'self-levelling' testing of the small scale 1.0m diameter U-HPC. The results of the large scale 'self-levelling' tests are given in Figure 8.7. This Subsection discusses the limitations of the larger scale testing, and explains why only a relatively small amount of data was acquired during the large scale tests.

The original intention had been to test multiple flow rates over five weir heights resulting in efficiency values over a range of d_2/d_1 ratios between 0.1 and 1.0, similar to Figure 8.1. Although the large scale U-HPC experiment was run for short periods of time at full flume capacity, around 300 l/s, experimental data could only be obtained for flow rates up to 160 l/s and d_2/d_1 ratios above 0.6. This was the result of limitations in the design of the experiment. Specifically, the flow measurement weir was installed within the flume and not at its end, as shown in Figure 7.4. This meant that the water could not clear the weir satisfactorily, and at higher flow rates the weir would not aerate as required, making the sharp crested weir equations inapplicable. Also, the Prony Brake could not provide sufficient load to achieve d_2/d_1 values below 0.6 due to overheating. These limitations could not be resolved due to time constraints. Referring to Figure 8.7, only three weir heights and three flow rates could be recorded.

8.1.4.2 Scale effect analysis

The cross sectional geometry of the large scale U-HPC model was similar to the small scale model, but 1.6 times larger. The width of the large scale model was 4.5 times wider than the small scale model, both models spanning the width of the flumes in which they were tested. Although the efficiency is not a function of width, it is known that the leakage through the gap beneath the blade is a function of width, referring to Figure 8.4. Accordingly, the data from both scales has been adjusted such that the efficiency has been re-calculated, excluding leakage. This has been achieved by calculating the leakage flow rate, using the dimensions of the wheel and gaps, the water depths d_1 and d_2, and Equations 8.1 to 8.4. The leakage flow rate was then deducted from the total flow rate in accordance with Equation 8.6, and this value was used to calculate the leakage-independent input power and efficiency. This analysis assumes that the leakage flow does not contribute to the power output of the wheel, instead flowing through the gaps without influence on the working blades.

The adjusted data from both the large and small U-HPC tests is plotted in Figure 8.8. The large scale data has less of a vertical spread than the small scale data, however this may be accounted for by the small range of flow rates tested. Referring back to Table 8.1, it has been demonstrated that d_2/d_1 ratios tested at higher flow rates can operate at lower efficiency.

- Despite the limited data from the large scale tests, it is concluded through induction that no significant scale effects were exhibited by the small scale testing. If the large scale data appears to be marginally higher in efficiency, this only supports the conclusion that the small scale data was not artificially boosted through scale effects. The small scale data can therefore be conservatively scaled using the Froude scaling laws to indicate the performance of larger scale U-HPC hydropower machines.

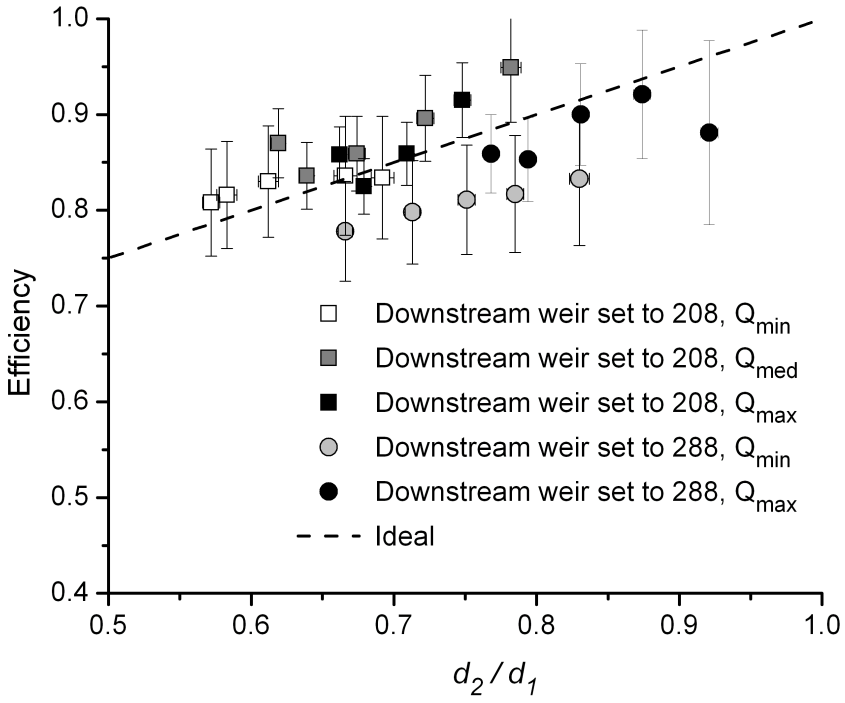

Figure 8.7: Results of the large scale U-HPC 'self-levelling' tests

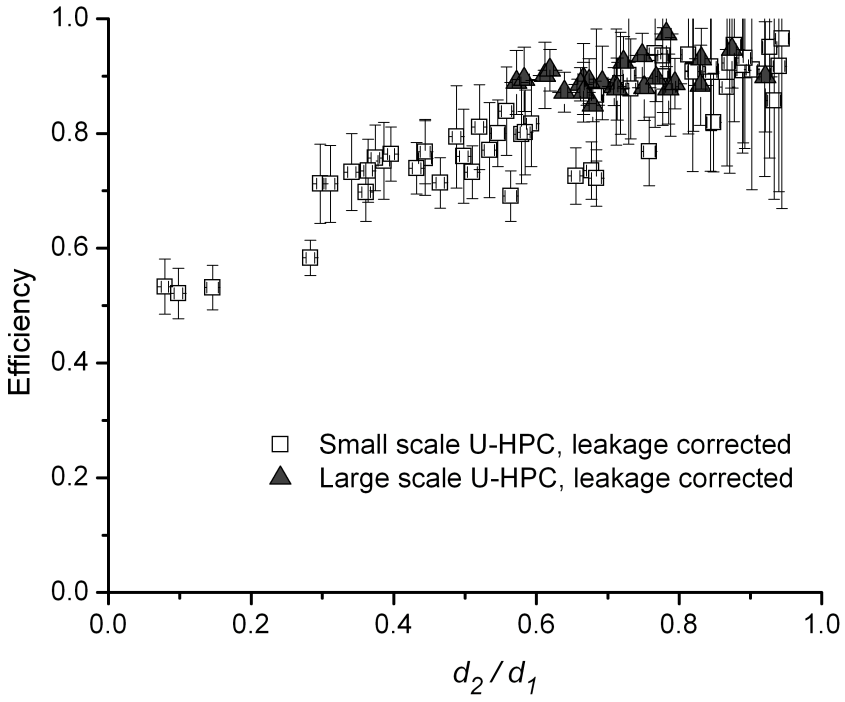

Figure 8.8: Combination of both scales of U-HPC tests

8.1.4.3 Indication of full scale performance

Scale	Head, m	Q_{max}, $\frac{m^3}{s}$ per m width	P_{max}, kW per m width	Upstream depth, m (prior to shroud)	Upstream velocity at $Qmax$, m/s	Downstream depth, m (beyond shroud)	Downstream velocity at Q_{max}, m/s
1:3.6	0.25	0.74	1.18	0.30	2.43	0.86	0.86
1:7.1	0.50	2.08	6.69	0.61	3.43	1.71	1.21
1:10.7	0.75	3.83	18.45	0.91	4.20	2.57	1.49
1:14.3	1.00	5.89	37.87	1.21	4.85	3.43	1.72

Table 8.2: Scaled estimates of full scale U-HPC performance

The 'constant level' tests of the small scale U-HPC model determined that the peak efficiency was ∼80%, P_{max} was ∼13W and Q_{max} was ∼30 l/sec at ∼12 rpm. This data and the dimensions and geometry of the model tests have been scaled using the Froude scaling laws to indicate the potential performance of larger machines for heads up to 1.0m. This is shown in Table 8.2, where the Q_{max} and P_{max} are provided per metre width of machine. Estimates beyond 1.0m head are not provided as the outside diameter of the machine is 14 times greater than the head difference, and machines larger than this, although possible, are considered unlikely. A limitation of the data is that the gap size and and the leakage flow rate are also scaled, the latter always being ∼6% of Q_{max}. In the case of the 1.0m head estimate, the gap size would be 35mm, which although not unacceptably large, could be significantly reduced. The effect of doing so would be to reduce the leakage flow rate and marginally improve the hydraulic efficiency.

Considering the example of the 1.0m head machine on the bottom row; a Q_{max} and P_{max} of ∼6 m^3/s and ∼40 kW per metre width are estimated. This machine would have a diameter of 14m and have a maximum rotational speed of 3.2 rpm. It must be noted however that the limiting factor in a practical installation would be the velocity of the flowing water. As an estimate, this should not exceed ∼1.5 m/s otherwise scouring could become an issue. Referring to Table 8.2, it is clear that for this specific design of a U-HPC operating with a d_2/d_1 ratio of 0.7, the limiting factor is the upstream water velocity. If the speed of rotation of this machine were to be limited such that the upstream velocity did not exceed 1.5 m/s, then the Q_{max} and P_{max} values are estimated to be ∼1.8 m^3/s and ∼17 kW per metre width. It should be noted that whilst the upstream velocities of the scaled estimates were high, the downstream velocities were acceptable. Adaptation of the U-HPC design, such as a reduced or more symmetrical shroud, could address the upstream velocity issue. These values are discussed further, being compared against traditional waterwheels in Section 9.2.

8.1.5 Assessment of U-HPC design compromises

The primary purpose of the U-HPC concept was to represent a 'type one' HPC, providing experimental data for assessment of the ideal theory. However, the U-HPC had two fundamental differences in its design when compared to the ideal representation. Practical considerations meant that instead of having a horizontal channel bed over which a vertical blade moved laterally, the U-HPC concept had a shroud and an axle about which multiple blades rotated. The aim of this subsection is to determine whether or not these differences resulted in a significant changes in operational characteristics, making the U-HPC unsuitable for verifying the 'type one' HPC theory. The impact of leakage and turbulent losses on the efficiency profiles have already been covered in the previous sections. The following analysis assesses the significance of the two design alterations independently, relative to the ideal theory assuming no leakage or turbulent losses.

8.1.5.1 Influence of the shroud on the head differential

The shroud beneath the U-HPC is an essential component introduced to minimise the leakage flow beneath the wheel. It is however a departure from the ideal representation of a 'type one' HPC, shown in Figure 5.3. When compared to the ideal model where the upstream depth is constant with a value of d_1, the U-HPC has a raised bed on approach to the installation which lowers within the wheel as the shroud. This drop in bed means that the depth of the water increases within the shroud.

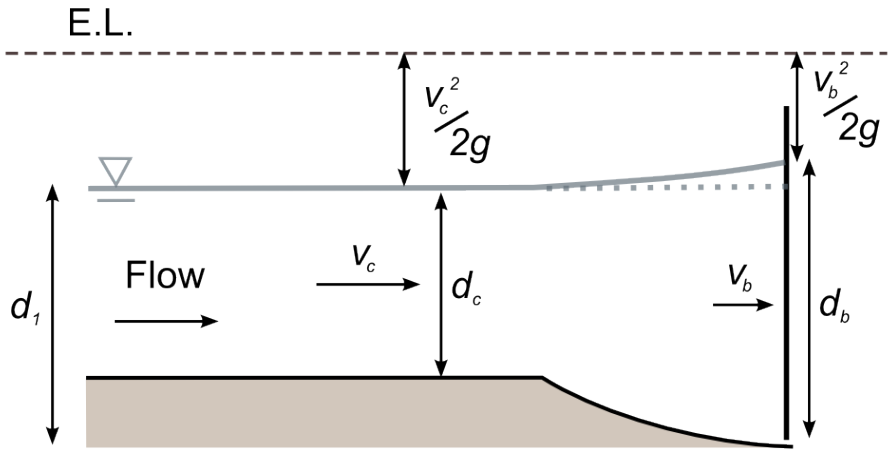

Figure 8.9: U-HPC design compromise: the potential impact of the shroud

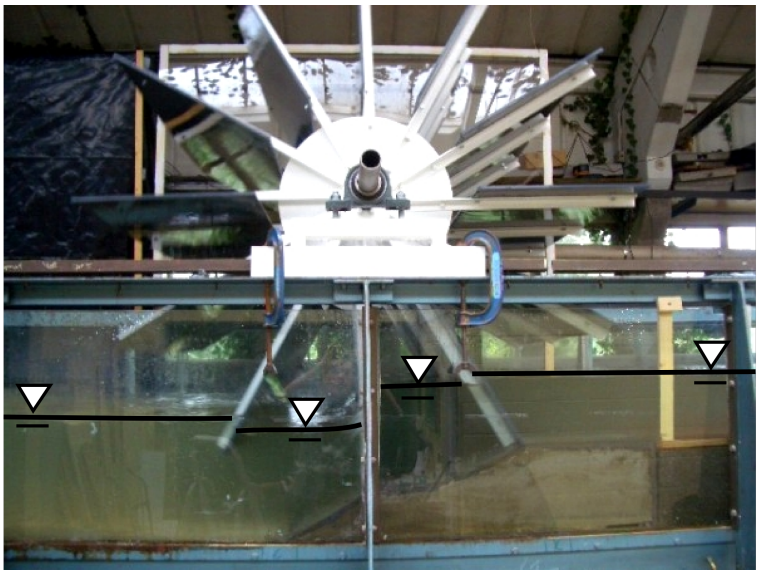

Figure 8.10: Demonstration of the water levels within the large scale U-HPC during operation

Assuming free flow conditions, application of flow continuity and the energy equation would suggest that the resulting deceleration of the water within the shroud would result in a slight increase in water surface level beneath the axle. This is depicted in Figure 8.9, where the terms d_c, v_c, d_b, and v_b represent the water depths and velocities within the upstream channel and at the blade. Using the dimensions and depths of the 'constant level' U-HPC tests at Q_{max} to demonstrate, the theoretical analysis suggests that the depth at the blade could increase by $\sim$6%. If present the consequence of this deceleration would be that in the ideal analysis, excluding leakage and turbulent losses, the U-HPC's efficiency would be a function of flow rate as well as the ratio d_2/d_1. In practice however, the water does not enter the machine in free flow conditions, instead interacting with the rotating blades. Referring to Figure 8.10 as an example, it was generally observed that the level within the wheel was level or even marginally lower than in the channel.

- Based on the observations made during testing, and the predominant trend between efficiency and the ratio d_2/d_1 outlined by Figure 8.1, it is concluded that the addition of the shroud to the U-HPC design did not significantly compromise the U-HPCs ability to represent a 'type one' HPC as intended.

8.1.5.2 Significance of rotating blades on power generation

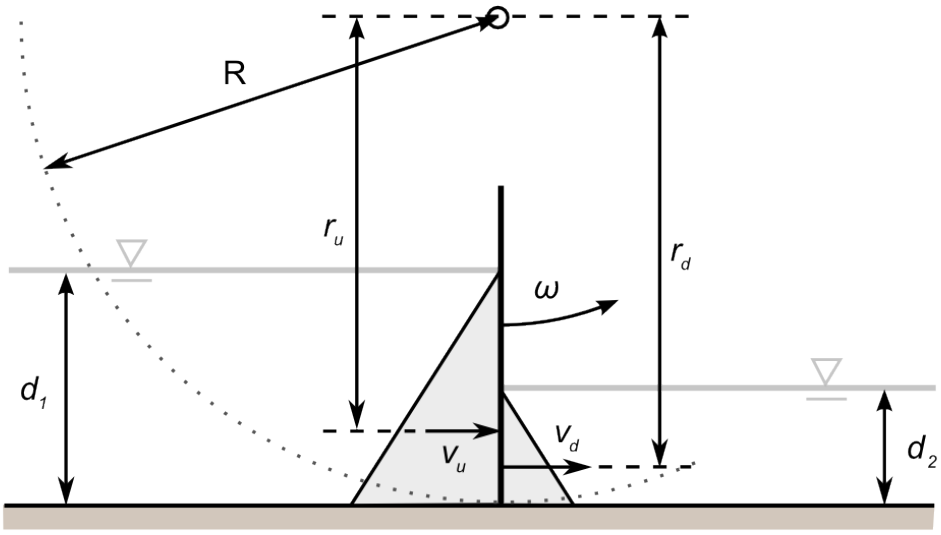

Figure 8.11: U-HPC design compromise: the potential impact or the radius-based blade velocity

In the ideal 'type one' HPC theory, the blade was modelled as vertical and moving laterally. This allowed the forces resulting from the upstream and downstream hydrostatic pressures to be multiplied by a common blade velocity when the calculating the output power, see Equation 5.6. In designing the U-HPC, it was not practicable to design such a blade movement, and instead multiple blades were positioned about a common axle, in the form commonly seen with traditional waterwheels. This departure from the the ideal model has significance on the machine's power generation.

Figure 8.11 represents the departure of the U-HPC concept from the ideal model, where lower case u represents the upstream and d represents the downstream. It can be appreciated that the velocities, v_u and v_d at the central positions on the blade where the upstream and downstream hydrostatic pressures act, are a function of the angular velocity of the blade, ω, and the radius at which that point is from the axis, r_u and r_d. Unlike in the ideal 'type one' HPC theory where the power was the product of the upstream and downstream forces multiplied by a common velocity, the power in this rotational scenario is now calculated as torque multiplied by angular velocity. The power generated is calculated using equations 8.13 to 8.18, where R is the radius of the wheel. Equation 8.13 is derived from Equation 8.5.

$$f = \frac{Q}{W\ (\pi\, r^2 - \pi\, (r - d_1)^2)} \tag{8.13}$$

$$P_u = \left(W\, \rho\, g\, \frac{d_1^2}{2} \right)\ r_u \times 2\, \pi\, f \tag{8.14}$$

$$r_u = R - \frac{d_1}{3} \tag{8.15}$$

$$P_d = \left(W\, \rho\, g\, \frac{d_2^2}{2} \right)\ r_d \times 2\, \pi\, f \tag{8.16}$$

$$r_d = R - \frac{d_2}{3} \tag{8.17}$$

$$P_{out} = P_u - P_d \tag{8.18}$$

Figure 8.12 plots the modified theory against the leakage adjusted, 'self-levelling' test U-HPC data. As the theory continues to assume no leakage or turbulent losses, it can be seen that the new line better represents the experimental data as it underestimates fewer data points. Compared to the ideal 'type one' HPC theory, calculating the blade velocity as a function of radius and angular velocity results in a 5% higher increase in efficiency for a d_2/d_1 ratio of 0.0. The increase in efficiency value decreases as the d_2/d_1 ratio tends to one. Figure 8.13 plots the modified theory against the 'constant level' U-HPC test data. The calculation of the blade velocity as a function of radius and angular velocity results in a 4% increase in efficiency when compared to the ideal 'type one' HPC theory. Referring back to Figure 8.6, the modified theory would have matched the experimental data more accurately, following the leakage and drag corrections.

- Analysis into the use of rotating blades by the U-HPC concept shows that the efficiency of such a design, when not considering leakage or turbulent losses, is more efficient than the vertical, laterally moving blade modelled by the ideal 'type one' HPC theory. This difference is marginal, at around 4% to 5%, and the fundamental operation of the machine is not altered; *the efficiency remains primarily a function of the ratio* d_2/d_1. It is therefore concluded that this design alteration does not compromise the U-HPCs ability to represent a 'type one' HPC. It should be noted that the increased efficiency of this analysis does not indicate an improvement in design, as it has been shown that rotating blades contribute to detrimental turbulent losses.

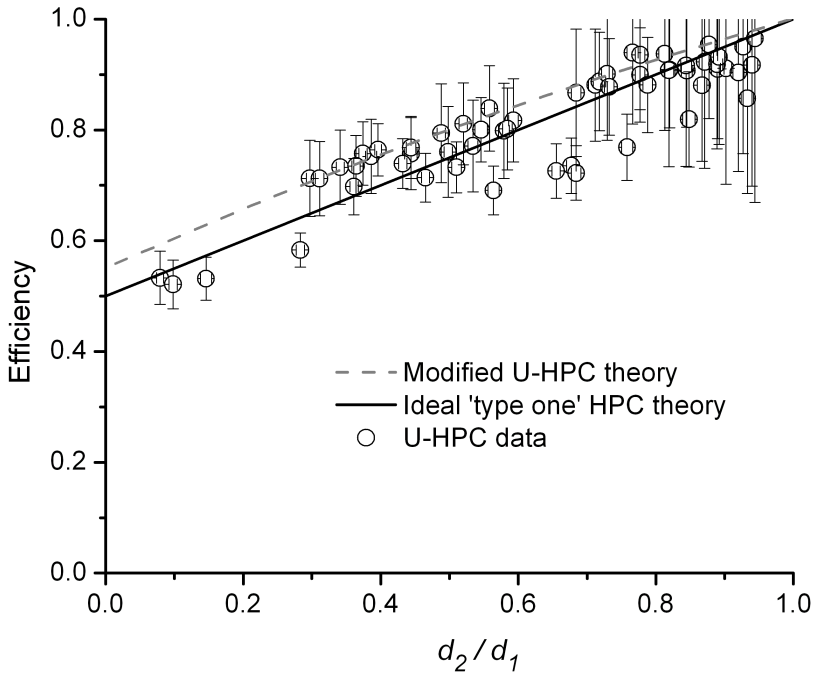

Figure 8.12: Impact of the radius-based blade velocity on the relationship between the ratio d_2/d_1 and efficiency

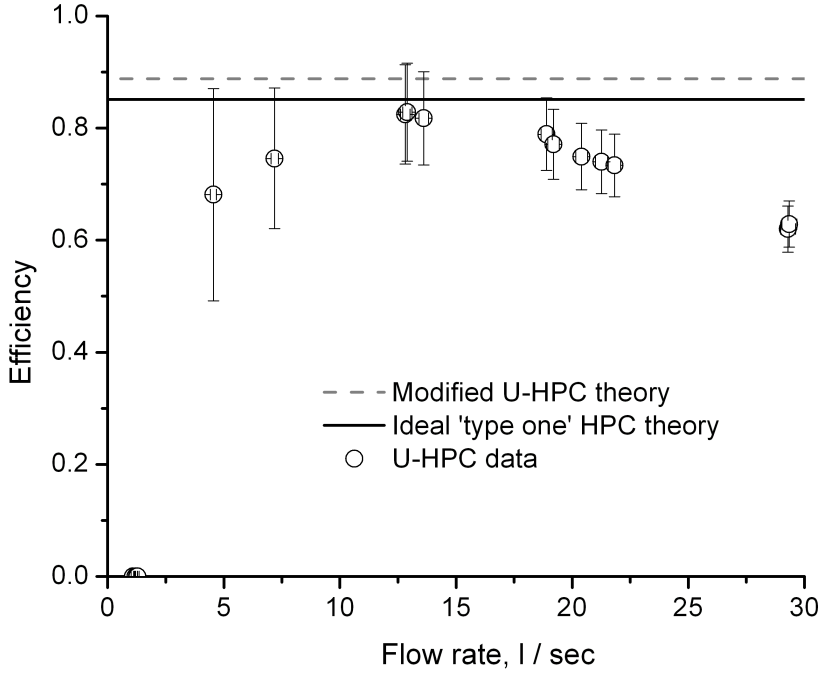

Figure 8.13: Impact of the radius-based blade velocity on the efficiency when operating with a constant d_2/d_1 ratio

8.1.6 Operational characteristics

The purpose of this Subsection is to portray the performance characteristics of the U-HPC model. Observations are provided without in-depth analysis, as the U-HPC model was a demonstration prototype, and not an optimised machine. The concept was devised only to represent a 'type one' HPC machine, and indicate the potential performance of such machines. Figure 8.14 shows the U-HPC operating in normal 'reasonable' conditions (pictures 1-3) and in extreme 'unreasonable' conditions which would result in poor efficiency values (pictures 4-6).

Picture 1 indicates the head difference which forms across a blade whilst it is within the shroud. The cell on the downstream side of this blade is seen in the fully evacuated state. Picture 2 shows the evacuation taking place once the blade has passed the lower extent of the shroud. During this process, the water level in the cell drops, and a head difference forms across the subsequent blade. Picture 3 shows how the water evacuating the blade can achieve sufficient downward momentum that the water level in the cell temporarily drops below that of the downstream. This 'overshoot' increases with rotational speed and also as the head difference through which the evacuation occurs increases. The net impact on the machine is negligible as the artificially increased head across the subsequent blade within the shroud is cancelled by the counter-acting head difference formed on the previous blade in the downstream.

Picture 4 shows the consequences of allowing the machine to rotate at higher speeds and flow rates whilst the downstream level is too high. Water is forced away from the machine by the reverse side of the blades as they exit the water. This generates severe waves in the downstream, and some water is raised above the downstream before it clears the cells fully, being thrown from the wheel. Such operation has reduced efficiency and the waves could potentially cause scouring in a real installation. This issue could however be addressed with curved blades similar to that of a traditional Zuppinger waterwheel as shown in Figure 3.6. Picture 5 shows how when the downstream water level is too low, the evacuating water leaves with excessive velocity. This can be sufficient to create a hydraulic jump - where the relatively shallow jet of water entering a relatively deep downstream has sufficient velocity that the deeper downstream water level can not reach the machine itself. Such conditions are highly turbulent and could result in severe scouring of sediment in a river installation. Picture 6 shows the final extreme condition. If the upstream depth is too shallow, the velocity of the water and the rotational speed of the wheel can become sufficiently high at low-load or high-flow, that the hydrostatic pressure difference does not form across the blades. Instead the water simply flows over and around the curvature of the shroud resulting in poor efficiency.

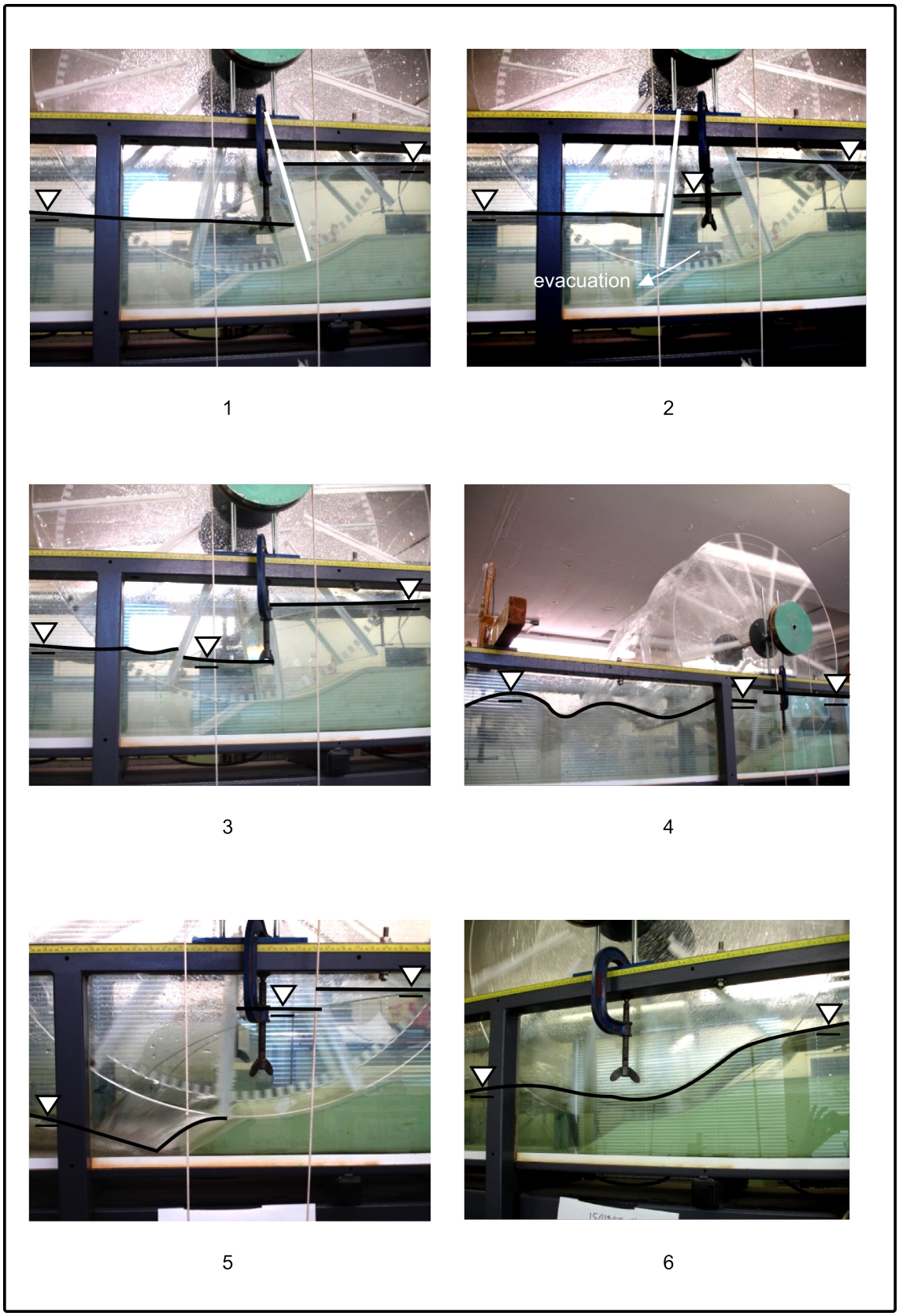

Figure 8.14: Operational characteristics of the U-HPC concept
(1-3: 'reasonable', 4-6: 'unreasonable')

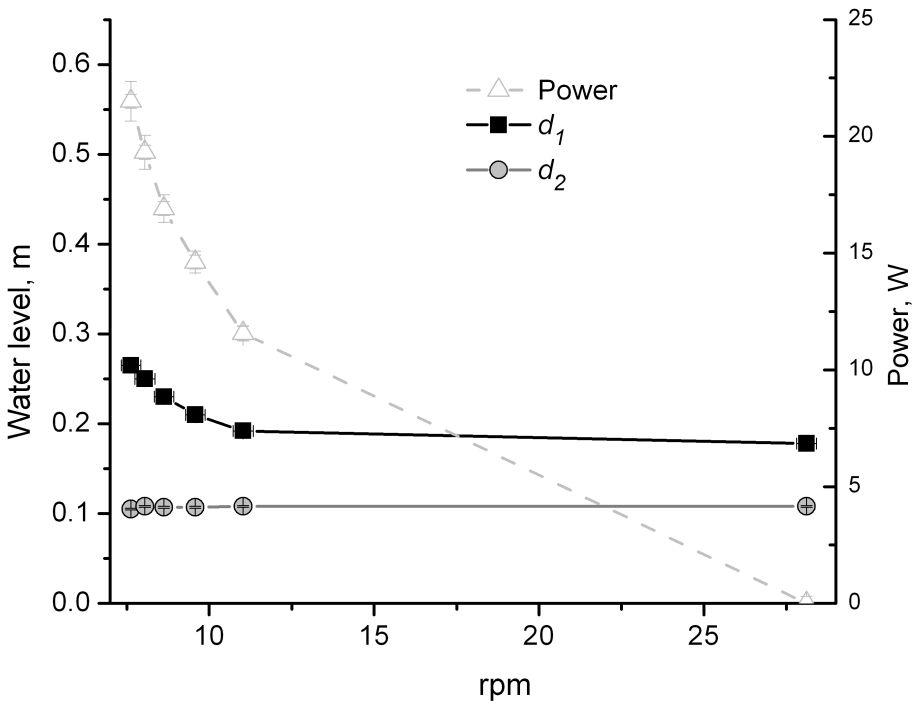

Figure 8.15: U-HPC: the relationship between the water levels and flow rate in self-levelling conditions

The depth of the upstream water at a U-HPC installation is a function of the rotational speed of the wheel and the flow rate. The downstream water depth by contrast is only a function of the flow rate, and is independent of the wheel. This is demonstrated by Figure 8.15 which shows a data set from the 'self-levelling' tests. The flow rate was constant and determined by the flume's pump, and the rotational speed of the wheel was controlled by the load. As the load was reduced and the speed of the wheel increased, the upstream water depth would reduce, whilst the downstream depth remained constant.

The evacuation of the cells into the downstream occurs after the working blade passes bottom dead centre and departs from the shroud, as shown in Figure 6.1. The process is effectively that of free-fall, being predominantly driven by gravity, whilst the speed at which the opening forms, through which the evacuation occurs, introduces a minor throttling effect at low speeds of revolution. The duration of the evacuation was, except at high speeds of rotation, shorter than the time between passing blades. The result of this energetic discharge from the wheel was two fold; wave generation in the downstream and pulsation in the wheel's rotation.

Wave generation

The generation of waves is illustrated by Figure 8.16. The wave profiles of the upstream and downstream are shown from one of the 'self-levelling' data points with a high efficiency of 84%. In the upstream there are practically no waves generated as the water enters the wheel without disturbance. In the downstream the evacuation process results in large wave forms with an amplitude equal to 25% of the head difference. One wave is generated per evacuated cell. Although wave generation was predominantly in the downstream and a result of the evacuation, wave generation was to a lesser extent also a function of the water depth and the interaction of the blades during entry and exit from the water. Analysis of all the 'self-levelling' data points found that in the upstream, the average amplitude of the waves was 4% of the head difference with a standard deviation of 3.2%. In the downstream, the average amplitude of the waves was 19% with a standard deviation of 7%.

$$P_{wave} = \frac{\rho g^2 H_{wave}^2 T_{wave}}{32\pi} \tag{8.19}$$

The power of the wave, P_{wave}, depicted in Figure8.16 has been calculated using Equation 8.19 where H_{wave} is the height of the wave and T_{wave} is the period (Chadwick 2004, p.223). At 0.3W per metre width of wave, it represents ~3% of the power output of the U-HPC. It is important to note that the wave does not represent a significant loss resulting from the hydrostatic pressure operational principle. It is generated by the 'evacuation' process; which occurs normal to the direction in which the working blades moves and is assumed not to contribute the power output of the U-HPC.

Rotational quality

The evacuation of the cells as a periodic energetic discharge and the manner in which the head difference would be generated on the following blade resulted in pulsation in the wheel's rotation. This is demonstrated by Figure 8.17, taken during the large scale U-HPC tests. The magnitude of the pulse is a function of the inertia of the wheel, which will be very different when comparing a perspex model to a full scale prototype manufactured from steel.

The important conclusion is that the evacuation process makes wave generation and pulsation a a fundamental property of the U-HPC.

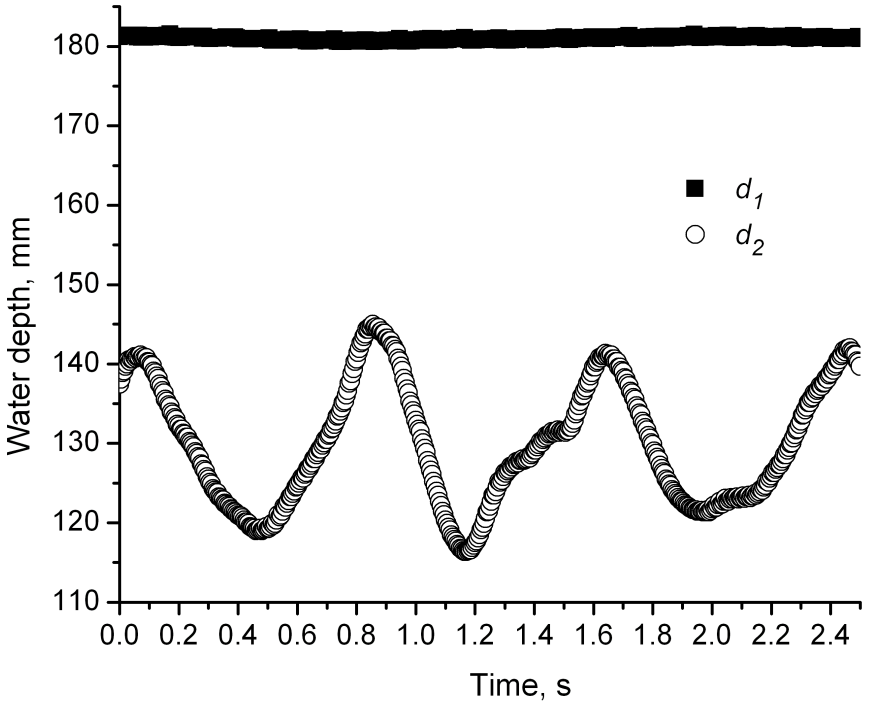

Figure 8.16: U-HPC: demonstration of wave generation

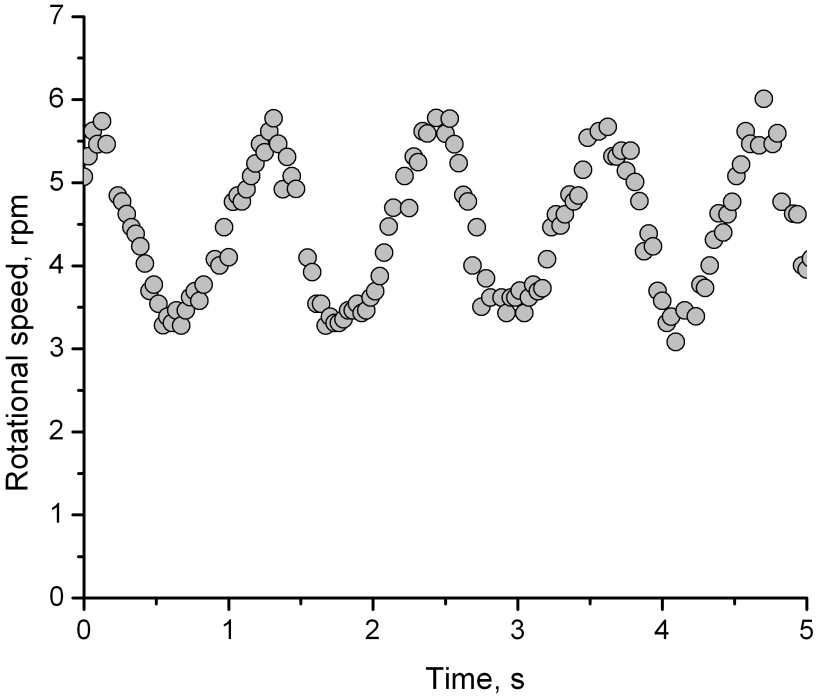

Figure 8.17: U-HPC: demonstration of pulsation

8.2 Middleshot - Hydrostatic Pressure Converter

The M-HPC concept was designed to test the principle of 'type two' HPCs as described in the theory, Chapter 5. The results and analysis of this machine are broken down into the following sections:

- Section 8.2.1 presents the data from the M-HPC 'constant level' tests, stating the values P_{max} and Q_{max} for use during the scaling exercise. A brief comparison is provided against the *Staudruckmaschine* from which the design was primarily inspired, and also against the ideal 'type two' HPC theory. This allows the influence of both leakage and turbulent losses to be observed, both of which are design related factors. These factors are then investigated in greater detail in the following section.

- Section 8.2.3 analyses the influence of leakage and turbulent losses on the hydraulic efficiency profile of the M-HPC.

- Section 8.2.3 utilises the Froude scaling laws to scale the experimental data and indicate the potential full scale performance of the M-HPC concept.

- Section 8.2.4 describes the operational characteristics of the M-HPC observed. These included the generation of waves and the quality of rotation.

8.2.1 Operation with constant water depths

The M-HPC concept was created to represent a 'type two' HPC, and in contrast with the U-HPC, was designed to operate with specific upstream and downstream water depths. A 0.45m diameter model of the M-HPC concept was tested in 'constant level' conditions as described in Section 7.4. The head difference between the upstream and the downstream was maintained at 0.15m, and the results are plotted in Figure 8.18. From this data it can be seen that the peak hydraulic efficiency occurs at a lower flow rate than the peak power output. Considering efficiencies over 60%, the efficiency profile is wide for a fixed geometry machine, covering flow rates between ~6 l/s and ~17 l/s. For the purposes of the scaling exercise, section 8.2.3, the peak efficiency was ~80%, P_{max} was ~16.5W and Q_{max} was ~17 l/sec at ~25 rpm.

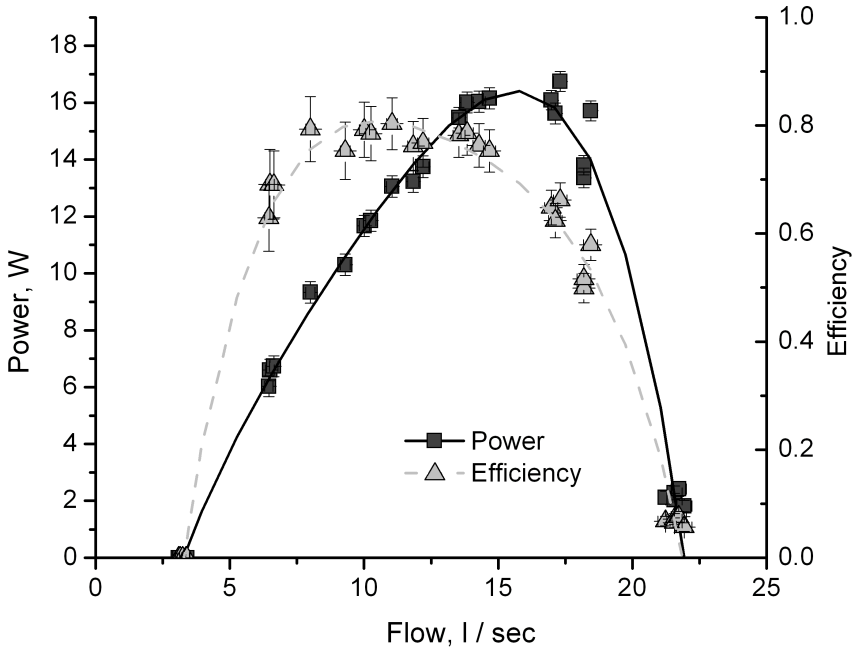

Figure 8.18: Results of the M-HPC constant level tests

The design of the M-HPC was initially inspired by the *Staudruckmaschine* introduced in the literature review. Major design additions and modifications were made, including the shroud and the side filling and ventilation regime. The purpose of these was to significantly reduce the leakage and turbulent losses observed on the *Staudruckmaschine* model, and as a result increase the efficiency and flow capacity of the machine per metre width. Although the M-HPC and *Staudruckmaschine* models were constructed with the same diameter and operated with the same head, they did not share a common width, at 235mm and 210mm respectively. Therefore the results from both tests, plotted in Figure 8.19, are adjusted to per metre width. It can be seen that the *Stauruckmaschine* (SDM) had a Q_{max} and P_{max} value of ∼40 l/sec and ∼18W per metre width, and a peak efficiency of ∼40%. In comparison, the M-HPC had a Q_{max} and P_{max} value of ∼70 l/sec and ∼70W per metre width, and a peak efficiency of ∼80%

- It has been shown that the M-HPC had a flow capacity 1.75 times greater, and a peak efficiency 2 times greater than the *Staudruckmaschine*. Overall, the P_{max} per unit width is ∼3.9 times greater than the *Staudruckmaschine*. It can therefore be concluded that the design of the M-HPC represents a significant improvement over its predecessor.

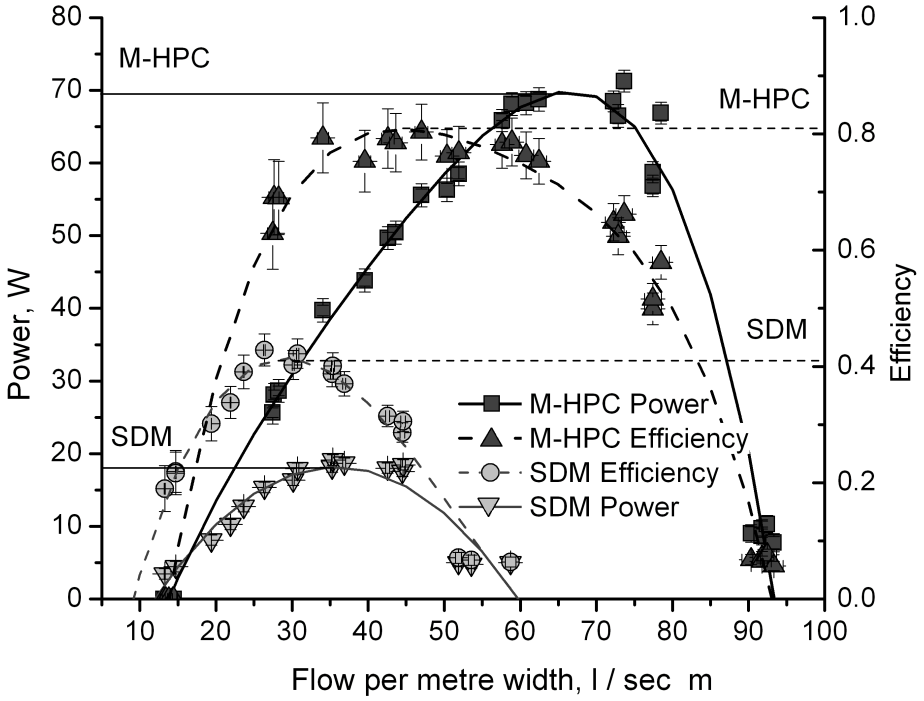

Figure 8.19: Performance comparison between the U-HPC and the *Staudruckmaschine*

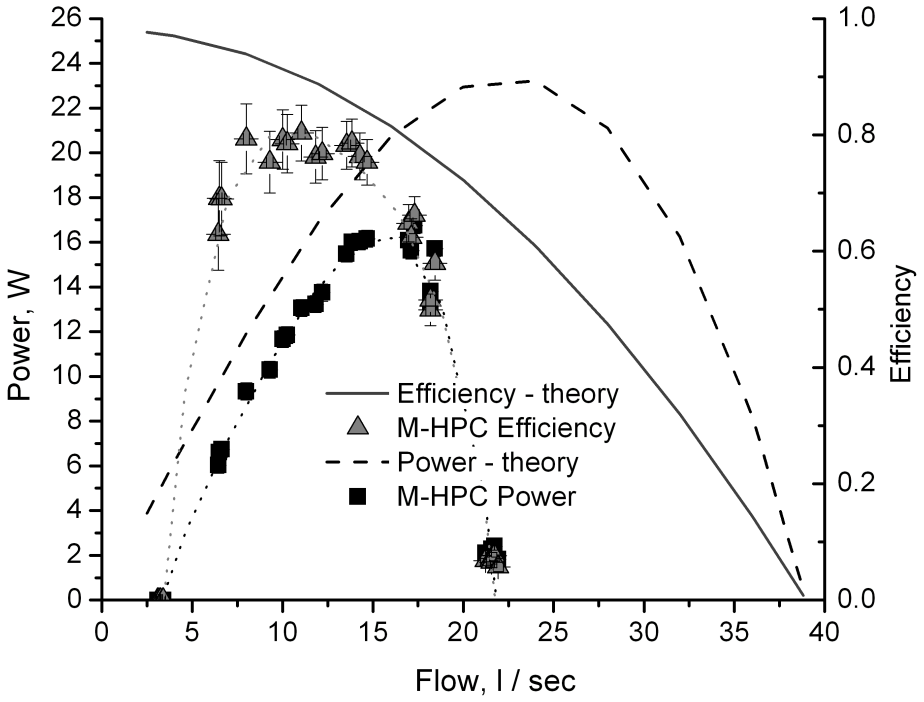

Figure 8.20: Comparison between the M-HPC results and the ideal 'type two' HPC theory

In order to compare the M-HPC experimental data with the ideal 'type two' HPC theory, a slight modification has been made to the theory. In Chapter 5, is was assumed that the width of the wheel and the channel were equal to avoid unnecessary complication. The design of the M-HPC required the channel to be wider to allow side filling and ventilation of the wheel. The channel had a width of 0.75m and the wheel 0.235m. Accordingly the original velocity relationship, Equation 5.10, does not hold and is replaced by equations 8.20 and 8.21, where v_1 is the upstream velocity, but the blade velocity is now given as v_b, and not v_2 as previously. This is because v_2, the downstream channel velocity is less than the blade, the downstream channel also being wider than the wheel. It is important to note that because of the free surface conditions in the downstream beyond the wheel, it is assumed that any deceleration of flow after the wheel occurs independently from the wheel, and does not contribute or otherwise to its output power. The new blade velocity term, v_b, has then been substituted into the remaining theory, giving equations 8.22 to 8.24.

$$v_1 = \frac{Q}{W_{channel}\, d_1} \tag{8.20}$$

$$v_b = \frac{Q}{W_{wheel}\, d_2} \tag{8.21}$$

$$\Delta d = \frac{v_b^2 - v_1^2}{2\, g} \tag{8.22}$$

$$F_A = \rho\, d_1\, v_1\, (v_b - v_1) \tag{8.23}$$

$$P_{out} = (F_P - F_A)\; v_b \tag{8.24}$$

Referring to Figure 8.20, it can be seen that the theory overestimates the efficiency of the M-HPC recorded during the experimental testing. Similar to Figure 8.2 for the U-HPC, the difference is greatest at very low and very high flow rates, and it is proposed that leakage flow through gaps and turbulent losses account for this difference. These design related factors are considered in the following Subsection.

8.2.2 Analysis of leakage and turbulent losses impact

This Subsection analyses the influence of leakage and turbulent losses on the hydraulic efficiency of the M-HPC in a similar manner to Chapter 8.1.3 for the U-HPC. The analysis is conducted by incorporating additional variables into the ideal 'type two' HPC theory. An assessment is then made; whether or not the leakage and turbulent losses can account for the difference observed between the experimental data and ideal theory shown in Figure 8.20, and therefore whether or not the ideal theory holds.

8.2.2.1 Leakage analysis

The M-HPC has a filling ratio of one, meaning that the cells between the blades fill entirely with water during operation. Therefore, as might be expected, there is a linear relationship between the speed of rotation of the wheel and the flow rate. This is shown by Figure 8.21 which plots the data from the M-HPC 'constant level' tests. Importantly there is a flow rate of $\sim$3.0 l/sec when the wheel is stationary, resulting from leakage through gaps between the wheel and the channel in which it was installed.

The theoretical analysis of the leakage flow rate through the M-HPC is similar to that of the U-HPC. Once more it is proposed that the leakage is driven by the head difference across the wheel. For the M-HPC, this head difference reduces by Δd with increasing flow rate, as discussed in the 'type two' HPC theory. Referring to Figure 8.22, the leakage analysis is broken down into three components. Q_1 is the leakage beside the central hub between the upstream and downstream water surfaces, and is calculated by Equation 8.25. The pressure and thus the velocity of the leakage flow increase with depth in this region. Q_2 and Q_3 are the leakage flows in the regions beside and beneath the blade respectively, and are calculated by Equations 8.26 and 8.27. The driving pressure and velocity of the leakage flow in these regions is constant with depth. The total leakage flow rate, $Q_{leakage}$, is calculated by Equation 8.28. The significance of the Δd term is that the leakage flow rate will reduce marginally as the total flow rate increases. Referring to Equation 8.29, the velocities used to calculate Δd are based on the flow rate through the wheel, Q_{wheel}, for simplicity. This is calculated using Equation 8.30, which assumes that the cells between the blades fill entirely with water.

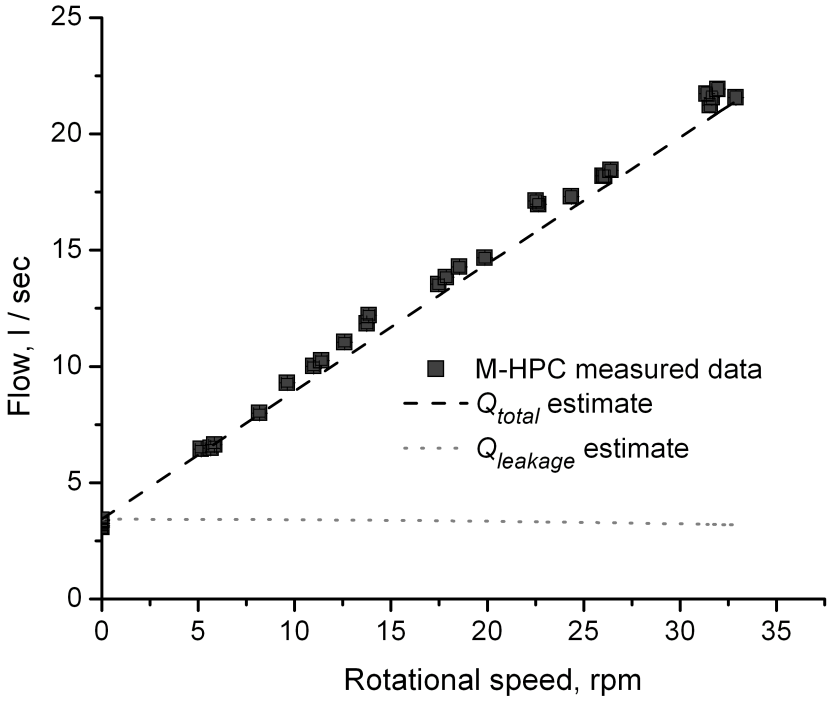

Figure 8.21: M-HPC: relationship between flow rate and rotational speed

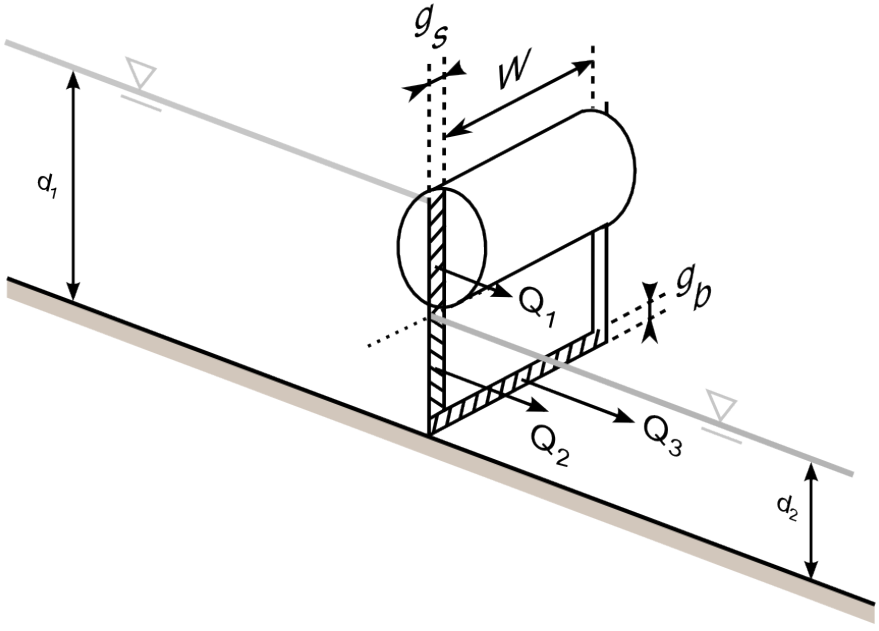

Figure 8.22: Representation of M-HPC leakage gaps

$$Q_{leakage} = velocity\,of\,flow \;\times\; area\,of\,gap$$

$$Q_1 = \frac{\sqrt{2\,g}\,(d_1 - d_2 - \Delta d)^{1.5}}{1.5}\,g_s \tag{8.25}$$

$$Q_2 = \sqrt{2\,g\,(d_1 - d_2 - \Delta d)}\,(d_2\,g_s) \tag{8.26}$$

$$Q_3 = \sqrt{2\,g\,(d_1 - d_2 - \triangle d)}\,(g_b\,(W + 2\,g_s)) \tag{8.27}$$

$$Q_{leakage} = 2\,(Q_1 + Q_2) + Q_3 \tag{8.28}$$

$$\Delta d = \left(\frac{Q_{wheel}}{(W + 2\,g_s)\,(l + g_b}\right)^2 - \left(\frac{Q_{wheel}}{W_{channel}\,(d_1 + g_b}\right)^2 \tag{8.29}$$

$$Q_{wheel} = f\,W\,\left(\pi\left(r^2 - (r-l)^2\right) - (n\,l\,t\right) \tag{8.30}$$

- $Q_{leakage}$ and Q_{total}, the sum of the leakage flow and Q_{wheel}, are plotted against the experimental data from the M-HPC tests in Figure 8.21. The correlation of the total flow estimate with the data supports the proposed theory; that the flow rate through the wheel is a function of rotational speed, and that the leakage flow rate is a function of the head difference only. It is interesting to note that despite the head difference reducing by Δd with increasing total flow, the velocity of the leakage is a function of the square root of the head, and thus the leakage flow remains practically constant relative to the total flow rate.

The impact of the leakage flow on the efficiency of the M-HPC is demonstrated in Figure 8.23. The 'flow adjusted theory' line has been generated by calculating the blade velocity, v_b, using the flow rate through the wheel itself, as seen in Equation 8.31. Thus, the calculation of the power and the hydraulic efficiency of this plotted line are independent from the leakage flow, assuming that the leakage flow does not contribute to the power output of the wheel.

$$v_b = \frac{Q_{wheel}}{W_{wheel}\, d_2} \tag{8.31}$$

It can be seen that the leakage adjusted theory underestimates the experimental data in the region up to ~15 l/sec. This difference is ~10%, but it should be observed that it results from a underestimation of the power output of ~2W, referring to Figure 8.24. For the leakage adjusted theory to underestimate the experimental data is noteworthy, considering that the un-modified theory does not take leakage *nor* turbulent losses into account. The cause is not thought not to originate from the experimental data, which has been plotted with suitable error bars. The difference can also not be accounted for by the components of the theory, as altering the assumptions on the water level drop and the inertial reaction force only significantly alters the theory in the higher flow region. This is discussed further in Section 9.1.2. It is proposed that the theory underestimates the experimental data as the hydraulic model experienced an additional force to that resulting from the hydrostatic pressure, which was not considered by the theory. It is proposed that the leakage flow, which represented between 100% down to 20% of the total flow in the region up to 15 l/sec, *did* contribute to the power output of the wheel. It was observed that with the wheel held stationary, part of the leakage flow departed the machine diagonally. This indicates that the flow through the gaps interacted with the tips and edges of the blades, being partially diverted through the wheel along the blades. The assumption that the flow existed in virtual channels beside the wheel (Figure 8.22) without acting upon the wheel does not hold. It must however be noted that the gap sizes around the M-HPC model and the leakage flow are relatively large when compared to what could be achieved on a larger scale machine. If the leakage has contributed to the power output of the M-HPC model, it should be noted that this does not represent a design goal. The efficiency of the machine could have been better increased by minimising the leakage flow.

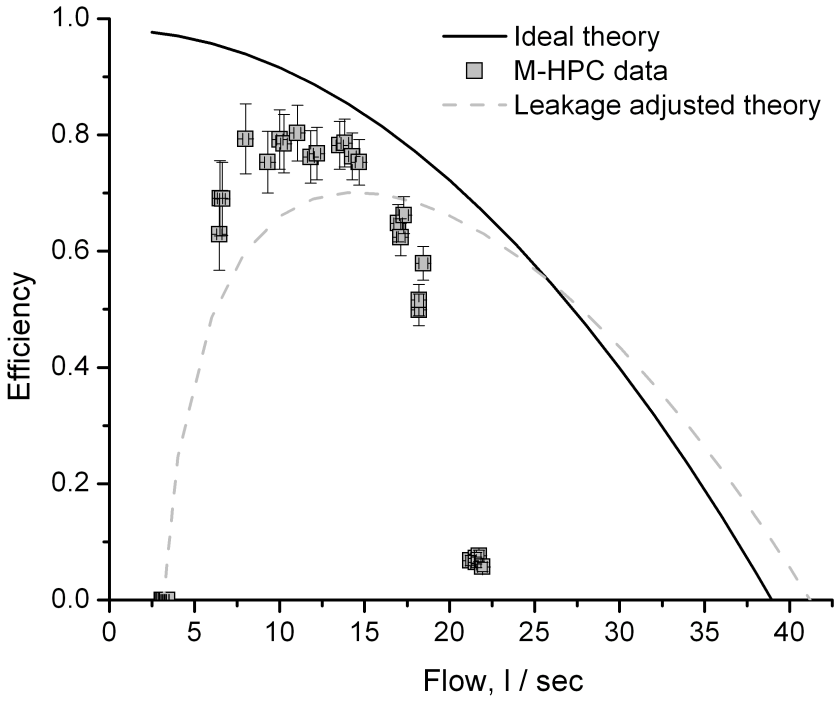

Figure 8.23: M-HPC leakage adjusted analysis

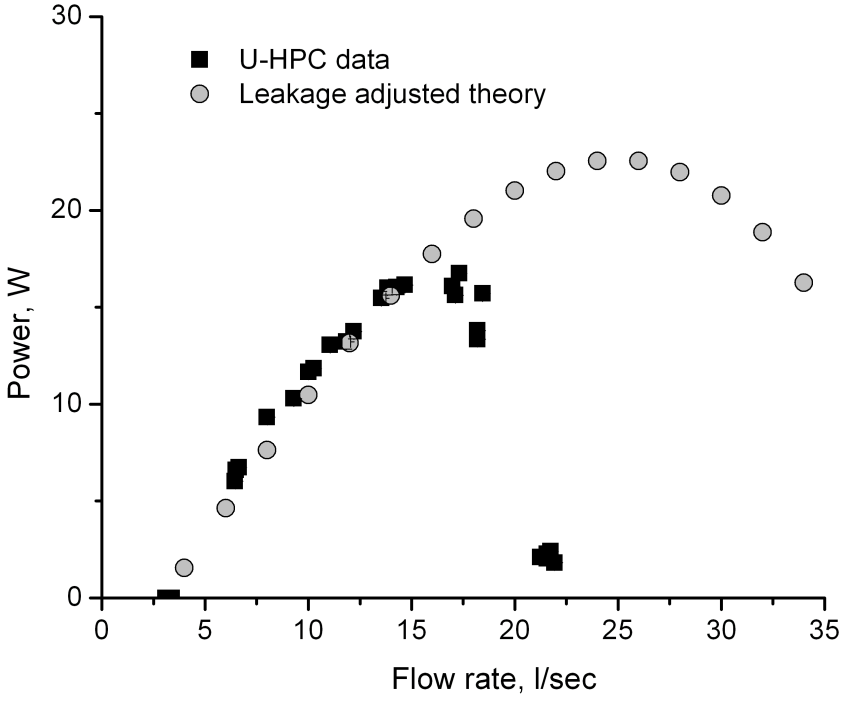

Figure 8.24: M-HPC data with leakage adjusted power calculation

8.2.2.2 Turbulent losses analysis

The difference between the M-HPC experimental data and the ideal 'type two' HPC theory at low flow rates can be accounted for by leakage flow through gaps around the wheel. Similar to the analysis of the U-HPC in section 8.1.3.2, it is proposed that the difference at higher flow rates results from turbulent losses between the moving blades and the relatively slow moving water into which the blades enter and exit. The magnitude of the turbulent losses of the M-HPC are dependent on the design of the installation in question, and are highly complex due to the geometry of the blades and the constriction the wheel poses in the channel of variable width. For demonstration purposes, the turbulent losses have been factored into the theory in the form of a velocity squared related force, F_T, Equations 8.32, 8.33 and 8.34.

$$F_T = K\, v_b^2 \tag{8.32}$$

$$P_{out,\, leakage\, and\, turbulence\, adjusted\, theory} = (F_P - F_A - F_D)\; v_b \tag{8.33}$$

$$\eta_{leakage\, and\, turbulence\, adjusted} = \frac{P_{out,\, leakage\, and\, turbulence\, adjusted\, theory}}{P_{in}} \tag{8.34}$$

The efficiency of the M-HPC, adjusted to include leakage and turbulent losses, demonstrates that the tubulent losses *contribute* to the difference in efficiency profile between the experimental data and the theory at higher flow rates. Whilst considering the influence of the leakage flow on the power output discussed in the previous Subsection, the matching of the theory to the experimental data is not as successful as it was for the U-HPC, Figure 8.6.

Modelling the turbulent losses only as a function of the blade velocity squared becomes too simplistic as the M-HPC model approached freewheel. Other sources of turbulence in the flow occurred at high speeds, such as air entrapment in the flow on blade entry and the lifting of water occurred on blade exit. These losses are discussed further in Subsection 8.2.4.

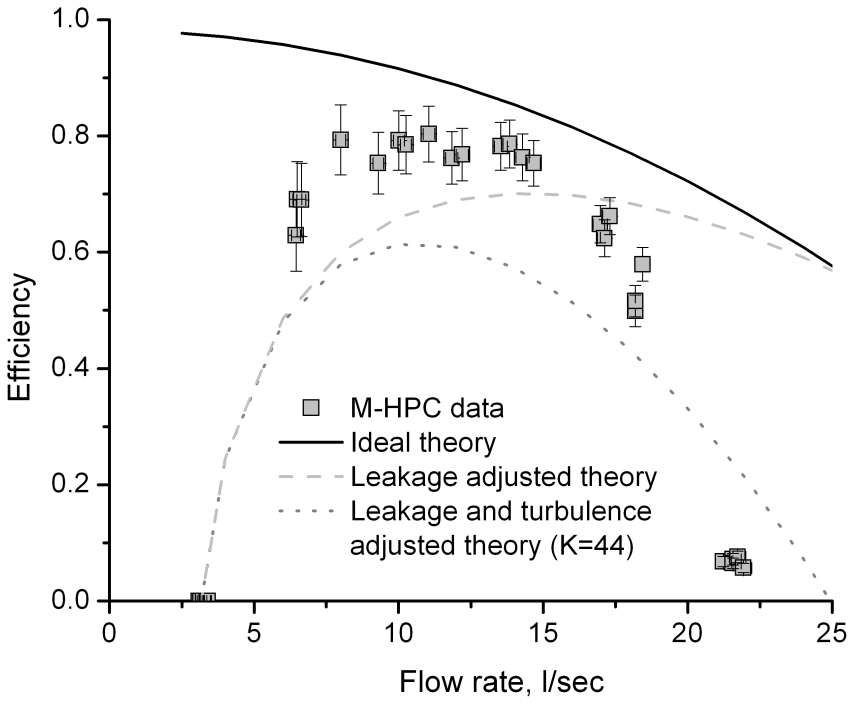

Figure 8.25: M-HPC leakage and turbulence adjusted analysis

- In the analysis of the M-HPC model tests, it has been proposed that the leakage flow may have contributed to the output power, increasing the apparent efficiency of the model at low flow rates beyond that indictated by the theory. This influence was design and manufacture related, and exaggerated at the small scale of the model by the relatively large gaps and leakage flows.

- Overall, it is concluded that leakage and turbulent losses can account for the difference between the M-HPC experimental data and the ideal 'type two' HPC theory. Therefore, it is concluded that the testing of the M-HPC supports the proposed ideal 'type two' HPC theory.

8.2.3 Scale estimates

Scale	Head, m	Q_{max}, $\frac{m^3}{s}$ per m width	P_{max}, kW per m width	Upstream depth, m	Upstream velocity at $Qmax$, m/s	Downstream depth, m	Downstream velocity at Q_{max}, m/s
1:3.3	0.5	0.44	1.42	1.05	0.13	0.55	0.25
1:6.7	1.0	1.25	8.06	2.10	0.19	1.10	0.35
1:10	1.5	2.29	22.20	3.15	0.23	1.65	0.43
1:13.3	2.0	3.52	45.58	4.20	0.26	2.20	0.50
1:16.7	2.5	4.92	79.62	5.25	0.29	2.75	0.86

Table 8.3: Scaled estimates of full scale M-HPC performance

The 'constant level' tests of the M-HPC model determined that the peak efficiency was ∼80%, P_{max} was ∼16.5W and $Q_{max}$was ∼17 l/sec at ∼25 rpm. This data and the dimensions and geometry of the tests have been used to indicate the performance of full scale machines by applying the Froude scaling laws. It has been assumed that the scale analysis conducted for the U-HPC model, Section 8.1.4, applies equally to the M-HPC testing, and therefore that no scale effects were present. Table 8.3 indicates the Q_{max} and P_{max} per metre width for M-HPC machines suitable for head differences up to 2.5m. Conservatively, the gap size and leakage of the M-HPC model have also been scaled. In the case of a 2.5m head installation, the gap size would be 50mm and the leakage flow rate would remain 18% of Q_{max}. Although not unacceptably large, these gaps could be significantly reduced. The effect of this would be to reduce the leakage flow rate and marginally improve efficiency.

Referring to the example of a 2.5m head installation, it is projected that a full scale M-HPC installation could have a Q_{max} and P_{max} of ∼5 m^3/s and ∼80 kW per metre width. The diameter of such a machine would be 7.5m and the maximum rotational speed would be 6.1 rpm. These values are discussed further, being compared against traditional waterwheels in Section 9.2. Table 8.3 also indicates the upstream and downstream depths and velocities for the projected installations, assuming that the relative widths of the M-HPC wheel to channel are similar to that used in the tests. When compared to the U-HPC scaling estimates, Table 8.2, it can be seen that high velocities which could potentially cause scouring within the channel do not occur. The velocity within the wheel itself will be greater than the downstream velocity, however the support structure and shroud of an M-HPC installation would be constructed from steel or concrete and would not suffer from scouring.

8.2.4 Operational characteristics

During normal operation, observations indicated that the M-HPC operates in a very calm manner with little turbulence. This is primarily the result of the central hub which presents a permanent structure beneath which the water flows in a continuous manner, between the upstream and the downstream. The water within the cells around the hub is passed directly into the downstream depth, and not released as an energetic evacuation as observed with the U-HPC. Figure 8.27 depicts a normal operational scenario viewed from the downstream end of the experiment. It can be observed that both the upstream and downstream water surfaces exhibit little disturbance. Figure 8.28 demonstrates the side filling of the cells which occurs as the blades enter the water. Wave generation by the machine was minimal and quickly dissipated into the channel which was wider than the wheel. As a result, wave profile measurements were not obtained.

Figure 8.26 depicts the rotational speed of the M-HPC during two entire revolutions, equivalent to the passing of 24 blades. The deceleration and acceleration of the rotation present *per revolution* of the M-HPC was due to slight variations in the geometry of the experimental model, and should be avoidable with better manufacturing consistency. The apparent scatter of the data at any time was actually the pulsation between the passing of each blade. Comparing Figures 8.26 and 8.17 (which showed the passing of only four blades), the M-HPC exhibited less pulsation in its rotation with the passing of each blade than the U-HPC. Although the response is a function of the inertia and rotational speed of the wheel, which was different for the two machines, the more consistent rotation can primarily be accounted for by the radially twisted blade design and the side filling and ventillation regime. This resulted in a more continuous flow through the machine, without an energetic evacuation of the cells.

It has been discussed in subsection 8.2.2.2 that drag type losses resulting from the blade's passage through the water contributed to efficiency losses. The M-HPC model exhibited two additional sources of turbulent loss which occurred during the blade's entry and exit from the the flowing water. Figure 8.29 shows how at *higher speeds* of revolution, some of the water would not run cleanly off the back of the blades as they exited the downstream, but be lifted out and

thrown clear. The quantities of water involved were small and this loss is not thought to have been significant. Figure 8.30 shows how the trailing tip of the blades on entry could result in an energetic ejection of water from within the cell into the upstream. This forcing of the water by the blade was energetic and represents a significant source of loss, but was only apparent at very high speeds of revolution. Both of these turbulent losses resulted from a slight compromise in the manufacture of the models; where the outside edges of the blades departed from their radial twist, curving back to parallel with the hub for fastening into the aluminium spokes. Development of the blade design and manufacture could reduce or eliminate these sources of loss.

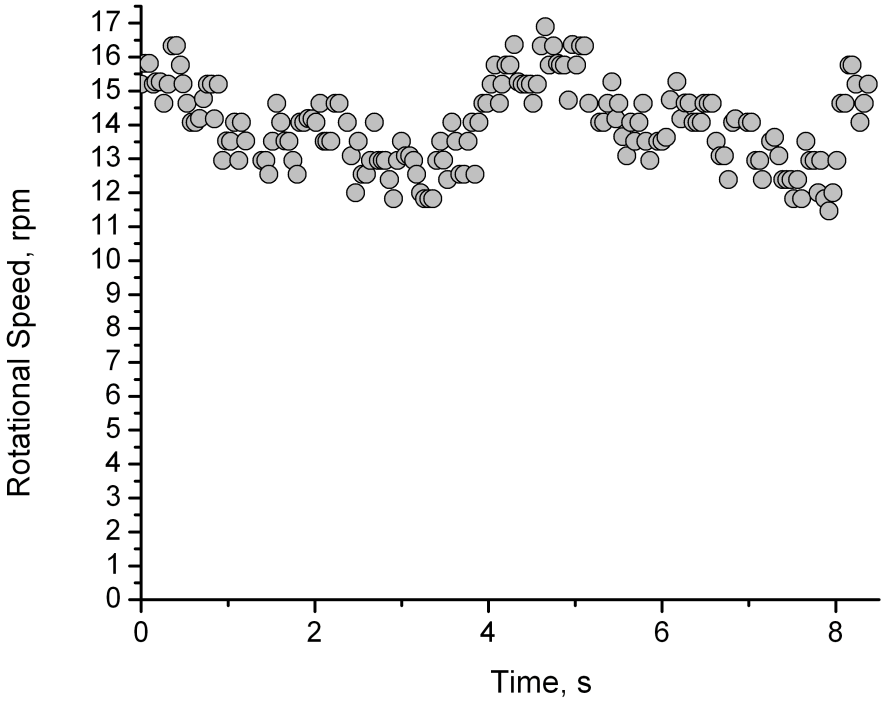

Figure 8.26: M-HPC: demonstration of rotational quality

Figure 8.27: M-HPC: picture of normal operation viewed from downstream

Figure 8.28: M-HPC: picture of side filling during blade entry into the upstream

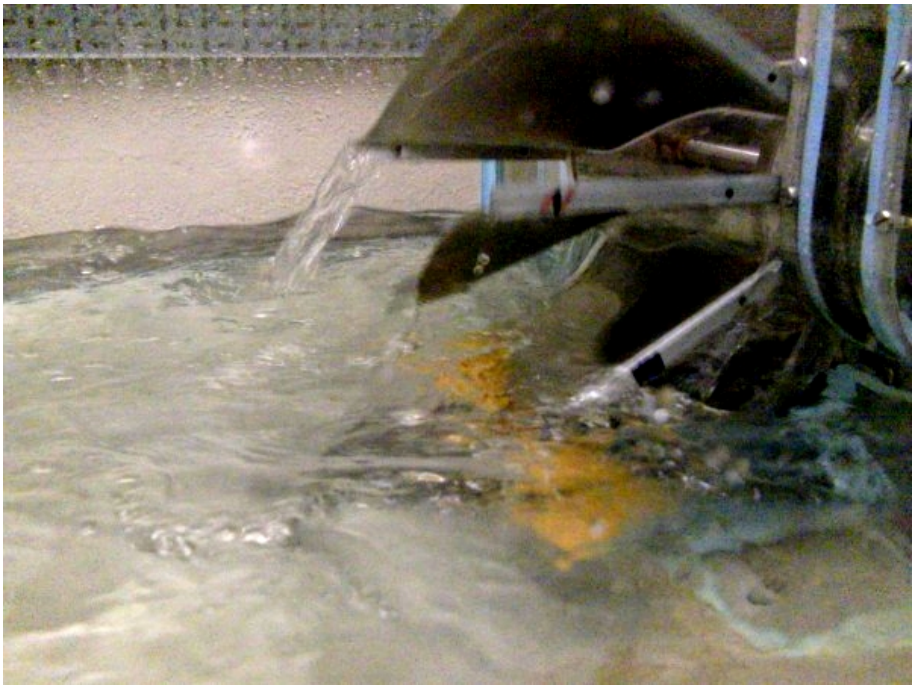

Figure 8.29: M-HPC: view of downstream at high rotational speed

Figure 8.30: M-HPC: view of upstream turbulence at high rotational speed

8.3 Summary

Three scale models of the U-HPC and M-HPC concepts have undergone hydraulic testing with the purpose of analysing the proposed 'type one' and 'type two' HPC theories, and also indicating the full scale performance of the two concepts.

It is concluded that the principles demonstrated by the proposed HPC theories are supported, whilst it has also been indentified that in practice the hydraulic efficiency of such machines would also be influenced by leakage and turbulent losses. Despite these losses, both concepts have relatively flat efficiency profiles, operating with hydraulic efficiencies greater than 60% from relatively low flow rates up to the Q_{max} values stated below.

Through the application of the Froude scaling laws, the full scale performance of the two concept machines in their current un-optimised forms has been indicated as follows:

- The U-HPC concept is suitable for head differences up to 1.0m, with a Q_{max} and P_{max} of $\sim$6 m^3/s (including a 6% leakage flow) and $\sim$40 kW per metre width, and a peak efficiency of $\sim$80%.

- The M-HPC concept is suitable for head differences between 0.5m and 2.5m, operating with a Q_{max} and P_{max} of $\sim$5 m^3/s (including a 20% leakage flow) and $\sim$80 kW per metre width, and a peak efficiency of $\sim$80%.

These values are put into context, relative to the established very low head turbine and tradtional waterwheel technologies, in Section 9.2.

Chapter 9

Discussion on Hydrostatic Pressure Converters

It has been shown in theory and practice that hydropower machines can be driven by hydrostatic pressure differences. This section discusses the application of the developed theories on the design and operation of 'type one' and 'type two' HPC installations. It also compares the indicated performance of the U-HPC and M-HPC concepts with other established hydropower technologies.

9.1 Application of the Hydrostatic Pressure Converter Theories

9.1.1 'Type one' HPCs

'Type one' HPCs were defined in Section 5.2 as machines where the working surface extends from the channel bed to the *upstream* water surface. The ideal theory developed to describe such machines determined that their hydraulic efficiency was fundamentally governed by the ratio of downstream to upstream submerged water depths on the working surface, d_2/d_1. Through the use of experimental testing, this relationship was verified to hold for the peak efficiency, whilst it was also determined that in practice, leakage and turbulent losses became dominant factors at the lower and higher flow rates of any machines' operating range. These three factors need to be considered together when designing any 'type one' HPC installation, as they not only affect the efficiency and ultimately the power output, but also the size and cost. These factors need to be balanced if the design of the installation is to be economically viable.

Referring to the top of Figure 9.1, consider 'type one' HPCs where the entire head difference is generated over a *single* working blade. Examples of such machines include the *Salford Transverse Oscillator*, the *Sundermann Turbine*, and the U-HPC concept.

- Initially considering the performance of the machine, for a given head difference, higher peak efficiency values can be obtained by increasing the blade length and the depth of the upstream and downstream water channels. Increasing the d_2/d_1 ratio in this manner does however have consequences. By increasing the submersed blade length, the size of the gaps and therefore the leakage flow increases. This will impact the efficiency in the low flow region. It should be noted however that low flow rates also equate to low input powers, so the effect of a reduced operating efficiency in this range is not too detrimental in terms of power output. In contrast, the increased blade length and water depths will result in lower blade and water velocities. The effect of this will be to decrease the turbulent losses with respect to the flow rate, thus increasing the flow capacity and peak power output for a given head difference per unit width of machine.

- From an economic perspective, a balance must be found between power output and the size and cost of the installation. Although increasing the d_2/d_1 ratio increases the flow capacity, efficiency and power output, it also increases the size and cost of the machine and the associated civil engineering works. For machines such as the *Salford Transverse Oscillator* where the blade reciprocates within the flow whilst remaining submersed, the increase in size will be linear with increasing blade length, and the visual impact of the installation above the water's surface will not alter. In contrast, the increase in diameter of machines which rotate about an axis, such as the U-HPC, will be double the increase in blade length. The visual impact of these machines will increase with blade length and diameter. The slower blade speeds associated with larger d_2/d_1 ratios also mean that the forces and torques which must be converted by the power take-off systems increase. Depending on the machine in question, this will require stronger connecting rods or higher ratio gearboxes, increasing the cost of the installation.

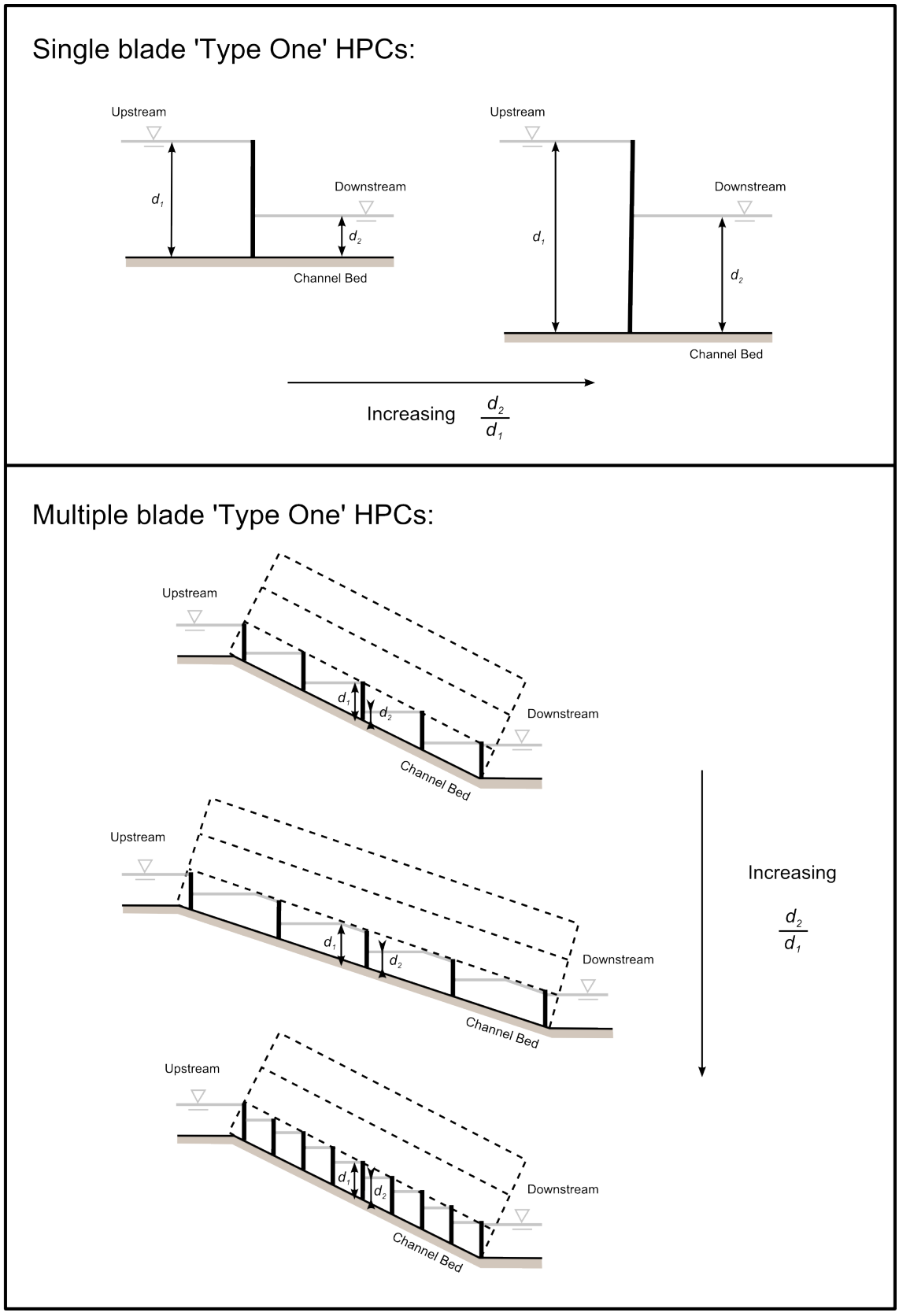

Figure 9.1: 'Type one' HPC discussion

Referring to the bottom of Figure 9.1, consider 'type one' HPCs such as the *Archimedes Screw*, where the entire head difference is generated over *multiple* working blades. The literature review indicated that the efficiency of the Archimedes screw operating as a pump was thought to relate solely to the losses of the machine, including leakage and turbulent losses. As a hydropower machine, it's power output was estimated using the equation shown in Appendix A. Whilst this also approaches the problem through an analysis of hydrostatic pressure, it does not easily lend itself to the understanding of design factors which influence efficiency. Compared to these previous analyses, the 'type one' HPC theory suggests that the efficiency is *also* a function of the ratio d_2/d_1.

- The d_2/d_1 ratio across the blades of an *Archimedes Screw* depends the gradient and the number of blades of the installation as shown in Figure 9.1. It also depends on the speed of revolution. Such machines are similar to traditional waterwheels in that they can operate with variable filling ratios. As such, the machines can handle varying flow rates whilst operating at constant speed, determined by the generator and controller. The result of this operational regime is that the filling ratio and thus the d_2/d_1 ratio alters with flow rate. The optimum operational regime would be to run the screw at variable speed, so that the maximum filling and d_2/d_1 ratio can be maintained at all flow rates. The leakage flow through the installation would increase as the length of submersed blade increases with the d_2/d_1 ratio. The greater the number of blades, or rather the turns of the thread, the higher the maximum speed of revolution must be for a given flow capacity. This could create higher turbulent losses at the inlet and outlet of the screw, reducing efficiency at higher flow rates.

- When designing an *Archimedes Screw* installation, a balance must be sought between performance and cost, which will increase with the d_2/d_1 ratio. This is because additional blades and shallower gradients, which result in longer screws, both require more material and labour to manufacture and install. Equally, maintaining high d_2/d_1 ratios through the use of variable speed generator and control system would increase costs.

9.1.2 Design of Type 2 HPCs

'Type two' HPCs were defined in Section 5.2 as machines where the working surface extends from the channel bed only up to the *downstream* water surface, such as the *Staudruckmaschine*, *Zuppingerrad* and *Aqualienne*. The ideal theory developed to describe these machines identified that the efficiency decreased with increasing flow rate. This was the result of the acceleration of the water from the relatively slow upstream situation into the machine, which resulted in a head and pressure drop at the working blade, and also a inertial reaction force to the acceleration of the water. This relationship between the efficiency and the acceleration was verified through the experimental testing of the M-HPC concept. This testing also identified the influence of leakage and turbulent losses on the efficiency profile of the machine. When designing an economically viable 'type two' HPC installation, a balance must be sought between maximising the power output and also the size, complexity, and ultimately the cost.

- From a performance perspective, figure 9.2 demonstrates how the efficiency, flow capacity (and thus the power output) vary with the extent of the acceleration. This is determined by the upstream velocity and the flow velocity within the machine. The upstream velocity will depend on the nature of the hydropower site, including the river depth and width for example. These can be altered through civil engineering works. The flow velocity within the machine is a function of the blade length, l, which defines the depth of the water between the central hub and the channel bed, d_2, as shown in Figure 9.3. Increasing the blade length to reduce the flow velocity also results in larger gaps through which leakage flow occurs. The result of this will be a slight reduction in efficiency at low flow rates. At low flow rates there is low hydraulic power available for exploitation, so a reduced efficiency in this region is not too detrimental to the economics of the installation. Reducing the flow velocity within the machine by increasing the blade length will result in a reduced speed of rotation. The turbulent losses which define the upper operating range of the M-HPC are a function of the blade length, hub radius and speed of rotation. How the turbulent losses alter by reducing the extent of the acceleration into the machine needs to be investigated further.

- From an economic persective, there is an inverse relationship between minimising the acceleration and the size and cost of the installation. Large diameters will require greater

material and labour, increasing the weight and the civil engineering works required. Reduced speeds of rotation will require gearboxes with higher gear ratios, being able to process a higher input torque. A balance would have to be sought between the efficiency and output of the machine versus its size and cost.

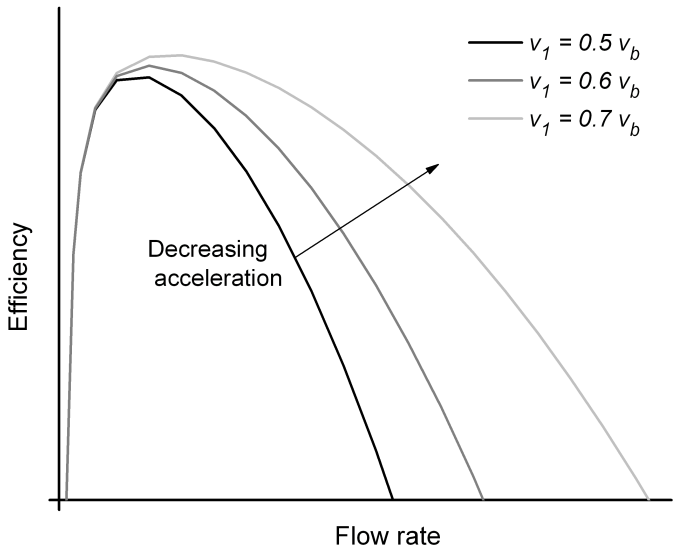

Figure 9.2: Effect on 'Type two' efficiency of decreasing acceleration

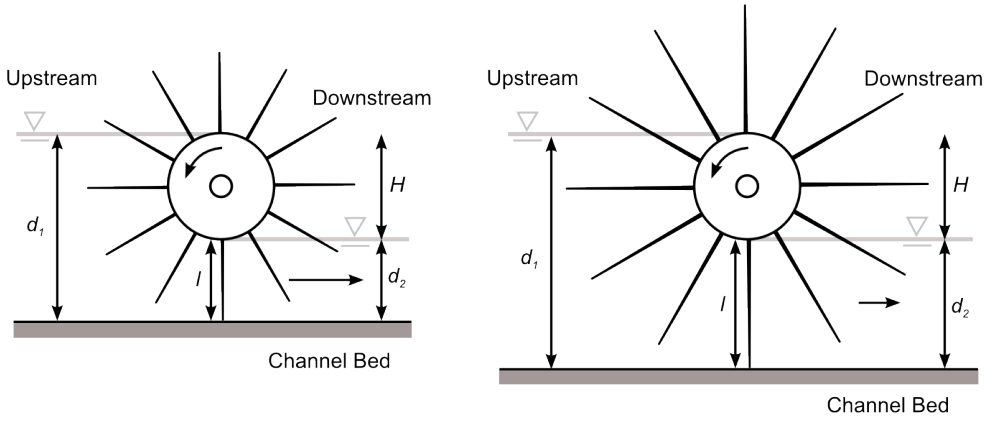

Figure 9.3: Demonstration of M-HPC with increased blade length for a given head difference

9.2 Indicated performance of concepts

The aim of this research was to develop a new technology to viably exploit very low head hydropower potential. Referring to Figure 9.4, the indicated full scale performance of the U-HPC and M-HPC concepts has been plotted along with the established waterwheel and viable turbine technologies, as originally plotted by Giescke and Monsonyi (1998) in Figure 2.2. It should be noted that the operational ranges indicated for the two concepts and the traditional waterwheels are based on a minimum wheel width of 0.5m and a maximum wheel width of 5.0m.

It can be seen that the U-HPC and M-HPC concepts are anticipated to be suitable for exploiting head differences between 0.0m - 1.0m and 0.5m - 2.5m respectively. In this region they provide an alternative to both traditional waterwheels and Crossflow turbines, with comparable peak efficiencies of around 80%, compared to 77% - 86% respectively. Whilst larger head differences may be possible, the outside diameters and channel depths may become excessive for river installations. Where the indicated performance of the two concepts excels, is the flow capacity per metre width.

- At its upper range of 1.0m head, the U-HPC has an indicated Q_{max} and P_{max} of $\sim$6 m^3/s and $\sim$40 kW per metre width. This is approximately $\sim$*5 times greater* than the largest traditional waterwheel for a 1.0m head, which had a Q_{max} and P_{max} limited to approximately $\sim$1.2 m^3/s and $\sim$8 kW per metre width.

- At its upper range of 2.5m head, the M-HPC has an indicated Q_{max} and P_{max} of $\sim$5 m^3/s and $\sim$80 kW per metre width. This is approximately $\sim$*3.5 times greater* than an equivalent crossflow turbine. It is also approximately $\sim$*5 times greater* than a traditional waterwheel for a 2.5m head, which would have a Q_{max} limited to approximately 1 m^3/s per metre width, with a P_{max} not exceeding 17kW per metre width.

In the head region 0.5m to 1.0m where the operational ranges of the U-HPC and M-HPC overlap, the most suitable choice would be determined on the basis of physical size and therefore the ability to integrate the machine into the environment, as well as the specific cost of the machines, which would need to be studied further. Whilst the M-HPC is relatively small compared to the U-HPC, with a diameter equal to $3.H$ instead of $14.H$ where H is the head difference being exploited, it is also more complex, with the radially twisting blades compared to the flat blades of the U-HPC.

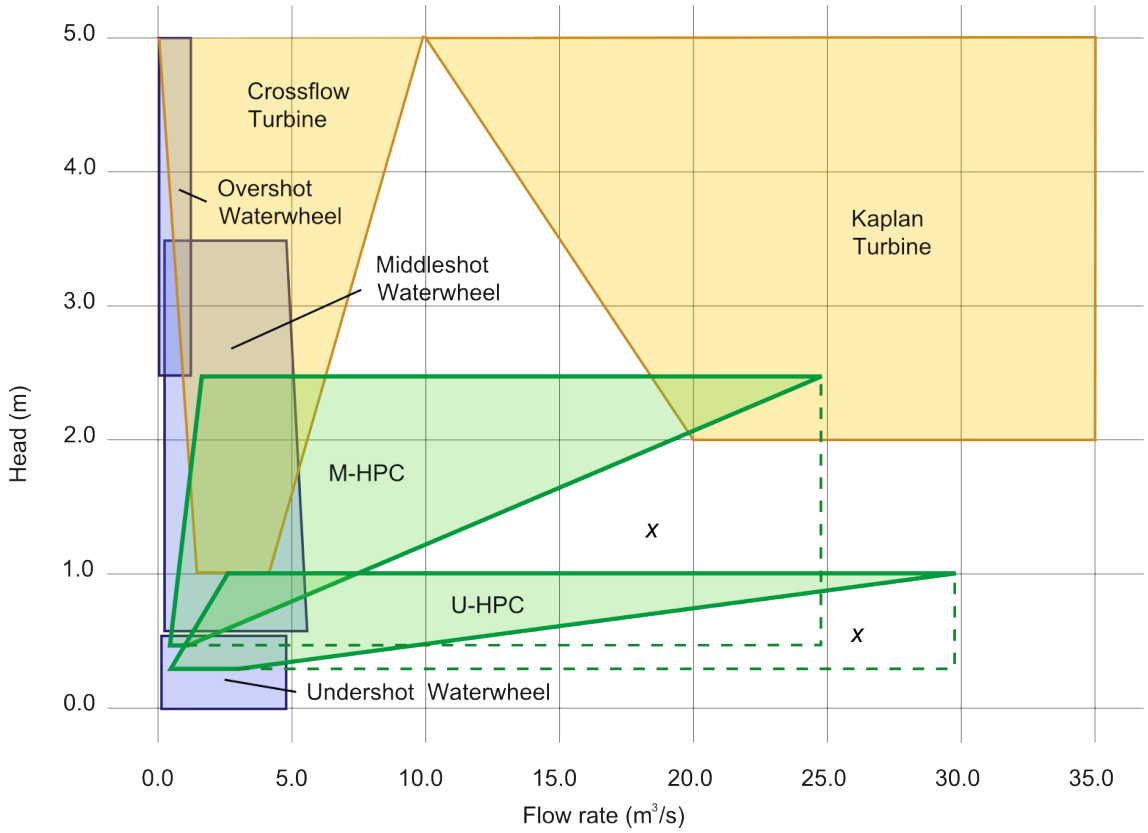

Figure 9.4: Operational ranges of the U-HPC and M-HPC relative to established technologies

The operational ranges indicated for the U-HPC and M-HPC in Figure 9.4 are limited by the Froude scaling process, which assumes geometric similarity between the model and estimated scales. For example, for all head projections the M-HPC has a head, hub diameter and blade length relationship of 1:1:1. It would be possible to combine larger blade lengths with smaller hub diameters, or in the case of the U-HPC, large diameter wheels relative to smaller heads. On this basis, the operational ranges of the U-HPC and M-HPC could be extended into the regions marked 'x' on Figure 9.4. It was shown in the Results and Analysis chapter that turbulent losses accounted for a significant reduction in performance with increasing rotational speed, potentially reducing the potential flow capacities and power outputs that could be achieved. The two concepts are mere prototypes and not optimised machines.

The U-HPC and M-HPC designs already represent a significant improvement over established technologies, but are in their infancy and have remaining development potential.

Chapter 10

Conclusion

The aim of this document was to develop a novel technology to viably exploit very low head hydropower installations in river environments. This has been successfully achieved by identifying and applying an unrecognised operational principle - that hydropower machines can be directly driven by the hydrostatic pressure of flowing water.

Analysis of the proposed operational principle has resulted in two approaches to exploiting hydrostatic pressure, and two idealised theories describing these approaches. These have been verified by conducting hydraulic testing of two concept *Hydrostatic Pressure Converters*, and improved through identifying empirical factors for turbulent and leakage losses. Both of these machines operated with high hydraulic efficiency, around 80%, and were predicted to be suitable for head differences below 2.5m. Significantly, the flow capacity and power output per metre width of machine was estimated, through scale analysis, to be up to 5 times greater than equivalent, traditional waterwheel technology conventionally used for exploiting very low head hydropower sites.

In conclusion, it has been identified and shown that *Hydrostatic Pressure Converters* are a promising alternative to the established very low head hydropower technologies. As their principle of operation is novel, being neither impulse, reaction nor potential, it is proposed that they should be recognised as a new classification of hydropower machine.

Chapter 11

Further work

11.1 Simulation

Whilst the proposed theories may be relatively simplistic, they do adequately demonstrate the principles behind 'type one' and 'type two' HPCs. Their use when it comes to prediciting the performance of real life machines is however limited by their inability to accurately predict the turbulent losses. These losses are very hard to estimate as they are heavily dependent on the quality of the proposed design. The complexity of the geometries and flow scenarios is such that satisfactory results may only be achievable through the use of computer simulation. Whether the profitability of such machines is sufficient to justify the time an expense of conducting simulations is not known. It may be acceptable to conduct further scale model testing, as this would be required in any case to verify any simulated model.

11.2 Further Testing

The proposal to conduct either computer simulation or further scale modelling is made for several reasons. The first is that both the U-HPC and M-HPC concepts were only first stage prototypes, and were not optimised. It was shown that the upper ranges of their flow capacity and power outputs were heavily limited by turbulent losses. It is anticipated that these concpets have remaining development potential, and the testing of alternative blade and shroud designs may result in not-negligible performance improvements. It is also anticipated that the M-HPC could be built with different ratios of central hub diameter to blade length to that testing in this document. Such machines would have different blade velocity and side filling and ventilation requirements, and overall their turbulent losses are an entirely unknown quantity. This work would be of great interest as it may be possible to design M-HPCs with significanly reduced levels

of acceleration and turbulent losses. It is also not yet known how the M-HPC would operate in an actual hydropower environment. Whilst the upstream water level would be determined by the machine itself through the appropriate control of the load, the downstream water depth would vary with the flow rate. The effect of such changes on the performance of such machines should be determined, as any unknown properties represent an avoidable risk.

11.3 Economic Assessment

If either of the concepts are to be recognised as feasible alternatives to established hydropower machines, it would be a worthwhile exercise to conduct some form of economic assessment. The increased flow capacities and power output of these machines when compared to traditional waterwheels would suggest a reduced specific cost of installation. This is indicated by a case study which was presented at the 2008 Hidrenergia conference in Slovenia (Senior et. al. 2008), see appendix E. Initially, it would be worthwhile conducting an additional case study but in greater detail; based upon an actual design for an installation, upon which manufacturers could provide quotes. In the longer term however, it is the experience of the author that the industry, and potential clients for such low head technologies, will only have confidence in such claims when a fully operational, grid connected prototype is functioning.

11.4 Environmental Impact Assessment

The final proposal for further work on HPCs, is an environmental impact assessment. It is proposed that these machines could be relatively fish friendly when compared to established technologies. This is because their large cells, slow speeds of revolution, relatively few blades and unique property of extending from the upstream water surface down to the channel bed, mean that no sudden pressure changes occur within the machine and the chance of mechanical strike is low. The relatively simple flow path and the property of extending from the upstream water surface down to the channel bed may also permit an improved transport of sediment within the river when compared to the established hydropower technologies. These proposed benefits are based on the physical properties of the two machines, but have not yet been investigated. If they could be confirmed, it would mean that HPCs not only represent a significant development in the field of very low head hydropower on the grounds of their hydraulic performance, but also on the grounds of economics and low environmental impact.

Reference List

ATRO, R, (2006), *Hydrodynamic Screws*, Available from http://www.ritz-atro.de/2006/downloads/Wasserkraft_GB.pdf [Accessed 23/01/2008].

BACON, I. (2004), *Low Head Hydro Power in the South-East of England - A Review of the Resource and Associated Technical, Environmental and Socio-Economical Issues*, TV Energy. Available from `http://www.tvenergy.org/publications.htm`, [Accessed 11/12/07].

BACH, C. V. (1886), *Die Wasseräder* , KonradWittwer Verlag, Stuttgart (in German).

BAKIS, R. (2007), *The Current Status and Future Opportunities of Hydroelectricity*, Energy Sources Part B, 2:259-266.

BRESSE, J. (1876), *Water Wheels or Hydraulic Motors*, reprint 2003, University Press of the Pacific.

BRINNICH, A. (2001), Wasserkraft-Staudruckmaschine. Neus, Konkurrenzlos Umweltfreundliches und Wirtschaftliches Kraftwerkskonzept, *Wasserwirtschaft*, 91, 70-74. (in German), Available from http://www.oewatec.de/Grafik/Gutachten%20SDM%2016.02.07.pdf , [Accessed 11/12/07].

BRINNICH, A. (2006), *Osterreichische Patentanmeldung AT 501 575 A1 2006-09-15*, Patent.

BRINNICH, A. (2008),Staudruckmaschine inventor's website, available from `http://www.staudruckmaschine.de/` (in German), [Acessed 09/01/09].

ELING, (2005), Eling Tide Mill Website, Available from `http://www.elingtidemill.wanadoo.co.uk`, [Accessed 11/12/07]

ENCYCLOPAEDIA BRITTANICA (1911), Encyclopaedia Brittanica, chapter *Waterwheels*, 95-97.

BROCKHAUS, F.A. (1903), Brockhaus Konversations-Lexicon, chapter *Wasserraeder*, 14th Jubilee edition, volume 16, Leipzig (in German).

BRYDEN, I. & COUCH, S. (2006), ME1 - Marine Energy Extraction: Tidal Resource Analysis, *Renewable Energy*, volume 31, 133-139.

CHADWICK, A. MORFETT, J. BORTHWICK, M. (2004), *Hydraulics in Civil and Environmentl Engineering*, 4th Ed., Spon Press, New York.

CHANSON, H. (2001), *The Hydraulics of Open Channel Flow*, Butterworth-Heinemann.

CIOCCI, L. (2003), *Hydropower Research and Development Reccommendations*, J. Energy engineering ASCE.

DAVIS, B. (1997), *Low Head Tidal Power: a Major Source of Energy From the Worlds Oceans*, IECEC-97. Proceedings of the Thirty-Second Intersociety Energy Conversion Engineering Conference (Cat. No.97CH36203) V 3, 1982-1989.

DENNY, M. (2003), *The Efficiency of Overshot and Undershot Waterwheels*, European Journal of Physics 25, 193-202.

DGCG (2004), *Technical Guide to the Connection of Generation to the Distribution Network* Available from http://www.energynetworks.org/spring/engineering/pdfs/DGSG/FES_00318_v040211.pdf, [Accessed 11/12/07].

ELY, R. (2003), *The Sagebien Project*, Technical report, The Davis Collaborative. Available from `http://daviscollaborative.com/projects/sagebien-abstract.htm`, [Accessed 11/12/07].

ETSU (1982), *Small Scale Hydroelectric Potential in the UK*, ETSU.

EURECA (2005), *FP7 Research Priorities for the Renewable Energy Sector*, EURECA.

EUROPEAN COMMISION (1997), *White Paper for a Community Stratergy and Action Plan - Energy for the future:Renewable Sources of Energy*, COM(97)599.

EUROPEAN COMMISSION (2007), *Small Hydro: Objectives - technical*, Available from `http://ec.europa.eu/energy/res/sectors/small_hydro_en.htm`, [Accessed 11/12/07].

FAIRBAIRN, W. (1849), *On Water-wheels with Ventilated Buckets*, Institution of Civil Engineers No.793.

FITZ, J. & MERRIMAN, M.LEE, L. (2004), *Overshot Water Wheels For Small Streams*, Algrove Publishing Limited.

FONFREDE (2004) Patent CA2506553, available from http://www.wikipatents.com/ca/2506553.html, [Accessed 11/12/07].

FONFREDE (2008a), Aqualienne brochure, available from http://www.h3e.fr/site_h3e2/plaquette_commerciale_v.9.1.pdf, [accessed 20/12/08].

FONFREDE (2008b), Aqualienne website, available from http://www.h3e.fr/pages/referencespag.html, [accessed 20/12/08].

GERHARDT, P. (1893), Ueber Aaleitern und Aalpässe, *Zeitschrift fuer Fischerei und deren Hilfswissenschaften*, 194-199, Neuman, Berlin (in German)

GIESCKE, J. & MONSONYI, E. (1998), *Wasserkraft-Anlagen*, Springer (in German).

GOLDSMITH, K. (1993), *Economic and Financial Analysis of Hydropower projects*, Norwegian Institute of Hydraulic Engineering.

HARKIN, S. (2007), *The Archimedes Screw as a Micro-Hydro Turbine*, MSc Dissertation, The Univeristy of Edinburgh, School of Engineering and Electronics.

HYDROLINK, (2008), Kaplan manufacturer's website, available from `http://www.hydrolink.cz/kaplan.php`, [accessed 20/12/08].

KALTSCHMITT, M. et al. (2007), *Renewable Energy*, Springer.

KHATER, F. (1996), *Power Electronics in Wind Energy Conversion Systems*, Proceedings of the Intersociety Energy Conversion Engineering Conference', IEEE, 1773 1776.

KILLER, F. (2003), *Einbau einer Kleinwasserkraftanlage an der Stadtbachstufe des WKW Isarwerkes 3 Diplomarbeit*, Master's thesis, FH Munchen (Fb Maschinenbau) (in German).

KROMPHOLZ, D. (2008), *Low Head Hydro Turbines*, Joule Centre Annual Conference, available from http://www.joulecentre.org/events/3apr08/Pres4VATECH%20HYDRO_Low%20Head%20Hydro%20turbines%20r2%20Dieter%20Kromphol.pdf, [accessed 20/12/08].

LAL, J. (1967), *Hydraulic Machines*, Metropolitan Book Company, Delhi.

LECLERC, M. (2008), The Very Low Head Turbogenerator Set Concept - Evaluation of 1^{st} Year Operation, *On the Crossroads*, Hidroenergia conference 2008, Bled, Slovenia.

LECLERC, M. (2009), Very Low Head Turbine manufacturer's website, available from `http://www.vlh-turbine.com`, [accessed 09/01/09].

LOCKETT, W. (2001), Jacob Leupold's analysis of the overshot water-wheel, *Water & Maritime Engineering*, 148 Issue 4, 211-218.

McGUIGAN (1978), *Small Scale Water Power*, Wheaton & Co. Ltd, Exeter.

MEYERS (1908), Meyers Grosses KonversationsLexikon, Bibliographisches Institut, chapter *Wasserraeder und Turbinen* (in German).

MÜLLER, G. DENCHFIELD, S. MARTH, R. SHELMERDINE, B. (2007), Stream Wheels for Applications in Shallow and Deep Water, *Harmonizing the Demands of Art and Nature in Hydraulics*, 32nd Congress of the IAHR, Venice, Italy.

MÜLLER, G. & KAUPPERT, K. (2004), Performance Characteristics of Water wheels, *Journal of Hydraulic Research*, 42, 451-460.

MÜLLER, G. & KAUPPERT, K. (2002), Old Watermills - Britain's New Source of Energy?, *Civil Engineering*, 150, 178-186.

MÜLLER, G. & WOLTER, C. (2004), The Breastshot Waterwheel: Design and Model Tests, *Engineering Sustainability*, ES4, 203-211.

MÜLLER, W. (1939), *Die Wasserraeder*, Reprint of the 2^{nd} edition, Moritz Schaefer, Detmold, 1999 (in German).

MÜLLER, W. (1899), *Die Eisernen Wasserraeder* (The Iron Waterwheels), Verlag von Veit & Comp (in German).

MÜLLER, W. (1899b). *Die Eisernen Wasserräder: Atlas.* (The Iron Waterwheels: technical drawings.) Veit & Comp., Leipzig (in German).

NAGEL, G, & RADLIK, A. (1988), *Wasserförderschnecken*, Bauverlag, Wiesbaden / Berlin (in German).

NRW (2005), *Handbuch Querbauwerke*, Klenkes-Druck & Verlag GmbH, Aachen (in German).

OSSBERGER, (2008), Crossflow turbine manufacturer's webiste, available from http://www.ossberger.de/cms/en/hydro/the-ossberger-turbine/, [Accessed 20/12/08].

PAISH, O. (2002), Small Hydro Power: Technology and Current Status, *Renewable & Sustainable Energy Reviews.*

RORRES, C. (2000), The Turn of the Screw: Optimal Design of the Archimedian Screw, *Journal of Hydraulic Engineering*, 72-80.

SAGEBIEN, (2007), Website on the Sagebien waterwheels, available from `http://www.a3i.fr/roueMilieur_vanne_sagebien1.htm` (in French), [Accessed 11/12/07].

SENIOR, J. MÜLLER, G. WIEMANN, P (2007), The Development of the Rotary Hydraulic Pressure Machine, *Harmonizing the Demands of Art and Nature in Hydraulics*, 32nd Congress of the IAHR, Venice, Italy.

SENIOR, J. MÜLLER, G. WIEMANN, P (2008), The Rotary Hydraulic Pressure Machine for Very Low Head Hydropower Sites, *On the Crossroads*, Hidroenergia conference 2008, Bled, Slovenia.

SMITH, N. (1976), *Man and Water, A History of Hydro-Technology*, Peter Davies, London.

SUNDERMANN (2008), Sundermann inventor's webite, avaiable from `http://www.sundermann.com.au`, [Accessed 20/12/08].

TNSHP (2005), *Proposals for a European Strategy of Research, Development and Demonstration (RD&D) for Renewable Energy from small hydropower*, ESHA.

WEC, (2004), World Energy Council, *Survey of Energy Resources*, Elsevier.

WEC, (2001), World Energy Council, *Survey of Energy Resources*, Elsevier.

WIEMANN, P. MÜLLER, G. SENIOR, J. (2007), Review of Current Developments in Low Head, Small Hydropower, *Harmonizing the Demands of Art and Nature in Hydraulics*, 32nd Congress of the IAHR, Venice, Italy.

WILSON, E. BULLOCK, G. JONES, I. (1984), Two New Machines for Hydraulic Power from Low Heads, 530-548, *Symposium on Hydraulic Machinery in Energy Related Industries*, 12^{th} IAHR Symposium, Stirling, Sweden, Natl Engineering Lab.

ZOTLÖTER, F. (2006), *Das Gravitationswasserwirbelkraftwirk* (in German), available from `http://www.watervortex.net/download/DE_Wasserwirbeltechnik.pdf`, [Accessed 09/01/09].

ZOTLÖTER, F. (2009), Gravitational Vortex Machine inventor's website (in German), available from `http://www.watervortex.net/?Leistungsdaten`, [Accessed 09/01/09].

Appendix A: A Mathematical Analysis of the Archinedes Screw

$$
\begin{aligned}
&\Lambda_{total} = \\
&n\omega\rho g \sin(\alpha)\Bigg[\Bigg\{\Big(r\sqrt{1-\tan^2(\alpha)}\tan(\frac{\pi}{2}-\alpha)\Big)\Big(\theta_b-\theta_a\Big) \\
&+\frac{L}{2n\pi}\Big((\pi-\cos^{-1}(\tan(\alpha)))(\theta_b-\theta_a)-\frac{\theta_b^2-\theta_a^2}{2}\Big)\Bigg\} \\
&\left\{\frac{-1}{4n^2}\frac{\sqrt{\frac{L^2+4n^2\pi^2R^2}{L^2}}(L^2+4n^2\pi^2r^2)-\sqrt{\frac{L^2+4n^2\pi^2r^2}{L^2}}(L^2+4n^2\pi^2R^2)}{\pi^2\sqrt{\frac{L^2+4n^2\pi^2R^2}{L^2}}\sqrt{\frac{L^2+4n^2\pi^2r^2}{L^2}}}\right\} \\
&+\tan(\frac{\pi}{2}-\alpha)\big(\cos(\theta_a)-\cos(\theta_b)\big)\Bigg\{\frac{L^3}{16n^3\pi^3}\Bigg[\frac{2nr}{L}\sqrt{\frac{L^2+4n^2\pi^2r^2}{L^2}}\pi- \\
&\ln\left(\frac{2n\pi r}{L}+\sqrt{\frac{L^2+4n^2\pi^2r^2}{L^2}}\right)+\ln\left(\frac{2n\pi R}{L}+\sqrt{\frac{L^2+4n^2\pi^2R^2}{L^2}}\right)- \\
&\frac{2nR}{L}\sqrt{\frac{L^2+4n^2\pi^2R^2}{L^2}}\pi\Bigg]\Bigg\}\Bigg]. \qquad (28)
\end{aligned}
$$

Figure 11.1: Archimedes Power output equation by Harkin (2007)

Appendix B: Froude Scaling Laws and Scale Effects

This document makes extensive use of scale models (i.e. smaller than the full scale intended) for physical testing, allowing the performance of full scale machines to be estimated and the theory analysed. Scale models were used not just for economic reasons, but also because of the flexibility and adaptability they allow in the laboratory environment. The flow conditions of the scaled *model* are said to be similar to the full scale *prototype* if the model displays similarity of form, motion and forces. These terms are shown as:

$$Geometric\,similarity,\ l_r = \frac{l_p}{l_m}$$

$$Kinematic\,similarity,\ v_r = \frac{v_p}{v_m}$$

$$Dynamic\,similarity,\ F_r = \frac{F_p}{F_m}$$

with:

r	ratio
p	prototype (full scale)
m	model
l	length
v	velocity
F	force

If the physical scale of a model is reduced linearly from $l_r = 1$, it will be observed that v_r and F_r do not reduce linearly with it. This is because important parameters, namely gravity, the density, dynamic viscosity, and bulk modulus of elasticity of water, and the surface tension of air and water, *remain constant*. Accordingly the relationship between these ratios for open channel flows with a free surface are governed by the *Froude number:* $F_r = v/\sqrt{gl}$, the value of which is constant for both the model and the prototype (Chanson 2001).

This number implies equation 11.1 from which all further relationships are determined in terms of l_r, with $\rho_r = 1$, as the same working fluid is used for the model as the prototype.

$$velocity: \; v_r = \sqrt{l_r} \tag{11.1}$$

$$Time: \; t_r = \frac{l_r}{v_r} = \sqrt{l_r} \tag{11.2}$$

$$Flow\,rate: \; Q_r = v_r\, l_r^2 = l_r^{2.5} \tag{11.3}$$

$$Mass: \; \rho_r\, l_r^3 \tag{11.4}$$

$$Power: \; P_r = \frac{M_r\, l_r^2}{t_r^3} = l_r^{3.5} \tag{11.5}$$

In the case of machines such as waterwheels, which are built to different widths, quantities such as flow rate are normally quoted per metre width of machine. This is calculated by dividing by $l_r\, W_m$, where W_m represents width of the model. The rotational speed of the prototype is calculated using the velocity relationship applied at the centre of the working blade.

The important point is that these relationships only apply when there are no *scale effects*. These can occur if the scale of the model is too small and effects other than gravity (in the case of free surface flows) become dominant. These can include exaggerated turbulence or air entrapment at the model scale due to their higher speeds resulting in an underestimated full scale efficiency. Equally, the higher surface area to volume of the scaled model when compared to the prototype can also result in an underestimated full scale efficiency (Ely 2003).

Appendix C: Test Matrix

Test model and conditions	Description:	Primary purpose:	Comments on testing:
Small scale U-HPC, self-levelling conditions	Test series conducted with variable flow, head and speed of rotation. Downstream depth determined by weir, set to 30mm, 80mm, 130mm, 180mm and 230mm	To determine the relationship between efficiency and the ratio d_2/d_1.	With the downstream weir set to 30mm, data could only be obtained at low flow rates. At higher flow rates, the 'evacuation' process made flow measurment over the sharp crested weir impossible.
Small scale U-HPC, constant level conditions	Test series conducted with variable speed of rotation and flow rate, but constant head.	To determine the relationship between efficiency and the speed of rotation/flow rate.	Following the Small scale U-HPC tests, the constant level tests were conducted with d_1 set to 165mm and d_2 set to 235mm, giving a d_2/d_1 ratio of 0.7.
Large scale U-HPC, self-levelling conditions	Repeat of small scale self-levelling tests using a 1.6 times larger model U-HPC. Downstream weir set to 48mm, 128mm, 208mm, 288mm, and 368mm accordingly.	To investigate whether scale effects were present at the small scale, and therefore whether the small scale U-HPC and M-HPC data could be used to produce full scale estimates with confidence.	Limitations in the performance of the Prony Brake and the positioning of the sharp crested weir arose, which could not be resolved in time. Only limited data was obtained at low flow rates using the weir set to 208mm and 288mm.
M-HPC, constant level conditions	Test series conducted with variable speed of rotation and flow rate, but constant head.	To determine the relationship between efficiency and the speed of rotation/flow rate.	-

Table 11.1: Test Matrix

Appendix D: Conference paper 1

Appendix E: Conference paper 2

THE DEVELOPMENT OF THE ROTARY HYDRAULIC PRESSURE MACHINE

James Senior [(1)], Dr. Gerald Müller [(2)], Patrick Wiemann [(3)]

[(1)] Civil Engineering Department, University of Southampton, Highfield, Southampton, SO17 1BJ, U.K., phone: +44 238059 4656; e-mail: pw1105@soton.ac.uk, web: wwwlowheadhydropower.com
[(2)] Civil Engineering Department, University of Southampton, Highfield, Southampton, SO17 1BJ, U.K., phone: +44 238059 2442; e-mail: g.muller@soton.ac.uk, web: wwwlowheadhydropower.com
[(3)] Civil Engineering Department, University of Southampton, Highfield, Southampton, SO17 1BJ, U.K., phone: +44 238059 4656; e-mail: js1301@soton.ac.uk, web: wwwlowheadhydropower.com

ABSTRACT

There currently exists a demand for economical hydro-electric machinery that operates at low heads and moderate flows; sites where the drop from a higher water level to a lower one is quite small, in the order of 1-3 m, with flows between 5 m^3/s and 15 m^3/s. The economics which determine a machine's viability are a function of its size and complexity, its efficiency characteristics and its power output. This paper analyses the *Staudruckmaschine* (SDM) in detail using scale model tests. These tests found that the SDM had many deficiencies resulting in unnecessarily low efficiencies and flow capacity, which is the volume of water which the wheel can process per second per metre width. The scale model tests also aided the development of a new detailed theory of operation for wheels operated by hydraulic pressure. Significant modifications are then proposed for the SDM to address its deficiencies. These revise its channel design, blade shape, and support structure. The result is effectively a new machine, the *Rotary Hydraulic Pressure Machine* (RHPM), which is expected to have over 20 % higher efficiency, greater flow capacity and smoother operation than the SDM. The RHPM can be built at any site; however it is especially suitable for incorporation into existing weir structures with minimal modifications being required to the weir structure itself. Furthermore, the RHPM is unlike most conventional rotodynamic machines as it is symmetrical and therefore fully reversible. This property means it also has potential application in tidal flow environments.

Keywords: Rotary Hydraulic Pressure Machine, Staudruckmaschine, Low Head, Hydropower

1 INTRODUCTION

The European Commission has set a target which requires 12 % of the total electricity production to come from renewable sources by 2010. Within Europe, over 70 % of the theoretically available hydropower output is already exploited (Giesecke & Mosonyi 2005). Of this, the development of hydropower over 1 MW installed capacity is virtually complete and what remains are sites with head falls between 1 m and 3 m. Until now this sector of hydropower has generally been considered un-exploitable and ignored by many resource surveys, e.g. ETSU (1982). An indication of the number of potential sites was made by NRW (2005) which counted the number of weir structures in a German federal state with an area of 1,000 km^2. This found 1,304 potential sites with heads between 0.2 m and 1.0 m which would suggest that tens of thousands of sites must exist throughout Europe. The majority of these sites have flow rates too small to make use of conventional turbines economically. This fact has been realised and many manufacturers are now developing new technologies to address this. The working principles range from kinetic energy conversion, the creation and utilization of vortex flow, siphon-action,

wave energy conversion for re-conversion into higher head differences, 'classic' stream wheels and a rotary hydraulic pressure machine. A study of these machines by Wiemann (2006) found most of these to have insufficient efficiency to be economical. This concluded that the technology with the most potential so far was the *Staudruckmaschine* which had the greatest efficiency and would have the least ecological impact.

2 THE STAUDRUCKMASCHINE

The *Staudruckmaschine* (SDM) shown in Figure 1 (comprising two symmetrical units) was patented in 2001 (Brinnich) as an attempt to exploit sites with low heads and moderate flows, that is with 1-3 m head and flows from 5 m^3/s to 15 m^3/s (assuming a 5 m wide wheel). *Staudruck* translates as dam-effect, and a definition is proposed:

A Dam-effect waterwheel restrains the flow of water thus maintaining the upstream water level, without the use of a sluice gate

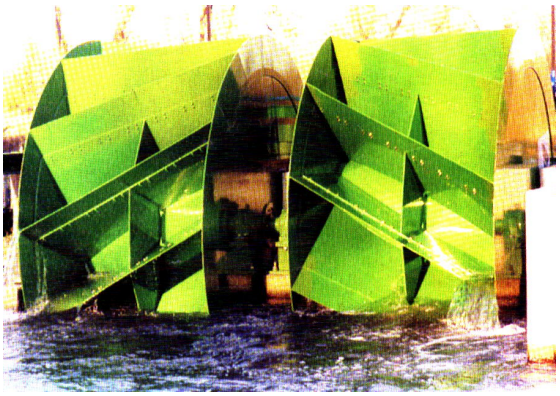

Fig.1. The *Staudruckmaschine*, SDM (Brinnich, 2001)

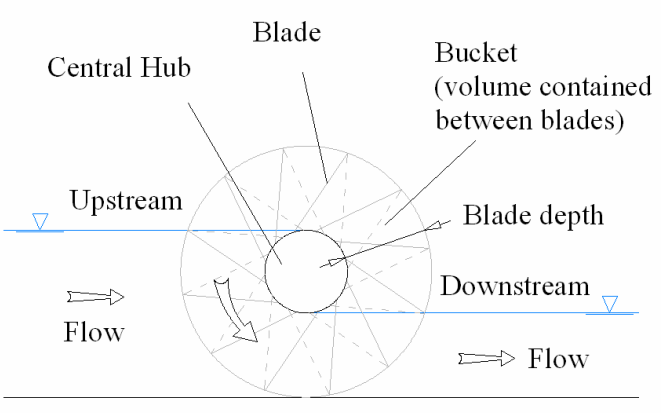

Fig.2. Detail of the SDM

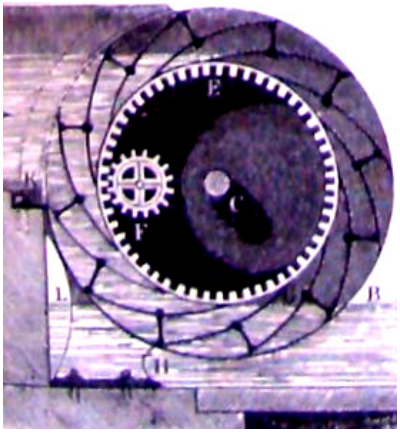

Fig.3. The *Zuppingerrad* (Brockhaus 1903)

Referring to Figure 2, the SDM has a central hub the same diameter as the head drop between the upstream and downstream water levels. When compared to traditional waterwheels for equivalent heads, it has a relatively large blade depth, roughly 2/3 of the radius, and the buckets fill completely with water. This means that the flow through the wheel is greater per revolution; however efficiency and flow rate are a function of speed of rotation. This type of wheel geometry is not entirely novel, as the hub's relation to the water levels was originally conceived as the *Zuppingerrad* shown in Figure 3. The unique feature of the SDM is its diagonally mounted blades which enter and exit the water continuously across the width of the wheel as it rotates, instead of at an instant as with traditional waterwheels. This allows the water to run into and out of the buckets more gradually and with less impulse. The blades are supported between two disks.

The inventor claimed that the SDM costs just 10-30 % of an equivalent turbine. Its efficiency would never drop beneath 90 % even when partially filled as the only source of loss was leakage through *air gaps*. This only loss was quantified as being 2-3 % and the maximum flow rate was stated to be 3 m^3/s per m width. The explanation indicates that the SDM exploits the energy of the current, similar to a 'classic' stream wheel. The pilot program was considered to be a success and has been shut down as testing is complete. A study by Killer (2003) found that no data was available from the pilot program and access was not granted. It was concluded that the claims did not seem reasonable and that the true efficiency was not known. As a result he concluded that obtaining planning permission for the SDM would be very difficult.

When compared to the other new technologies under development the SDM has several advantages. It is a relatively simple machine operating with just one phase (water) and having a continual rotational motion allows direct energy conversion. Due to its full fronted water entry mechanism it is least likely to have an adverse impact on fish and sediment transport.

3 IDEALISED THEORY OF OPERATION FOR THE SDM

The SDM and its channel bed have geometric similarities with stream wheels and this has often created confusion. It must be noted that no similarities exist in their operation; a stream wheel extracts kinetic energy from fast flowing water by decelerating it. Its blade speed is approximately equal to the velocity of the downstream which is **less** than the upstream velocity. The SDM also has a blade speed approximately equal to the downstream velocity, which unlike the stream wheel is **greater** than the upstream velocity.

The SDM rotates because of forces generated on the blades as they pass underneath the hub. The largest force is generated by the difference in hydraulic pressure either side of the wheel, resulting from the dissimilar depths of water. This is partially counteracted by a reaction force to the acceleration of the water as it is forced underneath the hub, acting similar to a nozzle. These two forces are assessed below using the following idealised model which illustrates the working principle:

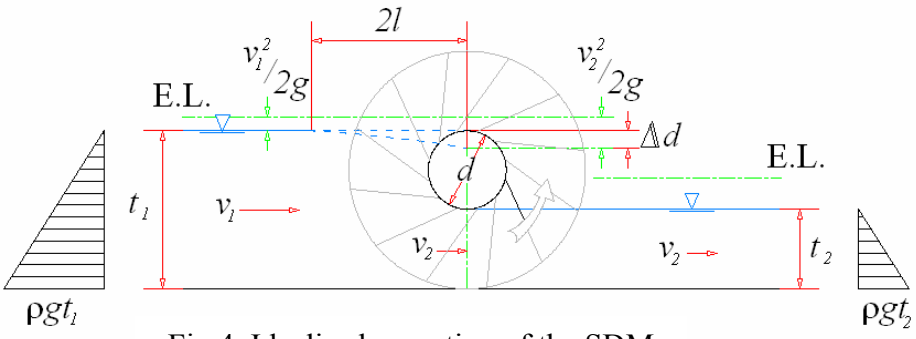

Fig.4. Idealised operation of the SDM

The model makes the following assumptions:

- The bearings are frictionless
- There are no losses as the blades enter and exit the water without influence
- The velocity of the blades as they pass beneath the hub is equal to the downstream water velocity, v_2
- There is no leakage around or underneath the wheel

Force due to hydraulic pressure differential

Referring to Figure 4 the head difference between the upstream and downstream water levels is t_1 - t_2. The flow rate Q and thus the speed v_2 are proportional to the rotational speed of the wheel. With the wheel stationary both v_1 and v_2 equal zero. As the wheel starts to rotate v_2 becomes greater than v_1, and in accordance with continuity we get equation 1:

$$v_2 = \frac{t_1}{t_2} v_1 \tag{1}$$

Assuming that v_2 is achieved beneath the hub, this acceleration of the water leads to a drop in water level, Δh:

$$\Delta h = \frac{v_2^2 - v_1^2}{2g} \tag{2}$$

The force on the blades due to the hydraulic pressure F_P acting on the blade therefore drops (F_P= Pressure × Area of blade A):

$$F_P = \rho g \left(t_1 - t_2 - \Delta h\right) A \tag{3}$$

Counter-acting acceleration force

The reaction force to the nozzle effect under the hub, F_A is equal to the mass flow rate × the acceleration. The acceleration is calculated assuming that the known velocity change took place over length l equal to twice the diameter of the hub.

$$F_A = Q\rho \frac{v_2^2 - v_1^2}{2l} \tag{4}$$

Idealised Output Power

The idealised power output is the total force acting on the blade under the hub ($F_P - F_A$) multiplied by its velocity:

$$P_{out,ideal} = \left(A\rho g \left(t_1 - t_2 - \Delta h\right) - Q\rho \frac{v_2^2 - v_1^2}{2l} \right) v_2 \tag{5}$$

Efficiency

$$\eta = \frac{P_{out}}{P_{in}} = \frac{P_{out}}{(t_1 - t_2)\rho g Q} \tag{6}$$

The idealised efficiency curve is shown alongside scale model test results in section 5.

4 MODEL TESTING OF THE SDM

For the purposes of comparison, a ~1/10 scale model of the original SDM machine shown in Figure 1 was constructed for testing in a hydraulic flume. This model is shown in Figure 5. The flume was 12 ×0.3 × 0.3 m in dimensions and had a maximum flow rate of 50 l/sec.

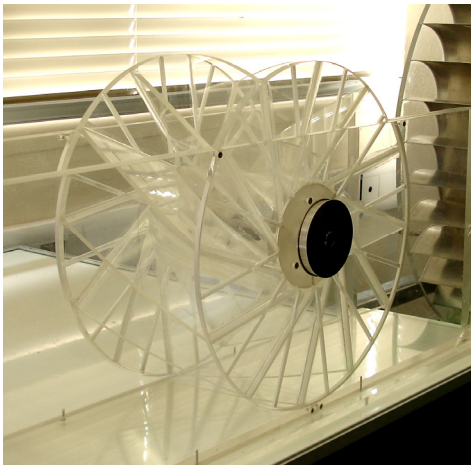

Fig.5. Scale model of the SDM

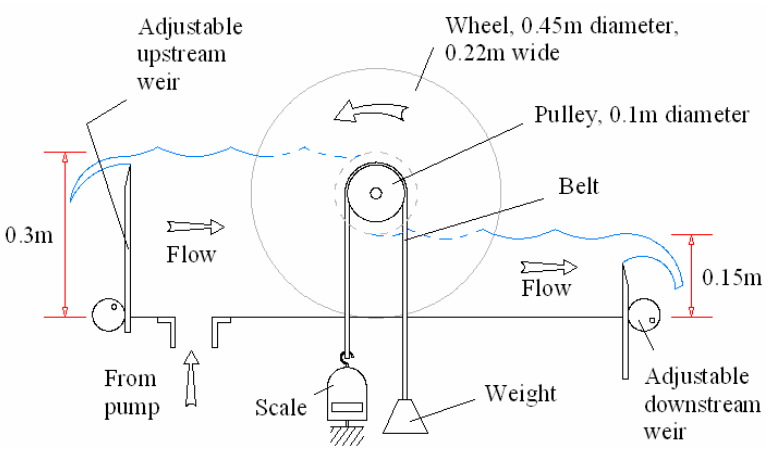

Fig.6. Setup of the scale tests

The experimental setup is depicted in Figure 6. Water from the pump entered the flume at the deeper upstream section, flowed through the SDM and exited via the shallower downstream section. Weights were added to the *Prony brake* power take off system to control the speed of rotation and measure the power output directly. This consisted of a pulley attached to the axel of the wheel, a weight and scale acting as a counter weight. The belt was made stationary, creating a friction force on the pulley equal to the difference between the two weights. Accordingly the measured power output was as follows:

$$P_{out,measured} = (w_1 - w_2)\, g\, 2\pi\, r\, f \qquad (7)$$

With: w_1 the mass of the weight (kg)
w_2 the mass of the counter weight (kg)
r the radius of the pulley (m)
f the frequency of rotation ($^1/_s$)

For the SDM, the speed of rotation, flow rate, upstream and downstream levels are four dependent variables, each influencing the other three. To simplify the set up process, weights would be added to the *Prony brake* and the flow rate from the pump would be set artificially high. Any excess flow from the pump which would otherwise have caused the other three variables to change would effectively bypass the SDM model by flowing over the upstream weir. This weir was adjustable in height so that the upstream water level could be set to within 1 mm of its designed level. This was measured using 0.1 m diameter water columns connected to the base of the flume via small diameter tubes. The water in these columns was not influenced by the waves generated by the rotating wheel. An adjustable weir was also used to obtain the designed upstream water level with variable flows. This doubled as a sharp crested measurement weir so that all flow passing through the SDM was accurately measured. The model was supported by two plain nylon bearings to prevent leakage around the wheel. These had more friction than desired so the speed/friction relationship was measured and the power output value was adjusted to eliminate this loss.

5 RESULTS AND ANALYSIS OF THE SDM

This section compares the idealised theory from section 3 to the data obtained from the scale model tests. Disparity is observed and the idealised theory is advanced accordingly. As can be seen in Figure 7 the model tests achieved a maximum efficiency of ~40 % and a maximum flow rate of 12 l/sec. Converted using the Froude scaling laws this is equivalent to 1.6 m^3/s per m width for the original 4.25 m diameter wheel, roughly half that claimed by the inventor.

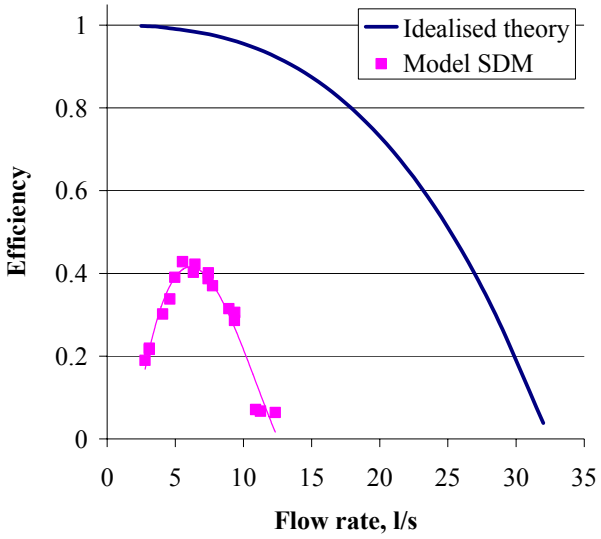

Fig.7. Ideal and scale model efficiency curves

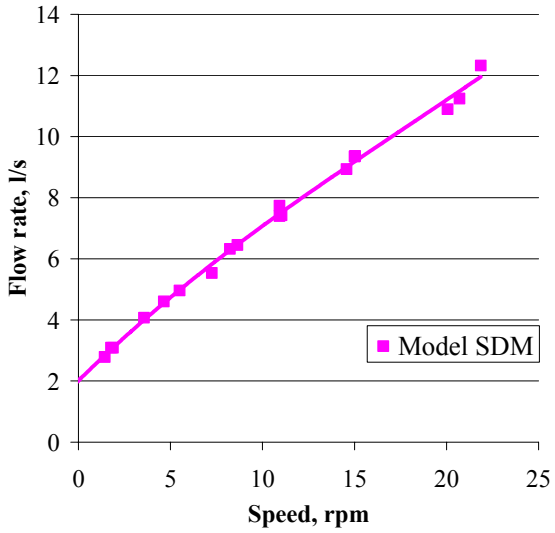

Fig.8. Scale model: flow vs. speed

The idealised theory and the model results shown in Figure 7 do not match well because two of the original assumptions were unrealistic.

The first of these assumptions was that there was no leakage under and around the wheel. Figure 8 indicates that the leakage when the wheel was not rotating was 2 l/sec or 1/6 of Q_{max}. The driving force behind the leakage is the difference in water levels either side of the wheel. As these levels are maintained at all flow rates the leakage is constant regardless of rotational speed. Therefore the idealised output power in equation 5 can be modified to take this constant leakage into account. See equation 8 which includes the leakage flow term Q_l.

$$P_{out\,\mathrm{modified}\,1} = (F_P - F_A)v_2 - \left((t_1 - t_2)\rho g Q_l\right) \qquad (8)$$

Figure 9 has the leakage flow Q_l set to 2 l/sec, which shows the improved correlation between the modified theory and the model results.

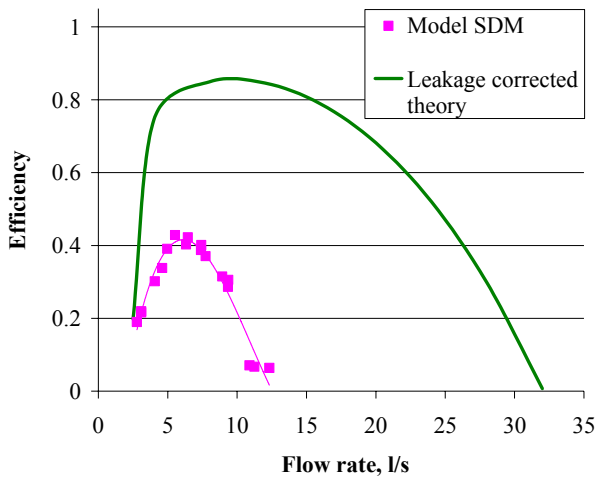

Fig.9. Leakage modified theory and scale model efficiency curves

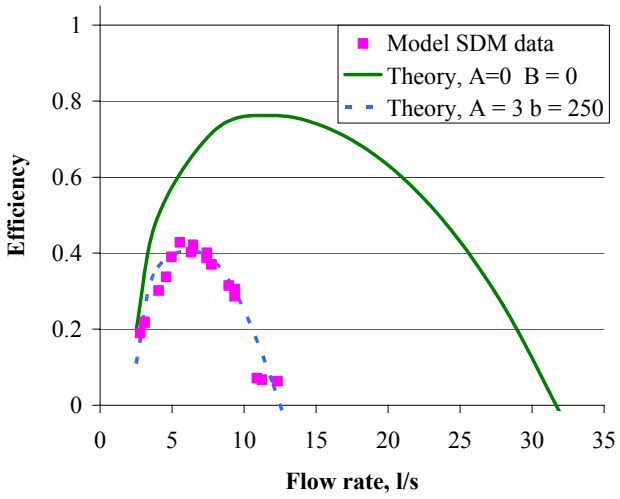

Fig.10. Modified theory adjusted to match scale model data

The second unrealistic assumption was that the blades would enter and exit without losses. In reality the blades would enter and exit with significant losses producing additional counteracting forces to the rotation of the wheel. Some of them were independent of speed (*e.g.* leakage) and others were proportional to speed (*e.g.* turbulent losses). Therefore equation 8 is modified further giving equation 9. This then matches the model tests using a correction factor to the force term:

$$P_{out\ \mathrm{mod}ified\ 2} = (F_P - F_A - (A + B v_2^2)) v_2 - \left((t_1 - t_2)\rho g Q_l\right) \qquad (9)$$

A and *B* are empirical constants, which have been adjusted to the data in Figure 10.

Before describing the blade losses it must be noted that as the SDM has diagonal blades, one side of each bucket always enters and exits before the other. Also, because these diagonal blades consist of flat plates in a single plane (see Figure 1), they do not protrude radially outwards from the hub across the width of the wheel. Instead they appear to lean forward when compared to the radial on one side of the wheel, and backwards on the other, see Figures 11 and 12. This results in different forms of losses on either side of the wheel.

On the side of the wheel where the buckets initially enter and exit the water, losses occurred with the passing of each blade. Figure 11 shows that for every blade, a volume of water *i* was initially displaced, only to be filled when the blade tip became level with the surface of the water. During this time a pressure force was exerted on the underside of the blade, counteracting rotation. This loss occurred at all speeds of rotation. When the water did enter this volume it ran down the top surface of the blade and impacted the subsequent blade, also counteracting rotation. This loss increased with the speed of rotation. This periodic filling mechanism produced waves in the upstream with an amplitude up to $1/15^{th}$ of the head difference. At the downstream side of the wheel, a volume of water *o* was raised with the passing of each blade. This required significant work by the wheel which was lost as soon as the blade tip passed the downstream water level, allowing air to ventilate the bucket. This loss also occurred at all speeds, and is also the main

cause of fast travelling waves at the downstream, and a pulsating rotation that would have negative effects on any power train connected to the SDM.

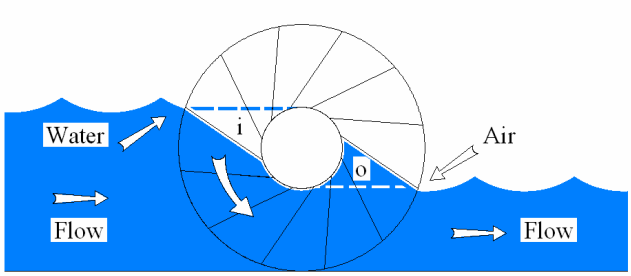

Fig.11. SDM losses 1

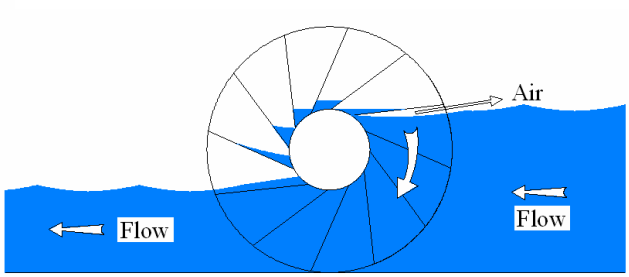

Fig.12. SDM losses 2

On the other side of the wheel where the end of each blade exits and enters the water, two final sources of loss remain. Referring to Figure 12, at the downstream side, a small quantity of water failed to run off the blade. This water was then effectively pumped back into the upstream. At the upstream, as the blades approached the water level and their buckets became fully filled, the angle of the blades being practically parallel to the water surface would eject fast blasts of air. This created turbulence in the water and introduced air into the flow. Both of these problems increased with the speed of the rotation.

All of the above losses were counter productive to the smooth running of the wheel. They not only reduced the efficiency but also the speed of the wheel, thus reducing its flow capacity.

6 THE ROTARY HYDRAULIC PRESSURE MACHINE

Two fundamental modifications have been determined to significantly reduce all of the losses witnessed on the SDM scale model in section 5. The first of these has been assessed and the second has yet to be implemented. The resulting machine, the *Rotary Hydraulic Pressure Machine* (RHPM) is expected to have efficiency and flow characteristics appreciably closer to that predicted by the idealised theory than the SDM.

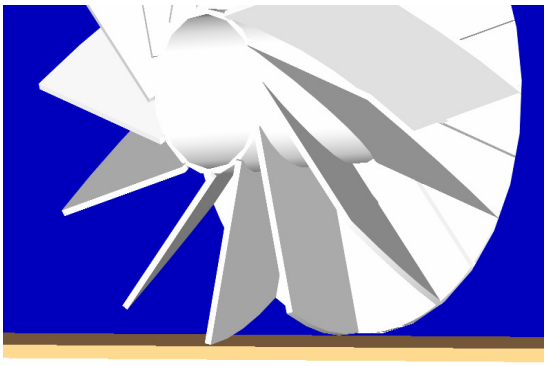

Fig.13. SDM leakage between blades

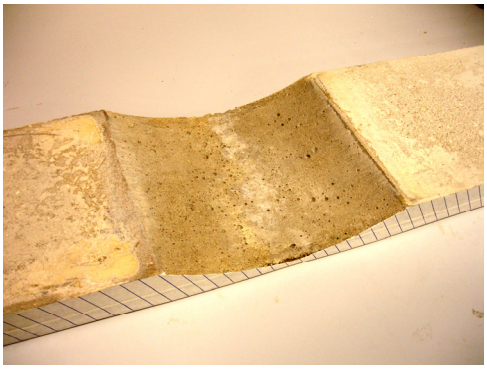

Fig.14. Shroud used in model tests

The first modification addresses unnecessary leakage underneath the wheel. Figure 13 demonstrates that diagonal blades in combination with a flat channel bed leaves passageways underneath the hub which allow water to flow along the blades without acting upon them. This

was addressed by creating a shroud. The shroud is a curved section of channel bed where the arc is equal in length to the arc between the two extreme corners of a bucket, see Figure 14.

Figure 15 shows that the addition of the shroud reduced the overall leakage by half, and the maximum efficiency of the wheel increased to just under 60 %. The maximum speed of rotation however did not increase as the blade inlet/exit losses are still dominant.

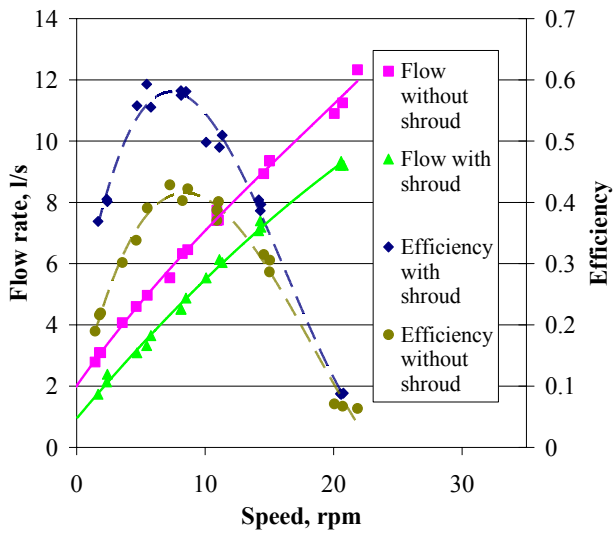

Fig.15. Model flow and efficiency curves with and without shroud

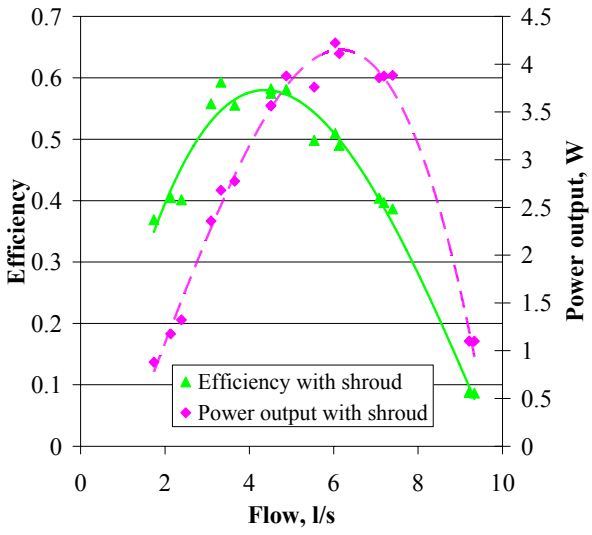

Fig.16. Model efficiency and power output curves with shroud

Figure 16 shows that the power output peaks at a higher flow rate than the efficiency. It is a function of flow and efficiency and can only be extended by addressing the problems highlighted by Figures 13 and 14. The second proposed modification is expected to alleviate these as it allows filling and venting from the sides of the wheel. This will increase the efficiency at all flows and raise the maximum speed of rotation and thus flow capacity. It is shown in Figure 17 and has not yet been implemented. It requires the removal of the side disks seen in Figure 1 and a new wheel support structure. This will similar to the shroud, preventing leakage through the buckets from their sides. The blades will protrude radially from the hub (and therefore twist along the width of the wheel) in order to minimise the required size of the support structure which must also prevent leakage.

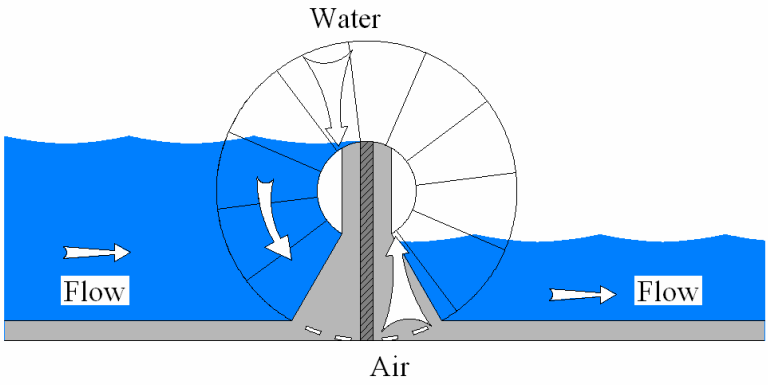

Fig.17. Proposed *Rotary Hydraulic Pressure Machine* with shroud and side filling and venting

7 APPLICATION OF THE ROTARY HYDRAULIC PRESSURE MACHINE

The RHPM is a very simple machine with few components requiring a simple support structure. The flow capacity is greater than with traditional waterwheels and the downstream flow velocity is not as fast as that from most turbines which can cause scouring. The way in which water flows into and out of the machine should not have any adverse effects on sediment transport or fish passage. These points make it suitable for relatively inexpensive installation into existing weir structures. Another unusual feature of the RHPM is that it is symmetrical. This means that it is fully reversible, being able to work in both directions of flow. Such ability could make it suitable for tidal flow scenarios.

8 CONCLUSIONS

The *Staudruckmaschine* does not have the operational characteristics claimed by its inventor. Many sources of loss have been observed using a scale model and two sets of modifications to its design have been determined. The result is a new machine called the *Rotary Hydraulic Pressure Machine*. Compared to the SDM, this is expected to have peak efficiency more than 20 % higher, a greater flow capacity per metre width of wheel, and a smoother less pulsating rotation. A theory has also been proposed to model the operation the SDM and the RHPM, both of which operate because of hydraulic pressure. A market for the RHPM exists as it can be used in scenarios where neither traditional waterwheels nor turbines would be economical. This is because of its simplicity in design, high flow capacity and ability to handle low heads. This market includes opportunities for installation into existing weir structures and use in tidal flow scenarios. Further information is available at www.lowheadhydropower.com.

REFERENCES

BRINNICH, A. (2001) Wasserktaft-Staudruckmaschine – Neues, konkurrenzlos wirtschaftliches Kraftwerkskonzept. *Wasserwirtschaft*, 91, 2, p. 70-74.

ETSU (1982) *Small scale hydroelectric potential in the UK*, ETSU Report.

GIESECKE, J. & MOSONYI, E. (2005) *Wasserkraftanlagen* 4th Ed., Springer Verlag, Berlin/Heidelberg.

KILLER, F. (2003) *Einbau einer Kleinwasserkraftanlage an der Stadtbachstufe des WKW Isarwerkes 3* Diplomarbeit, FH München (Fb Maschinenbau).

NRW (2005) *Handbuch Querbauwerke*, 1. Aufl., Klenkes-Druck& Verlag GmbH, Aachen, http://www.munlv.nrw.de/sites/arbeitsbereiche/boden/pdf/querbauwerk/handbuch_querbauwerke.pdf

WIEMANN, P. (2006) *Neue wirtschaftliche und technische Möglichkeiten der Stromerzeugung durch innovative Kleinwasserkraftwerke* (New economic and technical possibilities for energy generation with innovative small hydropower converters, in German), Diplomarbeit, Universität Kalsruhe/ University of Southampton.

BROCKAUS, F. A. (1903) *Brockhaus Konversations-Lexicon*, 14th Jubilee edition, Leipzig, volume 16, pages 527-8

THE ROTARY HYDRAULIC PRESSURE MACHINE FOR VERY LOW HEAD HYDROPOWER SITES

James SENIOR[1]
Patrick WIEMANN
Gerald MÜLLER
University of Southampton, U.K.

ABSTRACT
This short paper introduces a novel energy converter, the Rotary Hydraulic Pressure Machine (RHPM). This machine has been specifically developed to exploit very low head hydropower sites where the fall height is less than 5m. The RHPM is described and a theory behind its operation is outlined. This is followed by scale model testing, the results of which are used to estimate the full-scale performance. This found that hydraulic efficiencies up to 80% can be achieved, and estimated flow capacities for a 2m head installation of up to 3.6m^3/s per m width of machine. A case study demonstrates that the increased flow capacity and lower construction costs, compared to a traditional Zuppinger waterwheel installation, result in specific costs as low as 3000 €/kW installed capacity. This represents a significant improvement in very low head hydropower technology, making the economics more attractive to investors.

1. INTRODUCTION

In the western world much of the large scale, high output hydropower sites have now been exploited. Within Europe the focus has therefore shifted to Small Hydro-Power; installations with power outputs below 10MW. The target is to achieve an additional 2.4GW of power generation from Small Hydro-Power plants by 2010, relative to the 2005 generation levels (European Commission 2007). Within this bracket are sites with 'very low head' which refers to sites where the vertical distance through which flowing water falls over structures or terrain is less than 5m. At this point in time, no technology for this bracket satisfactorily meets the economic and ecological requirements required by investors and the authorities. As a result, the Seventh Framework Programme's 'Research Priorities for the Renewable Energy sector' set by the European Union includes the development of small turbines for very low heads under 5m as one of its long term targets (EURECA 2005).

2. THR ROTARY HYDRAULIC PRESSURE MACHINE

2.1 Description

The Rotary Hydraulic Pressure Machine (RHPM) is a novel energy converter developed at the University of Southampton in the UK for exploiting very low head hydropower sites, with fall heights under 5m. It is currently at the prototype stage, with a proposed theory and scale model results following in this paper.

[1] Civil Engineering Department, University of Southampton, Highfield, Southampton, SO17 1BJ, U.K., phone: +44 238059 4658; e-mail: js1301@soton.ac.uk

Depicted in Figure 1, the RHPM has just one moving part; a wheel with a diameter between 1.5m and 7.5m which rotates about a horizontal axis. The wheel has two critical components:

- The central hub: This is a horizontal cylinder which spans the width of the machine, and has a diameter equal to the head of the site. The top of the hub is level with the upstream water surface and the bottom of the hub is level with the downstream water surface.
- Twelve blades: The blades are the surface on which the water's energy is extracted. In the given example, they have the same length as the diameter of the hub or head of the site. They extend radially from the hub, whilst twisting as they progress across the width of the wheel. Overall they can be thought of as 'diagonally mounted', such that the termination of each blade coincides with the start of the subsequent blade on the other side of the wheel. This design is critical, allowing the large blades to enter and exit with minimal losses, and ensuring continual blade tip entry and exit from the water resulting in smooth consistent rotation.

Also depicted in Figure 1 are the main components of the wheel support structure, including:

- The shroud: This curved section of river bed ensures that at least one entire blade is enclosed within a close fitting channel. This prevents any leakage flow of water between and along the diagonally mounted blades, entering from beneath the wheel.
- Side walls: These not only provide a mounting for the wheel's bearings, but prevent any leakage flow of water between the blades entering from the sides of the wheel. Importantly, the side walls do not extend up to the water surfaces or along the entire length of the wheel. Instead the sides of the wheel remain exposed to allow water to enter the compartments between the blades from the side of the wheel as well as the front. They also allow air to 'ventilate' the compartments from the side of the wheel. This process allows the water to drain from the compartments with ease once they have reached the downstream.

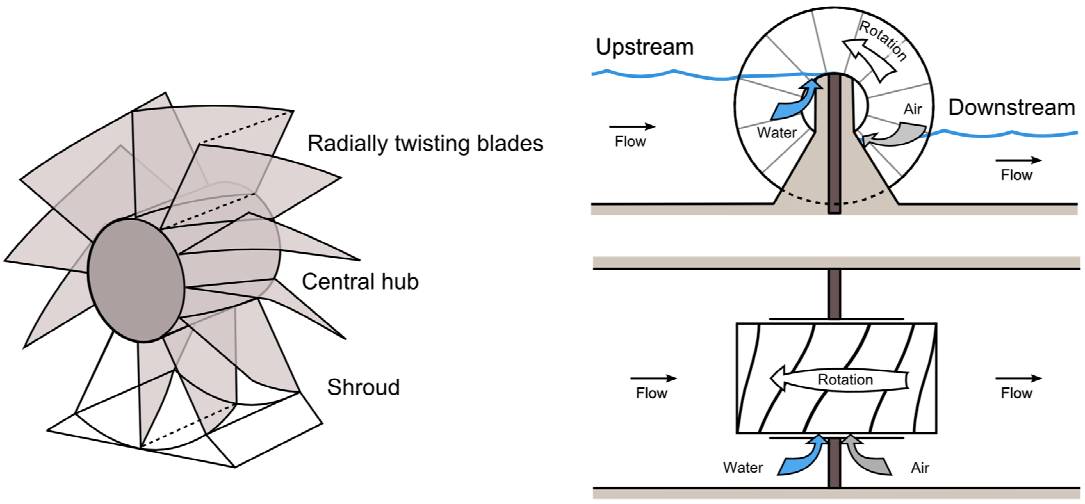

Figure 1: Depiction of the RHPM

The flow rate through the RHPM is proportional to the speed of rotation which is controlled by a 'load' such as a generator or mechanical power take-off.

It is envisaged that the RHPM could be employed in any conventional 'diversion' or 'run-of-river' installation, and would also be particularly suited for installation into bays of existing weir structures. Its complete symmetry would also allow it to operate with bi-directional flow, such as in tidal scenarios.

2.2 Theory

Starting from first principles, the Pressure, P at a depth of water, h with density, ρ of water, under the influence of gravity, g is:

$$P = h\rho g$$

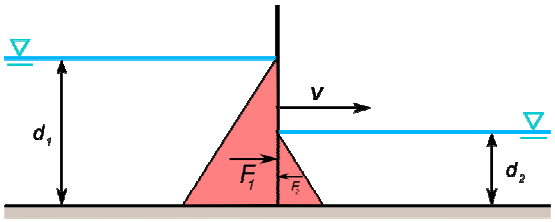

Figure 2: pressure acting on a simple vertical plate

Referring to Figure 2, consider a simple vertical plate which separates two dissimilar depths of water, d_1 and d_2. The triangles represent the hydrostatic pressure. The forces on either side of this plate of width, W, are F_1 and F_2:

$$F_1 = \rho g \frac{d_1^2}{2} W \qquad F_2 = \rho g \frac{d_2^2}{2} W$$

It can be seen that the force on the plate acting from the deeper water, F_1, is greater than that acting from the shallower water, F_2, and the total force acting on the plate, F, is:

$$F = \rho g \frac{(d_1^2 - d_2^2)}{2} W$$

If it is now imagined that the plate moves laterally with velocity, v, the power at the plate, P, is:

$$P = \left(\rho g \frac{(d_1^2 - d_2^2)}{2} W \right) v$$

The above example illustrates the most important principle behind the RHPM's operation: that two dissimilar depths of water acting across a vertical plate result in a force from which power can be extracted. In reality, it is not practical to have a vertical plate which moves laterally and indefinitely. Instead it is proposed that the plates, or *blades*, are mounted about an axle. This configuration adds additional complexity to the analysis as the water must flow from the deeper side of the RHPM to the shallower side.

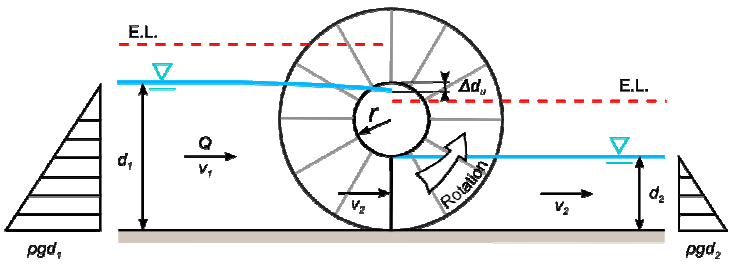

Figure 3: Operation of the RHPM

Referring to Figure 3 it can be seen in accordance with continuity that the velocity of the downstream water, v_2, is greater than that of the upstream water, v_1:

$$v_2 = \frac{d_1}{d_2} v_1$$

Therefore the water must undergo acceleration as it passes through the RHPM. Assuming for simplicity that the channel width is equal to that of the wheel, application of the energy equation gives the head drop associated with acceleration in the upstream, Δd_u as:

$$\Delta d_u = \frac{v_2^2 - v_1^2}{2\,g}$$

As all pressure forces acting directly on the central hub resolve towards the centre of the axel, only the pressure acting on the blade as it passes beneath the hub need to be considered. The force on the blade, F_p, is a function of the pressure difference across the blade and the area of the blade, A:

$$F_p = \rho\, g\, (d_1 - d_2 - \Delta d_u)\, A$$

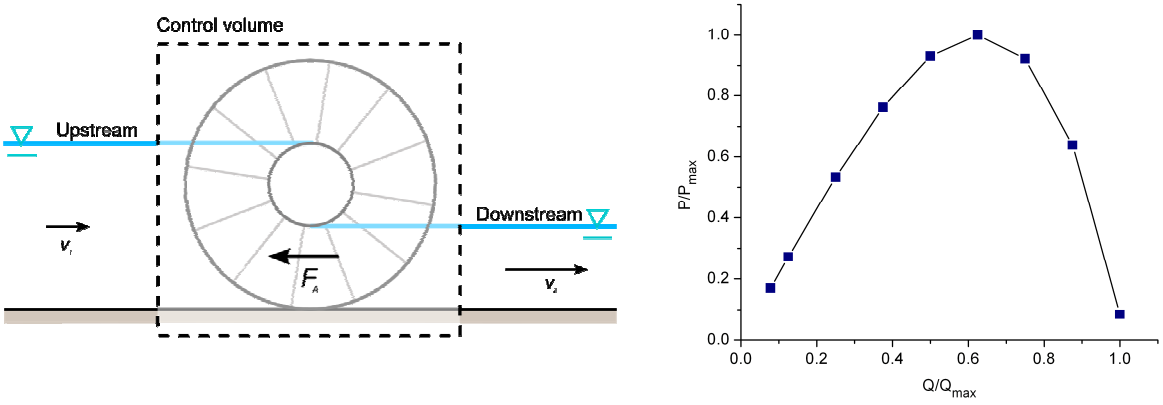

Figure 4: a) Reaction force on the RHPM, b) Theoretical power output of the RHPM

The force resulting from the pressure difference between the differing water depths, F_p, is not the only force that acts upon the RHPM. Figure 4a depicts a RHPM within a control volume, which can be thought of as a `black box' allowing the installation (wheel and all infrastructure) to be considered holistically. In passing through the control volume, a mass of water is accelerated from a lower speed, v_1, to a higher speed, v_2. In accordance with Newton's second and third laws, this acceleration must result in a force to which a counteracting force exists, provided by the installation itself. This counteracting force to the acceleration, F_A, is quantified by calculating the momentum change of the water, equal to the mass flow rate, Q, multiplied by the velocity change:

$$F_A = \rho\, Q\, (v_2 - v_1)$$

For simplicity it is assumed that all of the counteracting force to the acceleration of the water acts upon the blades. Also assuming no losses such as friction and turbulence, the theoretical power output, $P_{out\ ideal}$ is:

$$P_{out\ ideal} = (F_P - F_A)\, v_2$$

The theoretical output power for the RHPM is plotted in Figure 4b. The theoretical efficiency can also be plotted, however this requires analysis of the leakage flow through the gaps that exist between the wheel and the channel, and also all the sources of power loss including friction, turbulence etc. This part of the theory is design specific and is excluded from this short paper.

2.3 Differentiating properties

The RHPM can easily be confused with traditional waterwheels because of its large size and rotation about a horizontal axis. Such a comparison is misleading as the RHPM operates due to a different principle than traditional wheels.

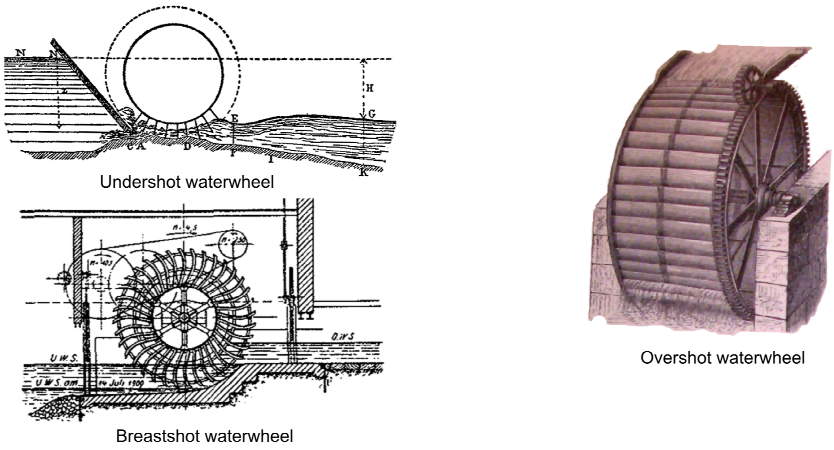

Figure 5: Common forms of traditional waterwheel

Figure 5 depicts the three regular forms of waterwheel. The *undershot* waterwheel was traditionally used for low heads and high flows; 0.5 – 2.5m head, 0.5 – 0.95m^3/s per m width (Müller and Kauppert 2004). The undershot waterwheel operated due to *impulse*, as a fast flowing stream of water impacted upon a blade moving at a slower velocity. Such waterwheels had maximum efficiencies in the range of 25% to 30% (Bresse 1876). The *overshot* waterwheel was used for relatively high heads and low flows; 2.5 - 10m head, 0.1 – 0.2m^3/s per m width (Muller and Kauppert 2004). The overshot waterwheel in comparison worked by *potential*, as it was the weight of the water within the buckets that drove the wheel. These had efficiencies up to 85% (Meerwarth 1935). The most common form of waterwheel built was the *breastshot* waterwheel, one form of which was the *Zuppinger* waterwheel shown in Figure 5. These wheels are a cross between the undershot and overshot waterwheel, being driven by both impulse and potential. The Zuppinger waterwheels were used for heads between 0.5 and 2m, with flow capacities not exceeding 1.2m^3/s per m width and efficiencies up to 73%(Müller 1939). These operating principles, impulse and potential, are clearly different to the RHPM, which is operated directly by the pressure of the water.

When compared to the Zuppinger waterwheel, the RHPM's operating principle allows for some significant design differences. The first of these is its small size relative to the head, with the upstream water level being above rather than below the axel height, reducing the machine's visual impact. Another is the large size of the blades of which there are relatively few; just 12 compared to 30 - 40. Being able to reduce the number of blades results in fewer losses detrimental to efficiency. The large size of the compartments between the blades, which fill 100% with water compared to the 60% of Zuppinger waterwheels (Muller 1939), allow a greater flow capacity per metre width of machine.

The RHPM extends from the water's surface down to the channel bed. This property should allow for improved natural sediment transport along the river when compared to Turbines and modern Zuppinger waterwheel installations. Turbines are normally designed to collect sediment upstream to prevent erosion of the blades and Zuppinger waterwheel installations require adjustable inlet gates to maintain a constant upstream water level. These act as barriers to flow resulting in a build-up of sediment upstream and prevent replenishment of sediment downstream. Similarly, the large open nature with which water enters the RHPM and the small number of blades may improve downstream fish passage conditions. This is because no large and sudden pressure changes take place and the chance of mechanical strike on small fish is reduced.

2.4 Model testing

The RHPM was hydraulically tested to ascertain its performance. This was done using a small scale model shown in Figure 6a. The model had a width of 0.245m, an outside diameter of 0.45m, and a hub diameter and blade length of 0.15m. Tests were conducted in a specially built flume of 2m length, 0.75m width, 0.4m depth and maximum flow rate of 25 l/sec.

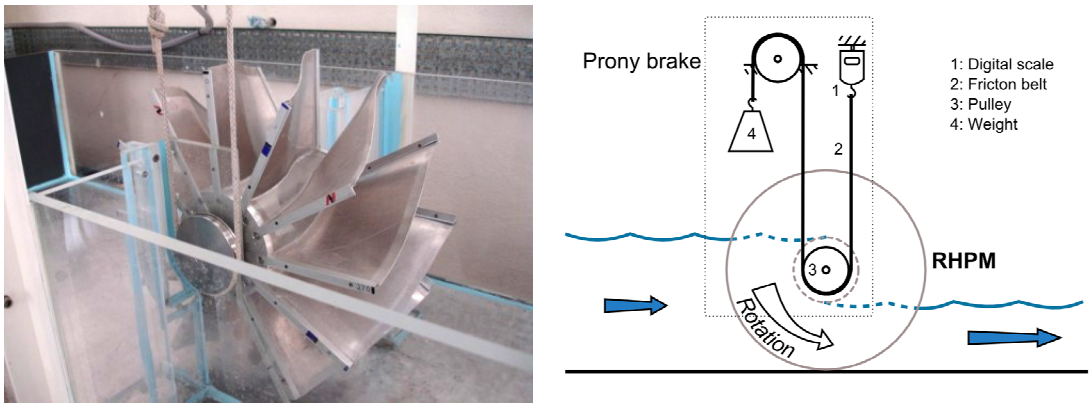

Figure 6: a) RHPM scale model, b) Prony brake power take off

The test series measured the flow rate, Q, power output, $P_{out\ measured}$, and efficiency, η, of the RHPM at several speeds of rotation ranging from stationary to maximum (freewheel at no load), whilst maintaining the upstream and downstream water depths to within 1mm to ensure a constant head.

The speed of the wheel was controlled using a 'Prony Brake'. This is a traditional means of applying a load to a rotating shaft which also allows the power output of the shaft to be measured. Shown in Figure 6b, the Prony brake uses a weight and a counterweight (scale) of mass, m_{weight} and $m_{counterweight}$, and a friction belt to apply a torque to a pulley rotating with frequency, f. The Prony brake is used to calculate the output power, $P_{out\ measured}$, by multiplying the torque by the angular speed:

$$P_{out\ measured} = (m_{weight} - m_{counterweight})g \times r \times 2\pi \times f$$

The flow rate was measured using a standard flow measurement weir and equations (Chanson, 2001):

$$q = \frac{2}{3} C \sqrt{2\,g(d_1 - \Delta z)^3} \qquad C = 0.611 + 0.08\frac{d_1 - \Delta z}{\Delta z}$$

The results of the model testing are shown in Figure 7a. It can be seen that the 'RHPM power' curve has a similar shape to that of the theory shown in Figure 4b, suggesting that the theory may be correct. The line does not intersect the axis at [0,0] as there was a constant leakage around the wheel of ~3 l/sec, driven by the pressure difference.

Figure 7a shows that the peak hydraulic efficiency is ~80%. The peak efficiency occurs at lower speeds of revolution and flow than the peak power output, P_{max}, which was 16.5W and occurred at 70% efficiency. The maximum acceptable flow rate, Q_{max}, can be taken as 18 l/sec, after which the efficiency and power output reduce significantly.

Assuming no scale effects, the Q_{max} and P_{max} of full scale installations have been estimated using the Froude scaling laws (Douglas, 2001), as shown in Figure 7b. The scaling maintains a head, hub and blade relationship of 1:1:1 as with the model. They suggest that for a 2m head, an RHPM could process 3.6m^3/s per m width of machine, which is ~300% that of a traditional Zuppinger waterwheel.

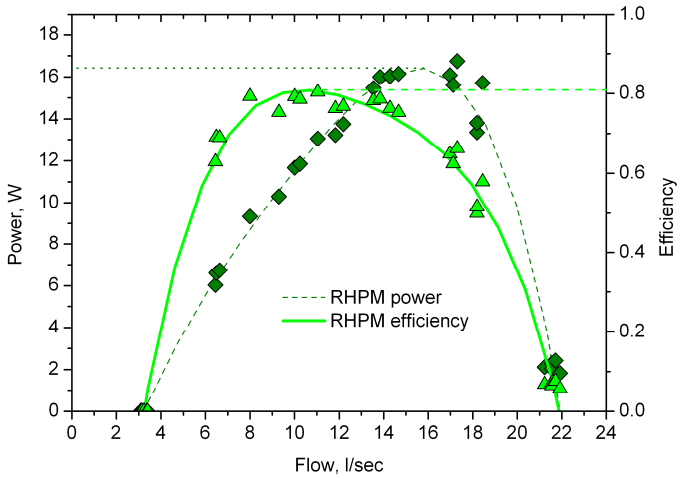

Head / Hub diameter / blade length, m	Q_{max}, m^3/s per m width	P_{max}, kW
0.5	0.5	1.4
1.0	1.3	7.7
1.5	2.3	21.3
2.0	3.6	43.7

Figure 7: a) RHPM scale model results, b) Full-scale estimates

3. CASE STUDY

A small case study is provided for a very low head hydropower site in the South of Germany. The site has a head of 0.9m, an average flow of $10m^3/s$ and a width restriction of 6m. Two reputable German manufacturers provided quotes for Zuppinger waterwheels for electricity generation, the average values of which are used to make a comparison with a RHPM installation, as shown in Figure 8. The quotes have been broken down into three cost groups:

- The wheel: The proposed Zuppinger waterwheels have a diameter and width of ~6m. They have 36 blades, each of which consist of wooden boards bolted to multiple curved and galvanised steel brackets. In comparison the RHPM only requires a diameter of 4.3m and a width of 5m. It would only require 12 blades and a central hub. Despite the RHPM requiring a greater quantity of steel, its smaller size (having a volume 40% that of the Zuppinger wheel), smaller quantity of parts and simple welded construction are expected to result in lower costs. Two scenarios are provided: the *best case* where the cost of the wheel is taken as 50% that of the Zuppinger waterwheel, and the *worst case* where the cost of the wheel is taken as 80% that of the Zuppinger wheel.
- The inlet gate: this component is required by the Zuppinger waterwheel to maintain a constant upstream water level. It is not required by the RHPM as the speed of rotation directly controls the flow rate and thus the water level.
- Common components and installation costs: These include the cost of the gearbox, generator, belts, control systems etc, and the costs of installation. They are applied directly to the RHPM from the Zuppinger waterwheel costs, as are the efficiencies of the gearbox, belt and generator.

Of importance *in this particular case study*, the RHPM with a hub of 0.9m and a blade length of 1.7m, has a flow capacity of $2m^3/s$ per m width. As a result, the full $10m^3/s$ flow at the site can be exploited, increasing the P_{max} by ~50% to 54kW when compared to the Zuppinger waterwheel installations which could only exploit ~$8m^3/s$ of the available flow. With the estimated cost of the complete RHPM installation being between ~70% and ~80% of the Zuppinger waterwheel installation, the *specific cost* also improves, being between ~50% and ~60% of the Zuppinger waterwheel installation. This is the cost per kW of capacity installed, and at approximately 3000 €/kW the RHPM looks economically very attractive for very low head hydropower sites.

	Zuppinger quotes (averaged)	**RHPM, *best case***	**RHPM, *worst case***
Diameter, m	6.25	4.3	4.3
Width, m	6	5.0	5.0
Q_{max}, m^3/sec	7.9	10	10
$Q_{max,}$ m^3/sec per m width of wheel	**1.32**	**2.0**	**2.0**
Wheel efficiency, maximum, %	73	80	80
Gearbox / belts / generator efficiency, %	87	87	87
$P_{elecrical}$, kW	37	54	54
Wheel, €	94,000	47,000	75,200
Inlet, €	15,200	0	0
Common components and installation, €	92,300	92,300	92,300
Total before tax, €	**201,500**	**139,300**	**167,500**
Specific cost, € / kW installed	**5,450**	**2,650**	**3,150**

Figure 8: Case study comparing Zuppinger waterwheel and RHPM installations

4. CONCLUSION

The RHPM is a novel energy converter for very low heads below 5m. A plausible theory of operation has been proposed which suggests that it is driven directly by the pressure difference between two dissimilar depths of water either side of the installation. This is unlike any conventional waterwheel or turbine. Model tests showed that the machine has an efficiency up to 80%, and scaling of the model data suggests that flow capacities up to 3.6 m^3/s and powers of ~40kW per metre width of machine are achievable. A case study was conducted comparing the RHPM to a Zuppinger waterwheel installation and found that the larger flow capacity and relative simplicity of the machine could result in a 40% to 50% lower specific cost of around 3000 €/kW installed capacity. Such values would suggest that the RHPM could be economically attractive. Combined with its potential for improved sediment transport and fish passage, the RHPM could satisfy the FP7's demand for a new economically and ecologically acceptable technology suitable for very low heads less than 5m.

5. ACKNOWLEDGEMENTS

The authors acknowledge the E.U.'s support for this research under FP7 contract number 212423.

References:

Bresse, J. (1876), Water Wheels or Hydraulic Motors, reprint 2003, University Press of the Pacific.

Brockhaus, F.A. (1903), Brockhaus Konversations-Lexicon, chapter Wasserräder, 14th Jubilee edition, volume 16, Leipzig.

Chanson, H.(2001), The Hydraulics of Open Channel Flow, Butterworth-Heinemann.

Douglas, J.et al. (2001), Fluid Mechanics, Pearson Education Limited.

EURECA (2005), FP7 Research Priorities for the Renewable Energy Sector, EURECA

European Commission (1997), White Paper for a Community Strategy and Action Plan - Energy for the future: Renewable Sources of Energy, COM(97)599.

Meerwarth, K.D. (1935), *Experimentelle und theoretische Untersuchungen am oberschlächtigen Wasserrad*, PhD Thesis, Technical University of Stuttgart, Germany (in German)

Müller, G. & Kauppert, K. (2004), Performance Characteristics of water wheels, Journal of Hydraulic Research, 42, 451-460.

Müller, W. (1939), Die Wasserraeder, Nachdruck der 2. Ausgabe, Moritz Schaefer, Detmold, 1991 (in German)